Nazarbayev University
School of Engineering and Digital Sciences
Department of Chemical and Materials Engineering

Capstone project Report 4

Design of Plant for industrial production of Styrene in Kazakhstan

Course instructor: Professor Dhawal Shah
Supervisors: Professor Stavros Poulopoulos
Professor Yanwei Wang

Sinister Six
Almas Askarov
Arailym Bekken
Gulnaz Ingkar
Kuralay Issabek
Alikhan Kalmakhanbet
Aizada Mels

April 20, 2025
Astana

Table of contributions of the team members

Section	Topic	Almas	Arailym	Gulnaz	Kuralay	Alikhan	Aizada
Chapter I. Process Introduction							
1.1	General physical and chemical properties of process elements		1^{st}			2^{nd}	
1.2	Styrene application and production rate	2^{nd}					1^{st}
1.3	Review of the selected manufacturing process			1^{st}		2^{nd}	
Chapter II. Process Summary							
2.1	Process kinetics	2^{nd}				1^{st}	
2.2	Separation of water and lights		1^{st}				
2.3	Final product purification			1^{st}			2^{nd}
Chapter III. Major Equipment Design							
3.1	E-101 Heat exchanger design	1^{st}					
3.2	Reactor R-101 and R-102 design				2^{nd}	1^{st}	
3.3	Cooler E-105 design		1^{st}				
3.4	Distillation column T-101 design			1^{st}			

3.5	Distillation column T-102 design						1^{st}
Chapter IV. Minor Equipment Design							
4.1	Storage tanks design for reactants				1^{st}		
	Storage tanks design for products						1^{st}
4.2	Heaters and condenser design		2^{nd}			1^{st}	
4.3	Decanter design			1^{st}			
4.4	Design of pumps		1^{st}				
Chapter V. Plant Location and Layout							
5.1	Plant site location		1^{st}	2^{nd}			
5.2	Plant layout		2^{nd}	1^{st}			
Chapter VI. Environment and Waste Streams							
6.1	Light gases treatment					1^{st}	
6.2	Wastewater treatment						1^{st}
6.3	Catalyst treatment						1^{st}
Chapter VII. Total Investment and Profitability							
7.1	Price of Raw Materials and Final Product	2^{nd}			1^{st}		

7.2	Capital Investment Estimation	$2^{n\ d}$			1^{st}		
7.3	Operating Costs (OPEX)	1^{st}			2^{nd}		
7.4	Cash Flow	1^{st}			2^{nd}		
7.5	Discounting, Depreciation and Analysis Period	1^{st}			2^{nd}		
7.6	Profitability Analysis	2^{nd}			1^{st}		
Chapter VIII. Conclusions and future work							
					1^{st}		

TABLE OF CONTENTS

LIST OF FIGURES

LIST OF TABLES

CHAPTER I. Process Introduction

1.1 General physical and chemical properties of the process elements

Styrene is an organic compound consisting of a vinyl group as a substituent for benzene, also known as vinylbenzene, ethenylbenzene, cinnamene, or phenylethylene with molecular formula C8H8) [1]. It is both a natural and synthetic substance, sometimes occurring naturally in foods such as coffee, cinnamon and cheese [2].

The industrial production of styrene dramatically increased during and after World War II, as it became crucial for producing synthetic rubber (SBR), especially for tyres, and various plastic products [3]. Nowadays, it is one of the most commonly used monomers with many applications(See *Appendix D*).

Styrene monomer is a base of many products ranging from flexible rubbers to plastic packaging(see *Appendix D: Table D1* for key applications of styrene). It is commercially available with a purity of 99.6% to 99.9%, ensuring it meets the high standards required across all of its applications [4]. This high purity is crucial for maintaining the desired quality and performance of styrene products like polystyrene, ABS, SBR, and other composites.

The **Table A1** (*Appendix A*) presents data on the physical and thermodynamic properties of the pure components (ethylbenzene, styrene, hydrogen, benzene, toluene) involved in the system. As can be seen in the table, literature data and that of Aspen Plus are fairly consistent with each other. All of the properties have been evaluated under standard conditions, namely, 25°C and 1 atm.

Furthermore, plots for temperature dependence of these properties are shown in *Appendix A*. Experimental values of properties were compared with Aspen plus simulation values, and density (*Appendix A: Figures A1-A4*), viscosity (*Appendix A: Figures A5-A8*), saturation pressure (*Appendix A: Figures A9-A12*), heat of vaporization (*Appendix A: Figures A13-A16*) and ideal gas heat capacity (*Appendix A: Figures A17-A20*) followed the same trend and values were close. However, liquid heat capacity values varied a lot from the Aspen Plus values with increasing temperature. The deviation from simulation values were between 9 to 15% (*Appendix A: Figures A21-A24*).

The plots of Henry's constant for the hydrogen-water system as a function of temperature, are shown in *Appendix A: Figure A25*. The Aspen Plus data displays a peak in around 310 K, followed by a decrease, whereas the experimental values show a consistent increase with temperature. The discrepancy between the two sets of data, particularly at higher temperatures, may arise due to differences in how the solubility model is handled in Aspen Plus versus the empirical data. In addition, at high temperatures, both hydrogen and water can exist in the vapor phase, making it challenging to predict their behavior accurately using models designed for gas-liquid equilibrium.

Literature review showed different root mean square errors for several theoretical models simulated in Aspen. Ideal and NRTL models showed the less mean square error, but

since the liquid phase consists of two compounds, ethylbenzene and styrene, the binary mixture exhibits non-ideal behavior [5]. Therefore, it is suitable to use the NRTL method for Aspen Simulation for modeling phase equilibria. The plots for thermodynamic model validation is shown in *Appendix B*.

1.1.1 Chemical hazards

Ethylbenzene is heavily involved in the manufacturing of the styrene monomer as an intermediate. According to the National Center for Biotechnology Information [6], human exposure to ethylbenzene mostly happens through inhalation. It is mainly toxic to humans in regard to their central nervous system, and is also an irritant of mucous membranes and eyes.

Table 1 illustrates the hazardous profile of ethylbenzene, including the Globally Harmonized System of Classification and Labeling of Chemicals (GHS) standards it falls under and hazard classification.

Percentages in brackets next to the standards refer to the purity of a relevant component.

Table 1. Ethylbenzene hazard profile

<table>
<tr><td colspan="4">GHS standards
[6]</td></tr>
<tr><td>H225 (99.97%)</td><td colspan="3">Highly flammable liquid and vapor</td></tr>
<tr><td>H304 (16.94%)</td><td colspan="3">Might be fatal if swallowed</td></tr>
<tr><td>H332 (99.91%)</td><td colspan="3">Inhaling is harmful</td></tr>
<tr><td>H373 (19.38%)</td><td colspan="3">Repeated exposure may damage vital organs.</td></tr>
<tr><td>Diamond</td><td>Hazard</td><td>Value</td><td>Description</td></tr>
<tr><td rowspan="4"> 

[7]</td><td>Health</td><td>2</td><td>Can cause temporary incapacitation or residual injury</td></tr>
<tr><td>Flammability</td><td>3</td><td>Can be ignited under almost all ambient temperature conditions</td></tr>
<tr><td>Instability</td><td>0</td><td>Normally stable even under fire</td></tr>
<tr><td>Special</td><td></td><td></td></tr>
</table>

Hazard indicating pictograms [6]


Styrene itself, a final product, might pose significant danger if exposed, too. As well as ethylbenzene, styrene is mainly exposed to humans through inhalation. According to the National Center for Biotechnology Information [8], a 3 hour exposure to styrene can result in immediate eye and throat irritation, drowsiness, vertigo and metallic taste. Long-term exposure results in more severe consequences such as dermatitis, blistering of the skin, depression, and damage to reproductive systems and other vital organs. **Table 2** depicts styrene's hazard profile.

Table 2. Styrene hazard profile

GHS standards [8]	
H226 (100%)	Highly flammable liquid and vapor
H304 (50.44%)	Might be fatal if swallowed
H315 (100%)	Causes skin irritation
H319 (99.93%)	Causes serious eye irritation
H332 (98%)	Inhaling is harmful
H335(54.02%)	May cause respiratory irritation
H361 (34.93%)	Might lead to fertility damage or damage the unborn child
H372 (75.94%)	Repeated exposure might damage organs
H412 (48.83%)	Harmful to aquatic life in a long term fashion

<table>
<tr><td rowspan="4"> 

Diamond
[9]</td><td>Hazard</td><td>Value</td><td>Description</td></tr>
<tr><td>Health</td><td>2</td><td>Can cause temporary incapacitation or residual injury</td></tr>
<tr><td>Flammability</td><td>3</td><td>Can be ignited under almost all ambient temperature conditions</td></tr>
<tr><td>Instability</td><td>2</td><td>Readily undergoes violent chemical changes at elevated temperatures and pressures</td></tr>
<tr><td></td><td>Special</td><td></td><td></td></tr>
<tr><td colspan="4">Hazard indicating pictograms
[8]</td></tr>
<tr><td colspan="4"> 
</td></tr>
</table>

Hydrogen might be irritating when inhaled at high concentrations. When in contact in confined areas, vapor hydrogen might cause dizziness and asphyxiation [10]. Below, in **Table 3**, is shown the hazard profile of hydrogen.

Table 3. Hydrogen hazard profile

GHS standards [10]	
H220 (99.93%)	Extremely flammable gas

<table>
<tr><td>H280 (76.76%)</td><td colspan="3">If heated, the gas under pressure might explode</td></tr>
<tr><td>H281 (13.76%)</td><td colspan="3">Contains refrigerated gas, might cause cryogenic burns or injury</td></tr>
<tr><td>Diamond</td><td>Hazard</td><td>Value</td><td>Description</td></tr>
<tr><td rowspan="4"> 

[11]</td><td>Health</td><td>0</td><td>No hazard beyond that of ordinary combustible material</td></tr>
<tr><td>Flammability</td><td>4</td><td>Burns readily. Rapidly or completely vaporizes at standard conditions</td></tr>
<tr><td>Instability</td><td>0</td><td>Normally stable even under fire</td></tr>
<tr><td>Special</td><td></td><td></td></tr>
<tr><td colspan="4">Hazard indicating pictograms
[10]</td></tr>
<tr><td colspan="4"> 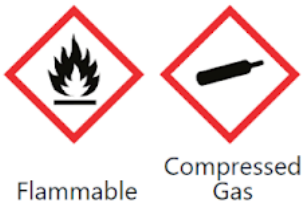
</td></tr>
</table>

The profiles of other major by-products, namely, **Benzene** and **Toluene**, are shown in *Appendix C*.

1.2 Styrene application and production rate

While polystyrene and styrene copolymers (ABS, SAN, etc.) have a significant share of all styrene uses, both face challenges due to their non-biodegradability and recycling difficulties, which makes them less environmentally sustainable. In contrast, Styrene-butadiene rubber (SBR), used for tyres and other elastomer applications, can be recycled and repurposed, making it less harmful to landfills compared to single-use materials [12]. Moreover, according to Market Forecast Analysis, the global SBR market size is predicted to increase from USD 10.2 Billion in 2022 to USD 16 Billion by 2032, meaning demand for styrene production is also increasing [13]. Therefore, considering its critical role in high-demand industries like tyre manufacturing,

potential for recycling and cost-effectiveness, SBR was selected as a primary focus application for this project.

For a production of styrene-butadiene rubber (SBR) styrene with a purity level of at least 99.7% is typically required to ensure high-quality polymerization [14]. This high level of purity minimizes unwanted reactions and potential contaminants that could affect the final rubber product. Common acceptable impurities include trace amounts of ethylbenzene and other hydrocarbons, but are generally kept below 500 ppm [15]. To inhibit premature polymerization during shipping, storage and handling, additives like tertiary butyl catechol (TBC) are present at a concentration of 10-15 parts per million (ppm) (**Table 4**).

Table 4. Styrene monomer requirements [14]

Property	**Specification**
Purity, min, weight %	99.7
Ethylbenzene, max, g/kg	1
Aldehydes(as benzaldehyde), max, weight %	0.02
Peroxides(as H2O2), max, mg/kg	100
Polymer, max, mg/kg	10
Inhibitor (TBC), mg/kg	10-15

The production rate can be predicted by considering either GDP or population growth. GDP can provide information on the level of economic industrial development of a country or a region, since GDP is an indicator of all economic activities. This is vital for chemical industries. From *Figure 1*, the average tons of styrene per million people is 2,666.79 and the average tons of styrene per billion of GDP is 298.084 in The CIS region. The results of the extrapolation are the following: 670 kilotons/year on population basis and 824 kilotons/year on GDP basis. Styrene production is more GDP-based than population-based because styrene is primarily used in industrial applications, such as plastics, and synthetic rubber, and is closely related to a region's manufacturing and economic activities, thus production of design will be assumed to be 824,000/4 = 206,000 tons per year. Rounding the value to the nearest integer will be assumed as 200000 tons/year.

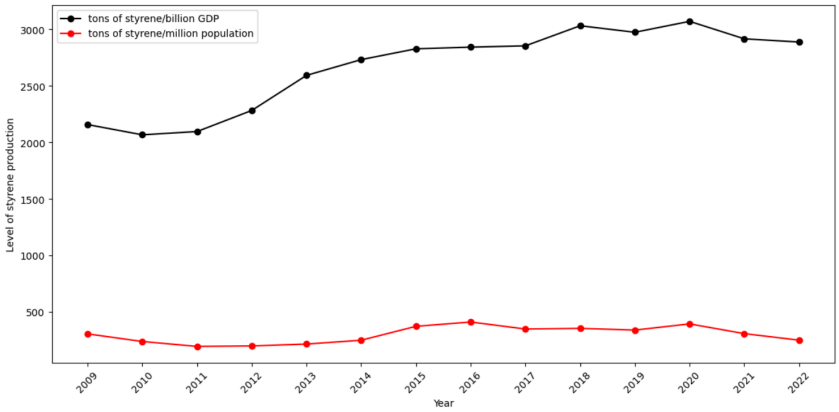

Figure 1. Production of styrene per unit variable

1.3 Review of the selected manufacturing process

The production route follows the direct dehydrogenation of ethylbenzene, which accounts for over 85% of global styrene production in the industry [16]. In this process, EB is mixed with high-temperature steam and proceeds with reaction to produce styrene and hydrogen gas under a catalyst (Fe_2O_3). Overall, the direct dehydrogenation of ethylbenzene is considered more beneficial compared to alternative processes such as oxidative dehydrogenation. It offers high styrene selectivity of around 90% and conversion rates up to 80%, while the use of steam helps prevent coke formation, preheats the feed, and shifts the reaction equilibrium toward products. Although it is endothermic and requires a large amount of steam, as well as being susceptible to polymerization, it avoids major drawbacks of oxidative dehydrogenation, such as rapid catalyst deactivation due to coke build-up and lower styrene selectivity caused by unwanted side products.

The overall reaction of dehydrogenation looks like this:

$$C_6H_5CH_2CH_3(g) \Leftrightarrow C_6H_5CHCH_2(g) + H_2(g) \quad (1)$$

$$C_6H_5CHCH_2(g) + 2H_2(g) \Leftrightarrow C_6H_5CH_3(g) + CH_4(g) \quad (1)$$

The reaction begins with liquid ethylbenzene mixed with recycled ethylbenzene from the distillation then changes its phase to be gas [17]. The reaction is endothermic, thus requiring high operating temperatures and low pressure [18]. Typical operating temperature is about 560−700 °C, and big temperature variations might lead to undesirable side reactions and equilibrium shifts as reaction is reversible [19]. The main side reactions producing methane, toluene, benzene, ethylene are listed below:

$$C_6H_5CH_2CH_3(g) \Rightarrow C_6H_6(g) + C_2H_4(g) \quad (2)$$

$$C_6H_5CH_2CH_3(g) + H_2(g) \Rightarrow C_6H_5CH_3(g) + CH_4(g) \quad (3)$$

$$2H_2O(g) + C_2H_4(g) \Rightarrow 2CO + 4H_2(g) \quad (4)$$

$$H_2O(g) + CH_4(g) \Rightarrow CO + 3H_2(g) \quad (5)$$

$$H_2O(g) + CO(g) \Rightarrow H_2(g) + CO_2 \quad (6)$$

Here, the side reaction leading to CO and CO_2 formation is not taken into account due to its insignificance.

1.3.1 Catalyst type

For the majority of styrene plants, potassium carbonate and iron oxide combined with a small amount of one or more of the following promoters— Cr_2O_3, Ce_2O_3, MoO_3, CaO, MgO, and V_2O_5—is the preferred commercial catalyst [17]. Potassium carbonate, water, and pigment-grade iron oxide are combined to form a paste that can be pilled or extruded [21]. Compared to unpromoted iron oxide, the K_2O promoted catalyst shows greater activity [22]. Moreover, the Potassium oxide continuously eliminates CO and CO_2 acts as an effective water-gas shift catalyst. This feature is responsible for the catalyst's prolonged lifespan, which spans one to two years [23].

By stopping sintering and the consequent loss of surface area, the Cr_2O_3 promoter in the 1-3 wt % range functions as a structural stabilizer [22]. As an alternative, different binders, such as cement, might be applied to guarantee structural strength [24]. Other promoters are used: Mo_2O_3, MgO without Cr_2O_3, and MgO with Cr_2O_3 and Ce_2O_3, in that order.

For many years, Shell 105 was the dominant catalyst, and it was the first to use potassium as a water-gas reaction promoter. Typically, this catalyst contains 13.3% potassium as K_2CO_3, 2.4% chromium in Cr_2O_3, and 84.3 percent iron as Fe_2O_3. It produces fair yields and has good physical qualities and activity [25]. Summary of characteristics of most acceptable catalysts are given in **Table 5.**

Table 5. Catalyst Characteristics and Composition

Form	Extrudates (Cylinders), macroporous [23]
Size, mm	0.84-1.68 [26]
Fe2O3, wt%	73.6 [26]
K_2O, wt%	9.7 [26]

Ce_2O_3, wt%	16.7 [26]
Activation energy, kJ/mol	103.7±8.2 [26]
Surface area, m2/g	1.5-3 [26]
Pore volume, cm^3g^{-1}	0.1-0.25 [26]
Pore radius, Å	150 [27]
Steam/ethylbenzene mole ratio	3-9 [26]
EB conversion, %	76.9 [26]
Styrene selectivity, %	91.4 [26]
Styrene yield, %	70.3 [26]

Catalyst deactivation can occur due to poisoning and potassium migration. Halides and compounds containing sulfur, phosphorus, and silica act as catalyst poisons by coating active sites and deactivating the catalyst [23]. While organic sulfur compounds temporarily poison the catalyst—allowing it to regain activity once the sulfur is depleted—halides are permanent poisons that cause irreversible damage. Therefore, it is recommended to maintain halide concentrations below 1 ppm in the feed, as they react with K_2O and diminish the promoting effect of potassium on the catalyst [22]. Over time, potassium promoters may migrate from the periphery to the center of the catalyst, leading to uneven distribution—high concentration in the core and low concentration at the edges—resulting in confined catalytic activity and inactive regions [22]. Additionally, steam treatment exacerbates potassium migration by converting K_2O into KOH, further reducing catalyst activity [28].

Endothermic nature of the reaction causes a significant temperature drop in the reactor, which in turn limits the conversion of ethylbenzene to styrene. Using **multistage reactors** with heating in between reactors is a very good method to decrease the temperature drop caused by the endothermic dehydrogenation reaction. Traditionally, **furnaces** are used as they offer more controlled heating, help to avoid steam-related complications and optimize steam distribution across stages [29]. In this production, a**diabatic reactors** were chosen as 75% of the industry uses it for styrene production. Their main advantage is a simpler design and lower capital costs. They manage the temperature drop caused by the endothermic reaction by staging the process. Most modern reactors operate at low pressures (around 0.5-2 atm) to improve the equilibrium conditions for dehydrogenation. This condition enhances conversion and allows for lower steam rates, leading to significant energy savings.

CHAPTER II. Process Summary

In *Figure 2*, the process flow description can be found. Overall process design was based on Luyben's design (*Appendix E*) [18]. Overall, the system has 20 streams.

Raw materials used are EB and low-pressure steam. EB enters a pump and is then heated (E-101 and E-102) to 500°C. This mixture is combined with a recycle stream heated in the E-107 unit. The resulting stream is then mixed with heated low-pressure steam (stream 6). After reaching 620°C (stream 7), it enters the first plug flow reactor (R-101), which operates at 620°C and 1.8 atm. As the reaction is endothermic, it leaves the first reactor at 550°C (stream 8), thus it is reheated (stream 9) up to operating temperature and enters the second PFR (R-102); it leaves R-102 unit at 590°C.

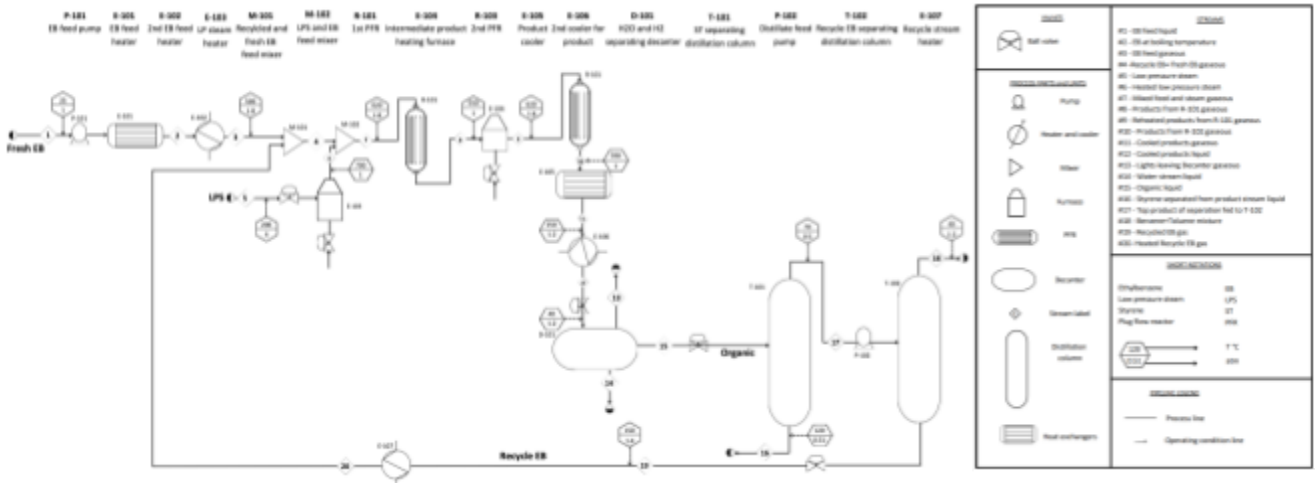

Figure 2. Process flow diagram of the plant for industrial styrene production

The product stream is then cooled to 40°C (stream 12) and enters the decanter (D-101), operating at 40°C and 1.2 atm. Most of the water (stream 13) and light gases (stream 14) are removed in the decanter, and the organic liquid (stream 15) is sent to separation units. In the first distillation column (T-101), a product containing 99.7% styrene with less than 900 ppm EB is collected (stream 16). The top product from T-101 is sent to the second distillation column (T-102), where recycled EB (stream 19) is collected as the bottom product, heated and mixed with the fresh feed. Benzene and toluene byproducts (stream 18) are removed as top products from T-102. The first distillation column operates at 70°C and 0.1 atm, while the second distillation column operates at 40°C and 1.2 atm.

2.1 Process kinetics

2.1.1 Kinetics model available in literature

The dehydrogenation of ethylbenzene to styrene is a complex industrial process requiring accurate kinetic models to capture the reaction mechanism, optimize selectivity and guide industrial reactor designs. Various kinetic models have been proposed to simulate this reaction, each tailored to specific catalysts and operational conditions. These models range from

mechanistically detailed approaches to empirical models suitable for industrial applications. The Hougen-Watson (HW) model is among the most widely used for EB dehydrogenation, particularly with potassium-promoted iron oxide catalysts. Lee and Forment use the HW kinetic model in a tubular reactor system. This model is suitable for high surface coverage conditions and allows for the intrinsic rate equations to reflect both the adsorption-desorption dynamics and reaction rates. Lee and Froment's work demonstrates that the HW model is robust in predicting conversion and selectivity under varying temperatures, steam-to-EB ratios, and space times in a tubular reactor setup. In addition, Potassium serves multiple roles: it enhances the catalyst's selectivity towards styrene by forming an active phase (potassium ferrite,$KFeO_2$) and reduces coke formation, allowing the process to operate effectively even at moderate steam-to-EB ratios. Potassium also aids in the gasification of carbonaceous deposits, thereby extending catalyst life under the high-temperature, endothermic conditions typical of industrial EB dehydrogenation [30].

The Langmuir-Hinshelwood-Hougen-Watson (LHHW) model offers a similar approach, focusing on the adsorption and surface reaction dynamics. It is especially effective for iron-based catalysts modified with potassium or chromium, which tend to exhibit high surface coverage and structure-insensitive behavior. Boudart discusses the relevance of the LHHW model for reactions involving catalysts with nonuniform surfaces, where high surface coverage causes uniform adsorption heat and reaction rates across sites. This model is particularly useful in simulating EB dehydrogenation on iron oxide catalysts, as it captures the adsorptive interactions between EB, hydrogen, and the catalyst surface [31]. Similarly, in the study by Tang et al. a two-dimensional quasi-homogeneous steady-state model was designed for a fixed-bed reactor setup. This model couples the reaction kinetics with reactor dynamics to simulate the temperature and concentration profiles under various operating conditions. The kinetic model is based on the Langmuir-Hinshelwood-Hougen-Watson (LHHW) mechanism, which assumes that the rate-determining step is the surface reaction of adsorbed ethylbenzene on the catalyst, specifically a phosphorus-doped boron nitride (PBN) catalyst supported on cordierite. The researchers found that high temperatures favor the main dehydrogenation reaction but also increase the formation of byproducts, particularly benzene and toluene, through secondary cracking reactions. Their two-dimensional kinetic model provides accurate predictions for optimizing reaction conditions to enhance styrene yield, showing high potential for scaling up this reaction in industrial settings [32].

For ODH or EB, the Mars-van Krevelen (MvK) mechanism is preferred. This redox-based model is applied primarily with reducible oxides like V_2O_5 and Cr_2O_3, which use lattice oxygen as the oxidant. Sharma et al. investigated EB dehydrogenation over a V_2O_5/TiO_2 catalyst, utilizing the MvK model to explain the catalytic cycle involving lattice oxygen. In this model, the catalyst's lattice oxygen participates in the reaction and is subsequently replenished

by molecular oxygen. This cycling of lattice oxygen allows the catalyst to maintain activity while minimizing coke formation, an advantage for high-temperature applications [33].

Lian et al. introduced the Eley-Rideal (ER) mechanism in studies of ODH, where it was found particularly suitable for systems involving nanocarbon catalysts. In the ER model, only one reactant (often hydrogen) adsorbs on the catalyst surface, and the other reactant (EB) remains in the gas phase, directly interacting with the adsorbed species. This model is especially relevant for catalytic systems where radical species play a role, or where one reactant absorbs weakly. Lian et al. demonstrated that the ER pathway was advantageous for nanocarbon catalysts in ODH, as it captures reaction dynamics where only partial adsorption of reactants occurs [34].

Lian et al.also employed microkinetic modeling (MKM) with density functional theory (DFT) for ODH studies, capturing complex interactions like adsorption, surface reactions, and desorption on nanocarbon catalysts. MKM, particularly when combined with DFT calculations, offers a highly detailed approach to understanding the elementary reaction steps in EB dehydrogenation. This approach enables researchers to quantify reaction orders and determine rate-limiting steps with high accuracy, providing a comprehensive understanding of catalyst behavior and interactions. While MKM provides the most detailed insights, it is computationally demanding and best suited for catalyst research and development rather than routine industrial applications [34]. In addition, Elnashaie et al. utilized microkinetic modeling to capture the complex reaction network of EB dehydrogenation within different reactor configurations, such as fluidized-bed and membrane reactors. These models require extensive data on surface kinetics but provide valuable information for optimizing catalyst formulations and understanding reaction mechanisms, therefore, microkinetic models are particularly advantageous for catalyst research and development [35].

2.1.2 Rationale behind choosing a specific model

The LHHW model was chosen for EB dehydrogenation to ST, due to its ability to account for the absorption and reaction processes on active catalytic sites. The model assumes that the reaction occurs via a surface mechanism, where adsorbed EB, ST, and hydrogen interact at active centers. It successfully describes reactions where the surface reaction is the rate-limiting step. This approach aligns well with *Fe*-based catalysts, as studies have shown the efficacy of Fe_2O_3 with *K* promoters in enhancing the reaction kinetics [36]. The LHHW model's assumption of competitive adsorption and surface reaction as the rate-limiting step aligns with the characteristics of Fe_2O_3-based catalysts, where potassium serves as a promoter.

In the context of Fe_2O_3-K_2CO_3 catalysts, this model was selected because it accurately fits the experimental data through its consideration of associative adsorption and reaction steps on a singular type of active site [36]. Additionally, *Fe*-based oxides, when promoted with K, offer active sites beneficial for stabilizing the potassium ferrite ($KFeO_2$) phase, which is crucial for effective EB dehydrogenation under high-temperature conditions. The LHHW model's

applicability here is supported by experimental and theoretical evidence showing that the Fe_2O_3 catalyst, particularly when optimized with *K* and potentially other promoters like Cr or Ce, yields improved catalytic performance for styrene production [37]. For instance, Fe_2O_3-K_2CO_3 catalysts promoted with *Cr* or *Ce* showed high stability and performance, achieving EB conversions up to 78.2% with selectivity to styrene under industrial reaction conditions (temperatures ranging between 540-650ºC and a steam-to-EB ratio of 2:1). The model's assumptions align well with the kinetic data from these systems, capturing both adsorption equilibria and reaction kinetics that are crucial for accurately simulating industrial-scale reactions [37].

It is widely accepted that the LHHW kinetic model with surface reaction rate-determining step can characterize the catalytic reaction kinetics very well. Thus, the Fe_2O_3-K catalyst system, employing the LHHW model, is appropriate for EB dehydrogenation, offering favorable conversion rates and selectivity for styrene production along with catalyst stability and model accuracy.

2.1.3 Parameters for kinetic modeling

The LHHW model was chosen for validation [38].

$$r_1 = \frac{k_1 K_{EB}[P_{EB} - (\frac{P_{ST}P_{H2}}{K_{eq}})]}{(1+K_{EB}P_{EB}+K_{H2}P_{H2}+K_{ST}P_{ST})^2} \quad (8)$$

$$r_2 = \frac{k_2 K_{EB} P_{EB}}{(1+K_{EB}P_{EB}+K_{H2}P_{H2}+K_{ST}P_{ST})^2} \quad (9)$$

$$r_3 = \frac{k_3 K_{EB} P_{EB} K_{H2} P_{H2}}{(1+K_{EB}P_{EB}+K_{H2}P_{H2}+K_{ST}P_{ST})^2} \quad (10)$$

$$r_4 = \frac{k_4 K_{ST} P_{ST} K_{H2} P_{H2}}{(1+K_{EB}P_{EB}+K_{H2}P_{H2}+K_{ST}P_{ST})^2} \quad (11)$$

Tables 6 and **7** were used to build kinetic models in the Aspen Plus. **Table 6** depicts necessary parameters, while **Table 7** shows how to implement it. The rate constants for reaction and adsorption steps are given by Arrhenius-type equations [38]:

$$k_i = A_i exp(-\frac{E_i}{RT}) \quad (12)$$

$$K_i = A_i exp(-\frac{\Delta H_{a,j}}{RT}) \quad (13)$$

Table 6. Parameters for the LHHW kinetic model [39]

Parameter	Symbol	Value
Pre-exponential factor of reaction rate constants k_i, [kmol/(kg-cat·s)]	A_1	1.276×10^{6}
	A_2	2.944×10^{11}
	A_3	3.461×10^{22}
	A_4	2.229×10^{7}
Pre-exponential factor of adsorption constants K_j, $[Pa^{-1}]$	A_{EB}	1.014×10^{-10}
	A_{ST}	2.678×10^{-10}
	A_{H2}	4.519×10^{-12}
activation energy [kJ/mol]	E_1	175.38
	E_2	296.29
	E_3	474.76
	E_4	213.78
adsorption enthalpy [kJ/mol]	$\Delta H_{a,EB}$	–102.22
	$\Delta H_{a,ST}$	–104.56
	$\Delta H_{a,H2}$	–117.95

Table 7. Implementation of Kinetic Model in Aspen Plus [39]

Reaction	Rate constant	Pre-exp [kmol/(kg-cat*s*Pa)]	E [kJ/mol]	Adsorption constant [bar^{-1}]
R1	$k_1^* = k_1 K_{EB}$	1.294×10^{-4}	73.16	$\ln K_{EB} = -23.012 + 12300/T$
R2	$k_2^* = k_2 K_{EB}$	29.852	194.07	$\ln K_{H2} = -26.123 + 14193.7/T$

R3	$k_3^* = k_3K_{EB}$	3.509×10^{12}	372.54	$\ln K_{ST} = -22.041+12582.4/T$
R3	$k_4^* = k_4K_{ST}$	5.969×10^{-3}	109.22	$\ln(\frac{1}{K_{eq}}) = -27.104+14931/T$

2.1.4. Validation of the Kinetic Model

In order to validate the LHHW kinetic model, the mathematical model was created using Python code and the parameters of the kinetic model were inputted into the Aspen, using the operating conditions from the chosen literature. The reactor was considered isothermal since the mathematical model was derived only for a constant 620C temperature. As can be seen in *Figure 3*, there was a perfect fit between the mathematical model, paper graph, experimental values and Aspen.

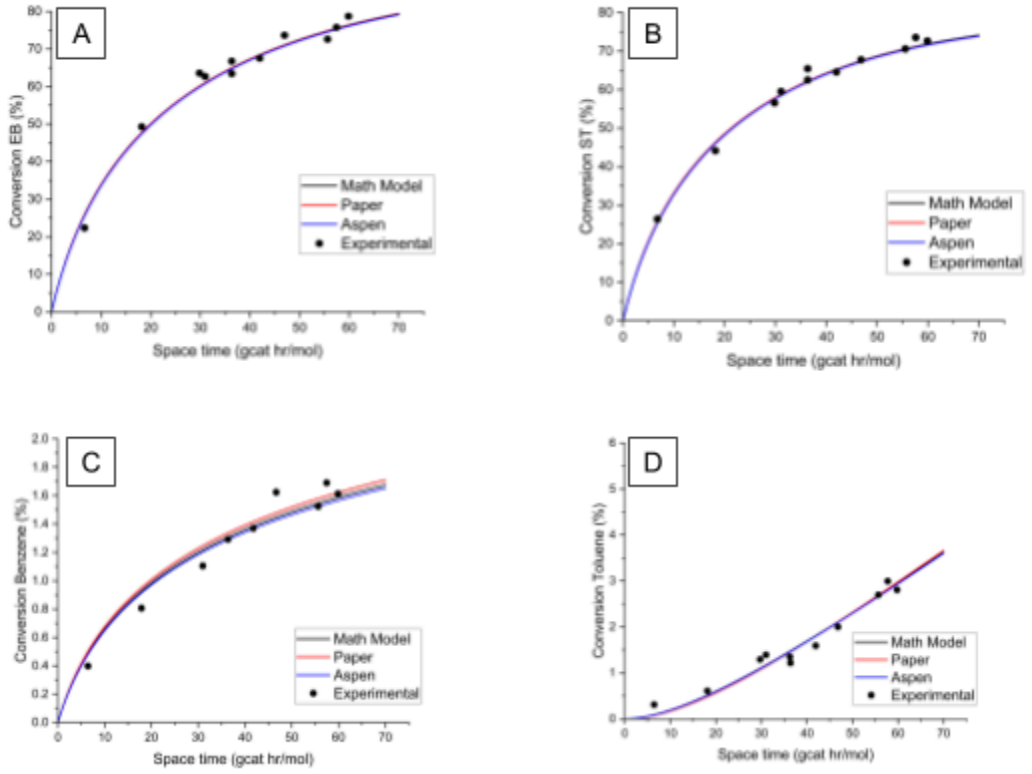

Figure 3. Conversion of the components over space-time. T = 620°C. H_2O/EB ratio = 11. P_T = 0.612 bar. A) Conversion of the ethylbenzene over space-time; B) Conversion of the styrene over space-time. C) Conversion of the benzene over space-time; D) Conversion of the toluene over space time [38]

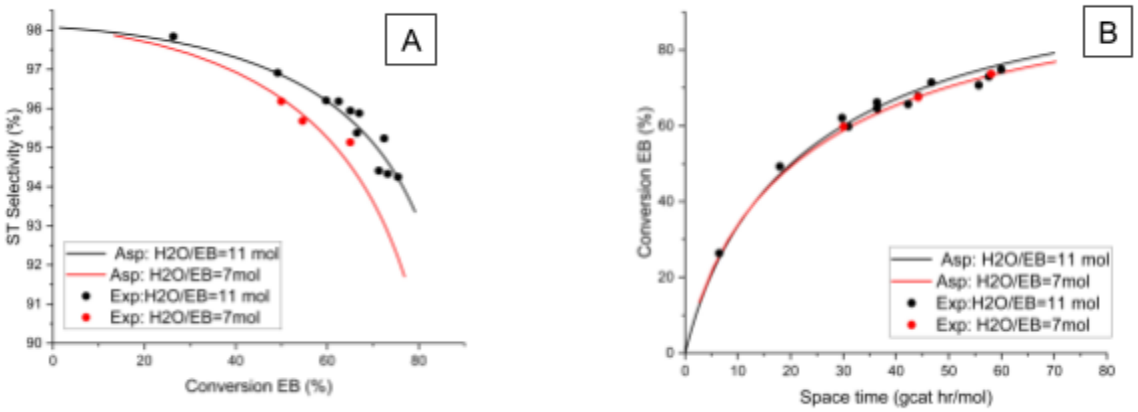

*Figure 4***.** Effect of H2O/EB ratio on the styrene selectivity and conversion of ethylbenzene. T = 620°C. H_2O/EB ratio = 11. P_T = 0.612 bar. A) Styrene selectivity over space-time; B) Conversion of the ethylbenzene over space-time [39]

The effect of steam to ethylbenzene ratio was investigated and compared with experimental data. As can be seen on *Figure 4***,** there was only a small difference between Aspen and experimental data. While the H_2O/EB ratio didn't affect the conversion of ethylbenzene that much, the higher ratio illustrated higher selectivity values for styrene. It was discussed in the literature that the optimum H_2O/EB ratio was between 11 to 13.

Consequently, after successfully validating the kinetic model, it was applied to our operating conditions of T = 620°C, 1 atm and H_2O/EB = 12. The optimum value of the catalyst weight was chosen from the graphs from Aspen analysis, as it was identified that it reached maximum styrene conversion at W/F_{EB} of 133.534 value. However, the conversion to styrene was approximately the same at around 100 and 133.534 values. By choosing 100 g cat hr/mol value, the conversion to styrene was near to maximum value, while opting for lower conversion to toluene. Considering that ethylbenzene in the feed was 372 kmol/hr, the minimum catalyst weight was chosen as 36,000 kg for the first reactor. The maximum conversion to styrene in the second reactor was observed at 216.72 space-time value, thus, a minimum of 46,000 kg for catalyst of loading was chosen for the 2nd reactor, considering the EB feed into the 2nd reactor was around 211.36 kmol/hr. For optimization of reactor design and maximizing ethylbenzene conversion, 50000 kg was chosen as catalyst loading for both reactors. The graphs used for the choosing of the optimal values are presented in the *Appendix F*. The stream results for both reactors are shown in **Table 8.**

Table 8. Stream results for R-101 and R-102

	7	**8**	**9**	**10**
Ethylbenzene	388.8	219.8	219.8	110.5

Steam/water	4665.5	4665.5	4665.5	4665.5
Styrene	7.4	168.6	168.6	251.1
Hydrogen	0	155.2	155.2	213.2
Toluene	0.03	5.9	5.9	30.4
Benzene	0	1.95	1.95	4.3
Ethylene	0	1.95	1.95	4.3
Methane	0	5.9	5.9	30.4
Total	**5061.7**	**5224.8**	**5224.8**	**5309.7**

2.2 Separation of water and lights

The gaseous product (stream 10) enters a cooling unit (E-105) at a total flow rate of 5310 kmol/h (126103 kg/h), where its temperature is cooled down to 252°C with the pressure remaining the same at 1 atm. Following the cooler, the product (stream 11) enters a condenser unit (E-106), where it is further cooled down to 40°C. In stream 12, the outlet stream of the condenser and the inlet stream of the decanter, the total flow rate remains unchanged. However, the product now is mostly a liquid after passing through E-106.

When the product enters a decanter unit (D-101), its pressure is increased to 1.2 atm with the pump employment, and the product is separated into three distinct outlet streams: lights or vapor phase (stream 13), aqueous or liquid 2 phase (stream 14), and organic or liquid 1 phase (stream 15). Temperature is maintained at 40°C for all the involved streams.

Stream 13 is all vapor and has a total flow rate of 268 kmol/h (1906 kg/h). Stream 14, on the other hand, is almost all water, accounting for 4647 kmol/h (83722 kg/h) of the total 4652 kmol/h. The remaining 5 kmol/h accounts for all the other components that are present in the system, which are dissolved in the water in some insignificant amounts. Majority of hydrogen, methane, and ethylene leave the system through streams 13 and 14, while the remaining amounts of the compounds enter the organic phase stream 15 at a total flow rate of 390 kmol/h (40227 kg/h). Hydrogen, methane, and ethylene amounts are neglected in stream 15 as they are very small compared to overall flow rate.

Table 9 presents the molar material balance for the cooler and decanter streams, which include streams from 12 to 15.

Table 9. Molar flow rate data and physical conditions of the streams associated with decanter

Stream #	**12**	**13**	**14**	**15**
Temp., °C	40	40	40	40
P, atm	1.2	1.2	1.2	1.2
Vapor fraction	0.13	1	0	0

Liquid 1	0.87	0	1	0
Liquid 2	0	0	0	1
Molar flow rates, kmol/h				
EB	110.5	1.8	0.6	108.1
Steam	4665.5	16.3	4647.3	1.9
ST	251.1	2.7	0.2	248
H2	213.2	212.9	0.3	0
Toluene	30.4	1.3	1.3	27.9
Benzene	4.3	0.4	0.01	3.9
Ethylene	4.3	3.5	0.8	0
Methane	30.4	29.0	1.4	0
Total	**5309.7**	**267.9**	**4651.9**	**383.9**

2.3 Purification of the final product

Organic phase produced from the decanter (D-101) enters the first distillation column (T-101) at a flow rate of 389 kmol/hour and composition of 63.5 mol% styrene, 28 mol% EB, 0.5 mol% water, 7 mol% toluene and 1 mol% benzene. Distillation column operates under vacuum with a reflux-drum pressure of 0.5 atm and separates the stream into two outlet streams, distillate (stream 17) and bottom product (stream 16). Stream 16 is a styrene product with 99.7% purity that further leaves the system with a flow rate of 240 kmol/h (**Table 10**).

Stream 17, consisting of EB, water, toluene, benzene and remaining small amounts of styrene at 148 kmol/h proceeds to the next distillation column, T-102, that operates at 1.2 atm. The top product (distillate) which is mostly benzene and toluene with some water, leaves the system (stream 18), while the bottom products from the column T-102, Stream 19 with a flow rate of 106.67 kmol/h is heated and recycled back to the feed part of the system (**Table 10**).

Tables 10. Molar flow rate data and physical conditions of the streams associated with distillation

Stream #	**16**	**17**	**18**	**19**	**20**
Temp., °C	120	70	40	150	500
P, atm	0.5	0.5	1.2	1.4	1.4
Vapor fraction	0	0	0	0	1
Liquid fraction	1	1	1	1	0
Molar flow rates, kmol/h					

EB	0.2	107.8	1.07	106.7	106.7
Steam	0	1.8	1.8	0	0
ST	240.6	7.4	0	7.4	7.4
H2	0	0	0	0	0
Toluene	0	27.9	27.8	0.03	0.03
Benzene	0	3.9	3.9	0	0
Ethylene	0	0	0	0	0
Methane	0	0	0	0	0
Total	**240.8**	**148.8**	**34.6**	**114.1**	**114.1**

CHAPTER III. Major Equipment Design

3.1 E-101 Heat Exchanger Design

Heat exchanger is an industrial equipment used to transfer energy between streams without their mixing. The main parts of each heat exchanger are hot and cold sides. Shell and tube heat exchangers are used widely as they are flexible, provide sufficient surface area and have comparatively low cost. Specifically, BEM as the most frequently used was designed for the assigned task. The E-101 is designed to heat fresh ethylbenzene to saturation temperature and plays a crucial role in the design process, since the main reaction is endothermic, supplying heat is important for overall performance of the plant. It is required to heat 282 kmol/hr from 25 °C to 136.15 °C for further evaporating and heating in the furnace.

Methodology of design:

1) Define known parameters as starting and final temperature, flow rate of process fluid (**Table 11**);
2) Define heat duty.
3) Choose a heat exchanger type;
4) Assume overall U form the physical nature of both fluids [40];
5) Assume length and diameter of tubes from required area;
6) Retrieve physical parameters of process and service fluids (viscosity, thermal conductivity, density, heat capacity);
7) Calculate the overall heat transfer coefficient and compare to the assumed value;
8) Calculate pressure drops;
9) If design does not satisfy requirements, repeat steps 5-8.

Table 11. Basic parameters for heat exchanger design

Parameter	**Unit**	**Shell side (ethylbenzene)**	**Tube side (low pressure steam)**

T inlet	°C	25	160
T outlet	°C	136.15	160
Flow rate	kmol/hr	282	180
Flow rate	kg/hr	29938.812	8061.543
P inlet	bar	1	6.05
P outlet	bar	0.967	5.875

The heat duty required was estimated by formula:

$$Q = \int_{T_1}^{T_2} C_p dT * m \quad \text{(Eq. 14)}$$

Where Q is heat duty, C_p is heat capacity, T is temperature, m is mass flow rate.

U was assumed to be 750, since the nature of fluids is Steam condensing - Organic solvents interaction is in the range of 500-1000, which is visible in Figure G1 in *Appendix G*. Low pressure steam condensation at temperature of 160 °C and corresponding saturation pressure 6.05 bar was used as water releases heat when condensation occurs and after condensation liquid water still would have energy for heating to some extent without temperature crossover. LMTD (log mean temperature difference) was estimated as:

$$\Delta T_{lm} = \frac{(T_1 - t_2) - (T_2 - t_1)}{ln\frac{(T_1 - t_2)}{(T_2 - t_1)}} \quad \text{(Eq. 15)}$$

Where $T_{h,in}$ is inlet of hot side, $T_{h,out}$ is outlet of hot side, $T_{c,in}$ is inlet of cold side, $T_{c,out}$ is an outlet of the cold side. Detailed calculations are provided at the spreadsheet of design of this equipment piece or *Appendix G Figure G3*, and the correction factor F_t = 1 calculated. Further, the area of tubes in contact with shell side fluid needs to be calculated. Assumptions for tubes are presented in **Table 12**.

Table 12. Assumed tubes used for heat exchanger design

Tube parameter	Inner diameter,	Outer diameter,	Thickness	Length, *L*

	D_I	D_O		
Value, m	0.0216	0.025	0.0017	3.66

$$Q = \int_{T_1}^{T_2} C_p dT * m = UAF_t \Delta T_{lm} \quad \text{(Eq. 16)}$$

$$A = \frac{Q}{F_t \Delta T_{lm} U} \quad \text{(Eq. 17)}$$

Area of a single tube, $A_t = d_o L_t \pi$ (Eq. 18)

Number of tubes, $N = \frac{A}{A_t} = 125.8048925$ (Eq. 19)

The internal shell diameter, $D_S = 0.012 + D_O * (N_{tot}/0.156)^{(1/2.291)}$ (Eq. 20)

D_S is 0.478 m. The values are taken from *Figure G4* (see *Appendix G*). From TEMA standards, minimal thickness for shell diameters between 330-580 mm is 3.2 mm stainless steel from Figure G6, thus D_{Sout} is 0.4844 m.

Tube condensation heat transfer coefficient:

$$\Gamma_h = W_c/(L * N_t) = 0.0009055877838 \quad \text{(Eq. 21)}$$

$$h_c = 0.76 * (\rho_l(\rho_l - \rho_g)g/(\mu_l * \Gamma_h))^{1/3} = 19539.76568 \quad \text{(Eq. 22)}$$

Where Γ_h is horizontal tube loading, W_c is total condensate flow, L is length of tubes, N_t is the total number of tubes in the bundle. ρ_l and ρ_g are liquid and gas densities respectively, g is gravitational constant, μ_l is liquid viscosity.

Shell heat transfer coefficient:

$$h_S = (k/d_e) * J_h * Re * Pr^{1/3} * (\mu/\mu_w)^{0.14} \quad \text{(Eq. 23)}$$

Where Re is Reynolds number, μ is viscosity, h_S is shell heat transfer coefficient, J_h is heat transfer factor taken form Figure 4A, μ_w is viscosity at the wall.

Overall:

$$\frac{1}{U_o} = \frac{1}{h_s} + \frac{1}{h_{od}} + \frac{d_o * LN(d_o/d_i)}{2k_w} + \frac{d_o}{d_i} \times \frac{1}{h_{id}} + \frac{d_o}{d_i} \times \frac{1}{h_i} = 1718.431619 \quad \text{(Eq. 24)}$$

Where U_O is overall coefficient, h_O outside fluid coefficient, h_I inside fluid coefficient, h_{Od} is outside fouling coefficient, h_{Id} is inside fouling coefficient, k_W is thermal conductivity of wall material. The calculated value is well above estimated U, and with some adjustments can be accepted. Final parameters for E-101 units are shown in the specification sheet **(Table 13).**

Additionally, the graphical representation of temperatures for both shell and tube sides is illustrated in *Figure 5*.

Table 13. Specification list of the heat exchanger

E-101 heat exchanger specification sheet		
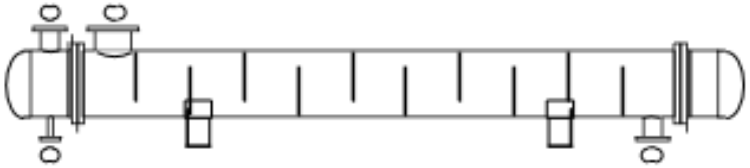		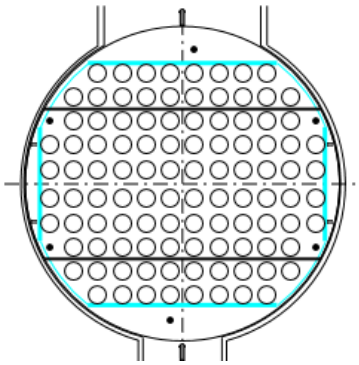
Parameter	Tube side	Shell side
Length, m	3.66	
Inner diameter, m	0.0216	0.478
Outer diameter, m	0.025	0.4844
Tube pitch/baffle spacing, m	0.03125	0.3824
Arrangement	90° square	Horizontal, 25% cut
Tube/shell passes	2	1
Number of tubes (tubes per pass)/baffles	126 (63)	10
Pressure drop, Pa(calculated)	3309	17307
Material	SS 304L stainless steel	
Estimated area, m^2	35.3382	

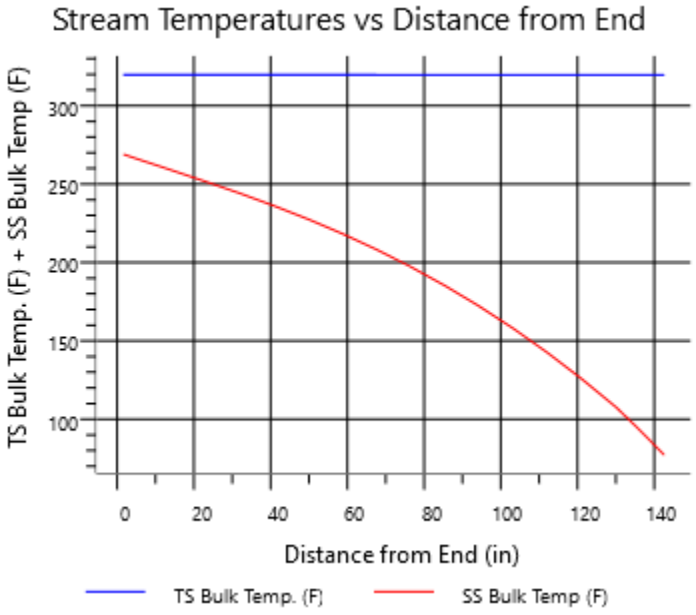

Figure 5. Graph of the temperatures for both sides

The absence of temperature change in tube side means that condensation occurs properly and heat transfer has moderate resistance, even if fouling large and heat transfer coefficient of steel is low. Detailed calculations of heat transfer coefficients and pressure drops are available in *Appendix G*.

3.2 R-101 and R-102 reactor design

3.2.1 Review of different reactor types

Dehydrogenation of ethylbenzene (EB) to styrene is endothermic, reversible, and typically carried out at high temperatures to drive the equilibrium toward styrene production. The choice of reactor significantly impacts the efficiency, conversion, and overall performance of the process.

Continuous Stirred-Tank Reactor (CSTR). A CSTR is a well-mixed vessel where reactants are continuously fed into the reactor, and products are continuously removed, maintaining constant volume. This reactor type is commonly used in liquid-phase reactions where uniform reactant concentration and temperature control are required. Due to its complete mixing characteristics, the conversion per unit volume in a single CSTR is often lower than other reactor types. However, when multiple CSTRs are arranged in series, the overall conversion can be improved. The CSTR is widely used in fermentation, polymerization, and pharmaceutical production due to its simplicity and ease of control [41].

The Plug Flow Reactor (PFR). The Plug Flow Reactor (PFR), also known as a tubular reactor, is characterized by a continuous flow of reactants through a cylindrical tube without back-mixing. This reactor type provides a higher conversion per unit volume than a CSTR

because reactants at the inlet remain at their highest concentration, ensuring a strong driving force for the reaction. PFRs are suitable for gas-phase and highly exothermic reactions, such as oxidation and nitration processes. However, temperature control can be challenging in PFRs, as heat removal must occur along the reactor length to prevent thermal runaway [40]

The Fluidized Bed Reactor. The Fluidized Bed Reactor involves a bed of solid catalyst particles suspended by an upward flow of gas or liquid, allowing for intense mixing and excellent heat transfer. This reactor type is widely used in catalytic cracking, polymerization, and biomass gasification. Fluidized bed reactors offer high mass transfer rates and uniform temperature distribution, making them suitable for highly exothermic reactions. However, their design is complex, requiring efficient gas-solid separation systems to prevent catalyst loss and attrition [42].

Fixed Bed Reactor. The Fixed Bed Reactor consists of a packed bed of solid catalyst through which reactants flow. This reactor type is commonly used in heterogeneous catalytic reactions, such as ammonia synthesis, hydrodesulfurization, and ethylbenzene dehydrogenation. Fixed bed reactors offer high catalyst utilization but can suffer from poor heat transfer and pressure drop issues. In exothermic reactions, hot spots may form within the catalyst bed, leading to thermal degradation, while in endothermic reactions, temperature drops along the reactor length can reduce conversion efficiency [42].

Reactor Selection for Ethylbenzene Dehydrogenation

The reactor that will be used for producing styrene from ethylbenzene dehydrogenation is an adiabatic fixed-bed tubular reactor. This reaction occurs at temperatures of approximately 620°C and low pressure of 1.8 atm. Because an adiabatic reactor does not exchange heat with its surroundings, the temperature drops along the reactor length, reducing reaction rates and conversion.

To counteract temperature drop, in industrial styrene production multiple reactors in series with interstage reheating are commonly used [18]. But in this specific case, the process utilizes six parallel reactor tubes with intermediate heat exchanger between reactors. This ensures that temperature remains sufficiently high in the second reactor to achieve the desired conversion.

Operating at low pressure or applying deep vacuum on the reactor effluent minimizes the partial pressure of ethylbenzene, thereby pushing the equilibrium toward styrene formation. Modern styrene plants use vacuum conditions and large steam dilution to maximize conversion per pass while maintaining selectivity [18].

3.2.2. Brief review for design methodologies

Several design methodologies exist for adiabatic fixed bed reactors, each method offering different levels of accuracy, complexity and computational effort. The main methods are:

Rules of Thumb

Design professionals may assume typical operating conditions, such as a catalyst bed height-to-diameter ratio within a standard range and a reaction temperature range of 550–650°C,

based on industry best practices and empirical knowledge. While rules of thumb are helpful for rapid estimations and feasibility studies, they are imprecise and may not take system-specific variations in kinetics, heat transfer, or pressure drop into account.

Heuristics-Based Design

Heuristic design is a more sophisticated method that uses engineering judgment and simplified models. Based on established reaction kinetics, heat balance factors, and catalyst performance, it employs semi-quantitative techniques. To determine ideal reactor dimensions, pressure decreases, and conversion rates, engineers may use empirical correlations. By combining basic concepts with useful approximations, this method enhances basic rules of thumb and is appropriate for reactor design in its first stages.

Rigorous Simulation

However, due to the intricacy of the dehydrogenation of ethylbenzene, the most reliable method for building an adiabatic fixed-bed reactor for the synthesis of styrene is rigorous modeling. Because of its high endothermic nature, this reaction necessitates careful thermal control to prevent sharp temperature decreases that could result in decreased conversion efficiency. Kinetic modeling is also essential since side reactions, like the production of benzene and toluene, rely on local temperature and residence time. Computational fluid dynamics (CFD) or process simulation tools such as Aspen Plus or COMSOL Multiphysics, as well as comprehensive reaction kinetics and catalyst deactivation models, are all used in rigorous simulation. By accurately forecasting temperature profiles, pressure drop distributions, and species concentrations, these simulations enable engineers to maximize reactor performance. Rules of thumb and heuristic design can help to avoid initial errors as well as make reasonable assumptions during the modelling stage. Rigorous simulation needs full data on the kinetic model and information on catalysts' properties.

The Non-Random Two-Liquid (NRTL) framework-based thermodynamic model was verified in Capstone Report I to precisely forecast phase equilibria and activity coefficients for the styrene manufacturing system. For subsequent separation procedures, this model made sure that non-ideal behavior in the vapor-liquid equilibrium was accurately represented. Building on this, Capstone Report II concentrated on creating a thorough kinetic model for ethylbenzene dehydrogenation that included reaction rate equations for the generation of styrene, benzene, and toluene. By incorporating these verified models into the design of an adiabatic fixed-bed reactor, temperature profiles, conversion rates, and selectivity may be rigorously simulated. The reactor design was improved for maximal styrene output while minimizing undesirable byproducts and thermal inefficiencies by combining the kinetic and thermodynamic models. The kinetic model was used to find catalyst loading of 50000 kg in both reactors which was used to determine the volume of the reactor required to achieve desired conversion.

The following adiabatic fixed reactor design assumptions were made:

1) A packed bed's void fraction, also known as porosity, normally falls between 0.35 and 0.45 for small particles that are randomly packed and between 0.4 and 0.6 for bigger

particles. Particularly for catalyst particles with variable forms utilized in industrial processes, a value of 0.5 is an acceptable approximation [43];

2) Reactor design frequently incorporates a safety margin of +25°C, particularly for temperature-sensitive reactions such as ethylbenzene dehydrogenation (which runs at about 600°C) [40];
3) . [1]By increasing the pressure margin by 10%, the design can account for pressure decreases brought on by fouling, catalyst deactivation, or changes in the feed's composition [40];
4) The gas velocity in fixed-bed reactors should be low enough to prevent fluidization and excessive pressure loss, yet high enough to reduce mass transfer resistance. Typical surface gas velocity estimates vary from 0.1 to 10 m/s, contingent on reactor scale and particle size [44].
5) L/D ≥ 2 enhances conversion, reduces back-mixing, and guarantees plug flow behavior [40];
6) In order to prevent hot spots and guarantee a consistent radial temperature distribution, industrial tubular fixed-bed reactors usually have diameters ≤ 2 m [40].

3.2.3 The working principle of reactor

The reactor operates as an adiabatic fixed-bed tubular reactor, where ethylbenzene (EB) is dehydrogenated to styrene in the presence of a solid catalyst. The catalyst is packed inside multiple tubes, ensuring efficient reaction kinetics and uniform operating conditions. Since the reaction is carried out under adiabatic conditions, no external heat is supplied during the reaction, leading to a temperature drop along the reactor length.

To ensure even distribution of reactants and steady-state operation, the reactor consists of six parallel tubes. The catalyst bed inside each tube provides active sites for the dehydrogenation reaction, enhancing reaction rates and selectivity while minimizing unwanted side reactions. This configuration allows for improved conversion efficiency and optimal utilization of the catalyst.

Since the reaction is endothermic, it requires heat to proceed, causing a temperature drop along the reactor length. If the temperature falls too much, the reaction rate decreases, leading to lower conversion. To counteract this, an interstage heat exchanger is placed between reactor stages to reheat the gases before entering the next reactor, maintaining optimal conditions for styrene production.

While the main reaction produces styrene, several side reactions occur within the reactor, forming undesired byproducts. These include thermal cracking of ethylbenzene, which leads to benzene and ethylene formation, and hydrogenation reactions, which produce toluene and methane. Additionally, steam reforming and water-gas shift reactions generate carbon monoxide, hydrogen, and carbon dioxide, further affecting process efficiency.

Effective heat and pressure management is crucial to maximizing styrene yield. Operating at low pressure (or vacuum conditions) helps reduce the partial pressure of ethylbenzene, shifting the equilibrium towards styrene formation. This reactor design ensures

continuous operation, efficient catalyst utilization, and high selectivity toward styrene, making it a reliable choice for industrial-scale production.

3.2.4 Material Selection for Reactor Tubes

The selection of construction materials was based on factors such as mechanical properties, temperature resistance, corrosion resistance, availability, and cost. To ensure corrosion resistance, the chromium content in the material must exceed 12%, with higher chromium content providing greater resistance to oxidation.

According to the ASME BPV 410 Code Sec. II Part D, stainless steels are among the most frequently used corrosion-resistant materials in the chemical industry. They also offer superior strength compared to plain carbon steels, particularly at elevated temperatures [40]. Based on these considerations, **SS304L** was selected as the construction material for the reactor tubes **(Table H2,** *Appendix H***)**. The wall thickness of the tubes was determined based on this material and the detailed calculations are provided in the *Appendix H*. The step by step algorithm and calculations are given in *Appendix H.* Specification sheet is shown in **Table 14.**

3.2.5. R-101 unit specification sheet

Table 14. Specification sheet of reactors

DATA SHEET FOR R101 AND R102		
Date: 10/03/2025		
Operating & Mechanical data for R-101 and R-102		
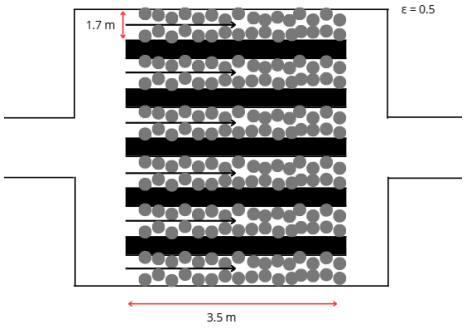		
	Operating	Design
Reactor type	Adiabatic Fixed Bed Reactor	
Pressure (atm)	1.8	2
Temperature (°C)	620	645
# tubes/ # parallel reactors	6	
Length (m)	3.5	
Inner diameter (m)	1.7	
Wall thickness (m)	0.001	

Working Volume of Reactor (m^3)	48	
Volume of Reactor (m^3)	49	
Working Volume of a Parallel Tube (m^3)	8	
Volume of a Parallel Tube (m^3)	8.2	
Bed Voidage	0.5	
Material specification	SS304l	
Construction code	ASME B31.3	
Allowable stress, S (atm)	218	
Corrosion allowance (in)	0.0625	
Quality factor, E	1	
Coefficient, Y	0.7	
Process Data for R-101 and R-102		
	R-101	R-102
Catalyst Loading (kg)	50000	50000
Superficial Velocity (m/s)	4.2	4.34
Actual Velocity (m/s)	8.41	8.68
Pressure Drop (atm)	0.72608	0.78572
Catalyst Data		
Catalyst type	Fe_2O_3 doped with K	
Catalyst Density (kg/m^3)	2500	
Particle Size Diameter (mm)	5.5	
Shape Factor	0.8736	

3.3 Cooler E-105 design

The heat exchanger (E-105) plays an important role in the styrene manufacturing process as it is responsible for cooling the hot reaction effluent (Stream 10) before further processing. The main function of the unit is to subcool the styrene-rich vapor stream via transferring heat to a cooling medium to ensure that the phase conditions are met for subsequent separation and purification stages. To optimize the heat exchanger area, 4 identical exchangers in a parallel arrangement are to be employed.

This section provides detailed information on design and analysis of the cooler unit, including thermal and mechanical design, and material selection.

3.3.1 Design selection and justification

E-105 is a shell-and-tube heat exchanger. This choice is based upon the fact that this type of heat exchanger is the most commonly used one in the industry due to its advantages: such configuration provides a large surface area in a small volume; possesses a good shape for

pressure operation; requires easy cleaning maintenance; and has well-established design procedures [40].

Among four types of shell-and-tube heat exchangers, namely, fixed tube sheet, U-tube, internal floating head, and external floating head designs, the best choice falls on the external floating head design as its design takes into account high temperature differentials and eases the cleaning of both tube and shell sides.

Table 15 below summarizes the advantages and disadvantages of each type.

Table 15. Comparison of types of shell-and-tube heat exchanger [40]

Type	**Advantages**	**Disadvantages**
Fixed tube sheet	● Cost-effective ● Simple maintenance with straight tubes	● Limited thermal expansion ● Tube bundle cannot be removed for cleaning
U-tube	● Requires only one tube sheet ● Cheaper than the floating-head types	● Limited in use to relatively clean fluids ● Tubes and bundle are difficult to clean
Internal floating head	● Suitable for high temperature differentials ● Easier to clean ● Can be used for fouling fluids	● Risk of leakage ● High cost ● Large clearance required between the tubes and the shell
External floating head	● Allows for large thermal expansion ● Easy tube bundle removal	● Risk of leakage ● Shell-side pressure limitation to 20 bars ● High cost

3.3.2 Design methodology

The general design methodology is described as the following [40]:

1) Define heat duty;
2) Collect the fluid physical properties like density, viscosity, and thermal conductivity;
3) Choose a type of exchanger to be used;
4) Assume the initial overall coefficient, U;
5) Calculate the log mean temperature difference, LMTD;
6) Calculate the trial area of the heat exchanger;

7) Choose the exchanger layout;
8) Calculate tube-side and shell-side coefficients;
9) Calculate the overall coefficient and compare to the assumed value; iterative process;
10) Calculate pressure drop; if not satisfactory, return to step 7, 4, or 3, in this order.
11) Optimize the design if needed by repeating steps 4 to 10.

3.3.3 Thermal design

E-105 cooler is divided into 4 identical exchangers in parallel to reduce the flow rate of the product in the stream and, subsequently, obtain an optimal velocity. Basic information on the streams associated with E-105 is provided below in **Table 16**.

Table 16. Streams data for Shell and Tube sides

	Tube side	**Shell side**
Fluid	Process fluid	Superheated steam
Flow rate, kg/s	8.75	21.1
Inlet temperature, ℃	590	110
Outlet temperature, ℃	252	270
Pressure, bar	1	1
Heat duty, MW	6.5	

The calculations start with evaluating LMTD, which will serve as the major driving force for heat transfer. Then, the values of R and P ratios are calculated by Eq.G.1 and G.2 *(Appendix G)* to estimate the correction factor for LMTD, and are equal to 2.1 and 0.33, respectively.
Using Eq. 2, LMTD is calculated as follows:

$$\Delta T_{lm} = 221.08$$

The LMTD correction factor is calculated using the formula designed for a heat exchanger with 1 shell pass and even number of tube passes:

$$F_t = (R^2 + 1)^{0.5} LN(\frac{1-P}{1-RP}) / (R - 1) LN(\frac{2-P[(R+1)-(R^2+1)^{0.5}]}{2-P[(R+1)+(R^2+1)^{0.5}]}) \quad \text{(Eq. 25)}$$

$$F_t = 0.76$$

$$F_t \Delta T_{lm} = 168.02$$

The correction factor value is considered generally acceptable, although low, and the corrected LMTD still yields a comprehensive value, so the 1 shell pass and 2 tube passes design is valid.

Based on *Figure G1 (Appendix G)* , considering the process fluid as heavy organics, and the service fluid as air and gas, trial value of U = 40 W/m-K.

Provisional heat exchanger area, A, can be calculated using Eq. 4:

$$A = 955.65\ m^2$$

3.3.4 Mechanical design

Table 17 below provides information on tube design necessary to estimate the values needed for the mechanical design of the shell and tube.

Table 17. Summary of tube sizing

Material	Stainless steel 304
Length of tube, L_t, m	3.64
Tube thickness, mm	1.7
Tube outer diameter, d_o, mm	37
Tube inner diameter, d_i, mm	33.6
Material thermal conductivity, k_t, W/m-K	21.4

Using Eq. 18 and 19, heat transfer area of a single tube is $A_t = 0.425\ m^2$, and number of tubes is $N_t = 2246.3 \simeq 2246$. Tube pitch, P_t, (the distance between tube centres) is estimated using Table 2A, and is equal to P_t = 46.25 mm. Eq. G.6 yield a bundle diameter of D_b = 2.29 m.

To identify shell inside diameter, D_s, the chart illustrated in *Figure 3A* can be used with known bundle diameter and heat exchanger type. For pull-through floating head type and a bundle diameter of 2.29 m, D_s is 2.4 m.

3.3.5. Tube side and shell side coefficients and pressure drop

Table 18 summarizes the properties of the fluids for both sides at different temperatures for different heat transfer ranges. All the properties are evaluated at the mean temperatures of their respective regions using Aspen Plus software.

Table 18. Tube and shell side fluid properties at different heat transfer regions

	Tube side	**Shell side**
Mean temperature, ℃	337.73	159.71

Viscosity, μ	2.45×10^{5}	1.60×10^{5}
Density, ρ_l, $\frac{kg}{m^3}$	0.44	0.47
Thermal conductivity, k, W/m-K	6.37×10^{-2}	3.32×10^{-3}
Heat capacity, C_p, J/kg-K	4452.8	1937.1
Mass flow rate, $\overline{m}$, kg/s	8.76	20.7
Equivalent diameter d_e, mm	3.36	26.3
Friction factor, j_f	0.005	0.029

Since both shell and tube sides contain vapor without any phase change, correlations designed for single-phase heat transfer are used.

For estimating heat transfer coefficient for the tube and shell side, the Nusselt correlation is used. It is noteworthy that the viscosity correction factor is ignored during the calculations, as it is assumed that it has a negligible effect on the coefficient. C is a constant value, and is 0.021 for gases. j is a heat transfer factor which can be found on the chart illustrated in *Figure 4A*.

$$h_{tube} = \frac{0.023 Re^{0.8} Pr^{0.4} C\, k}{d_i} \quad \text{(Eq. 26)}$$

Eq. 26 yields h_{tube} = 87.55 W/m^2-K, and Eq. 23 yields h_{shell} = 76.1 W/m^2-K.

According to the calculations, pressure drop values are 0.006 bar for the tube side, and 0.11 for the shell side.

3.3.6. Overall heat transfer coefficient

Table 19 breaks down the components of Eq.24 and provides details related to the heat transfer process occurring in E-105.

Table 19. Overall coefficient equation components

Outside fluid film coefficient, h_s, W/m^2-K	87.55
Inside fluid film coefficient, h_i, W/m^2-K	76.1

Outside dirt coefficient, h_{od}, W/m^2-K [40]	5000
Inside dirt coefficient, h_{id}, W/m^2-K [40]	7000
Thermal conductivity of the tube wall material, k_w, W/m-K	21.4
Tube inside diameter, d_i, m	0.037
Tube outside diameter, d_o, m	0.0336

Using Eq. 24, the overall transfer coefficient is calculated as U_o = 38.22 W/m^2-K, which is not far from the assumed 40 W/m^2-K, meaning that the design of the heat exchanger is satisfactory.

3.3.7. Material selection and overall sizing

The following table summarizes the important moments of the specification sheet and is retrieved from the sheet designed by the Aspen Plus software. Additionally, the sketch and the tube layout of the unit are also included in the table.

The chosen material for all the parts of the unit is type 304 stainless steel alloy. The material has been chosen based on the fabrication characteristics, mechanical properties, corrosion-resistivity and material cost [45]. Overall specifications of the unit are shown in **Table 20.**

Table 20. Specification sheet for E-105

Schematic representation of the unit	
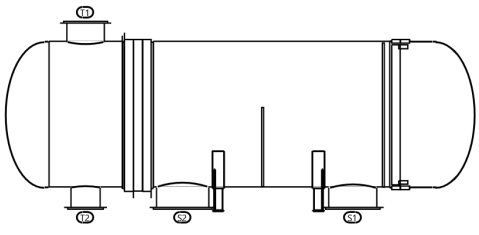	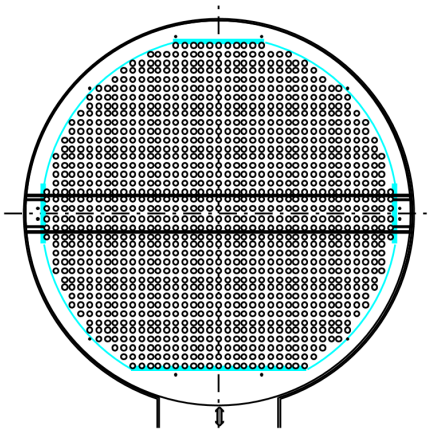

Parameter	Tube side	Shell side
Length, m	3.66	
Inner diameter, m	0.0336	2.08
Outer diameter, m	0.037	2.099
Pitch, m	0.04625	
Baffle spacing, m	1.7094	
Tube pattern	90° Square arrangement	
Number of baffles	1	
Number of tubes	1260	–
Tube passes	2	–
Shells in series	–	1
Shells in parallel	–	2
Pressure drop, bar	0.020	0.062
Material	Stainless steel 304	

Comparing the results obtained via Aspen Plus with the hand-calculated ones, there are some minor differences regarding the shell side properties, mainly, the shell-side velocity. Such discrepancy can be explained by the fact that the software employs built-in constraints based on common industrial practices. In the meantime, the manual calculations are derived from fundamental heat exchanger design equations. The difficulty with higher velocities are mainly associated with their effect on pressure drop and some concerns such as flow-induced vibration. Such issues can be solved if the selected materials and baffle configurations are properly designed to withstand the effect of higher velocities.

3.4 Distillation Column T-101 unit design

3.4.1 Brief description of the unit

Vacuum distillation is used for ST separation because of its high boiling temperature (146°C) and thermal instability [18]. By operating under vacuum the boiling point of ST is

reduced thus preventing the polymerization. The packed bed distillation column operates on the principle of separation based on the relative volatility of key components to the reference component (mainly the heavy-key component, styrene in this case). More volatile components, such as benzene, toluene, and ethylbenzene, rise with the vapor phase and are collected as distillate, while the less volatile styrene is discharged as the bottom product. In *Appendix J,* it is evident that a packed column is more suitable for this application.

In a packed column, vapors ascend from the reboiler, interacting with the descending liquid reflux from the condenser. The packing inside the column provides a large surface area for vapor-liquid contact, facilitating mass transfer between the phases. Unlike tray columns, which rely on distinct stage-wise separation, packed columns allow for a continuous contact process, improving efficiency and minimizing pressure drop—making them highly suitable for vacuum distillation applications [46]. A key operational factor in packed columns is the reflux ratio, which influences the separation efficiency by altering the equilibrium conditions within the column. An optimal reflux ratio and proper column design—including packing type, column diameter, feed location, and temperature control—ensure high-purity styrene separation. Since relative volatility varies throughout the column due to temperature gradients, it is typically estimated as the geometric mean of values at the condenser and reboiler conditions. The design of the packed bed column must account for this variation to achieve effective separation while maintaining a low-pressure drop, reducing energy consumption, and preventing unwanted polymerization of styrene.

Structured packing was chosen for the styrene/ethylbenzene separation process due to its performance under the specified operating conditions. The system operates near-vacuum conditions, making low-pressure drop a critical factor. Structured packing offers a significantly lower pressure drop (~0.02 psi/stage) than random packing, enhancing relative volatility and separation efficiency while minimizing energy consumption. Available in corrosion-resistant materials, it is also well-suited to handle potential impurities in the feed [47].

Aspen Plus simulations enabled us to identify possible azeotropes, providing insights into separation limitations and necessary design considerations. In addition, all material balance data from Report 2 were used as input for the distillation column design, ensuring that feed compositions, flow rates, and recovery targets aligned with process requirements. The previously specified purity and allowable impurity constraints defined the separation objectives, guiding key design parameters such as the number of stages, reflux ratio, and operating pressures. Furthermore, component volatility data, calculated using saturated pressure data, helped determine relative volatilities, influencing separation's feasibility.

3.4.2 Column operating design

Assumptions made during calculations:

1) EB is a light key (LK) compound, and ST is a heavy key (HK) compound;

2) Packed bed column distillation with structured packing;
3) Packing material: Mellapak Plus 252Y;
4) Reflux ratio / Min. reflux ratio = 1.5.

All extensive calculation methods and equations are shown in *Appendix J.* To start calculations, the relative volatility of all compounds relative to HK was required. To find P_{sat} for each compound in the condenser (0.5 atm, 70℃) and reboiler (0.51 atm, 120℃,) the Antoine equation (Eq. 1E) was used. After two relative volatility values were obtained for different parts of the column, the geometric mean of these two was used in the following calculations (**Table 21**).

Table 21. Relative volatility of components

$\alpha_{j/HK}$	**Condenser**	**Reboiler**	**Geometric average**
EB/Styrene	1.49	1.31	1.40
Toluene/Styrene	4.14	2.69	3.34
Benzene/Styrene	12.8	6.10	8.84
Water/Styrene	3.86	3.71	3.78

Firstly, heuristic calculations were made to find rough values for the number of stages, minimum and actual reflux ratio. The Fenske equation was used to find the minimum stages. Calculations showed that the minimum **number of theoretical stages is 35**.

Further, the Underwood equations were employed to estimate the minimum reflux ratio (RR_min). It was found that θ = 2.56781, and using Eq. 4E, **RR_min = 7.0**, and **RR_actual = 10.5.**

Using the reflux ratio values and Gilliland correlations (Eq. 5-7E), the **actual number of theoretical stages** was calculated to be **57.**

In packed bed columns, the HETP (height equivalent to theoretical plate) factor is a key factor in estimating the height of the column. According to the industry data for the packing material (Mellapak Plus 252Y), the HETP value with our system's pressure drop is about 0.5 [12G]. Using the following formula:

$$H = HETP * N = 50\,m \quad \text{(Eq. 27)}$$

As max bed height per section is 8-12 m, to prevent maldistribution the number of beds needs to be [9G]:

$$N_{bed} = \frac{H}{10} = 5 \quad \text{(Eq. 28)}$$

3.4.3 Column internals

Further, the inner diameter of the column was estimated using these data. Flooding conditions were used extensively to assess the flooding velocity, gas superficial velocity, pressure drop and diameter of the column. For that, the reflux ratio and individual parameters of packing material were used. As EB and ST are abundant in our system, calculations assumed a binary non-dilute system.

Flooding data for packed columns were first correlated using a liquid-to-gas kinetic-energy ratio (F_{LV}). Then, a generalized pressure-drop chart for structured packing developed by Strigle, Kister and Gill was used to find the modified empirical capacity factor (F_C). For modern structured packings with packing factors between 9 and 60 ft^{-1}Kister and Gill [13G] showed that the simple empirical correlation gives the specific pressure drop at flooding. Thus u_{Vf} = 10.6 ft/s = 3.2 m/s. To avoid flooding in the column, vapor superficial velocity should be between 50-80% of this flooding velocity. It was assumed to be 0.7. Internal diameter (D_T) equation for column based on a fraction (f) of flooding velocity, and the continuity equation became [48]:

$$D_T = \left(\frac{4VM_V}{f^* u_{Vf} \pi \rho_V}\right)^{0.5} \quad \text{(Eq. 29)}$$

Thus, estimated D_T = 4.2 m.

Packed distillation columns require essential accessory components to ensure efficient operation. The key accessory components of the packed distillation column and the proper types selected are summarized in *Appendix J*.

3.4.4 Simulation approach using Aspen Plus

The design process began by comparing the minimum reflux ratio (RR) through manual calculations with those obtained from the Aspen Plus DSTWU unit. The difference between the two methods was within an acceptable range 6.3 and 7 for DSTWU and hand calculations respectively, confirming the validity of our calculations. Based on this, we proceeded with the rigorous design phase (Screenshots of inputs and results are shown in *Appendix J*).

First, we defined the required styrene (ST) and ethylbenzene (EB) compositions in the DSTWU unit to determine the actual reflux ratio (RR) and number of stages (N) required for separation. These values served as initial inputs for detailed simulations in the RadFrac unit, where equilibrium-based calculations were conducted.

For the packed bed system, we utilized Aspen Plus' interactive sizing tool, incorporating the values obtained from DSTWU. A sensitivity analysis was performed on key parameters, including the reflux ratio (*Appendix J Figure J11*), feed stage location (*Appendix J Figure J10*),

and number of stages (*Appendix J Figure J12*), to identify the optimal conditions for achieving the desired separation efficiency. Next, we transitioned to a rate-based simulation approach, which required manual input of column diameter and height. Using the equilibrium-based design as a starting point, we iteratively adjusted the column diameter, reflux ratio, and number of stages until the desired separation was achieved, while maintaining acceptable hydraulic performance.

To evaluate the feasibility of such a system the pressure, temperature, flow rate and molar composition profiles were plotted against a number of stages. As shown in *Appendix J, Figure J9,* a linear pressure profile in the distillation column staying within operating pressure range is observed. A linear gradient suggests a uniform pressure drop, which typically indicates well-distributed vapor flow. *Appendix J, Figure J8* shows the temperature profile of the distillation column. It shows a sharp initial increase, followed by a rise until it stabilizes near the 37th stage. This trend is due to the removal of lighter components at the top, while heavier components dominate the lower stages, requiring more heat for vaporization. A slight temperature drop is observed at stage 37, the feed stage, due to the introduction of a cooler feed disrupting the thermal equilibrium. The similarity in vapor and liquid phase temperatures indicates equilibrium at each stage, confirming proper separation within the column. Plot on flow rate profile shows (*Appendix J, Figure J13*) that due to internal reflux and vaporization, the circulating vapor and liquid flow rates exceed **2200 kmol/h** in most stages, with a step change at the feed stage as additional mass and energy are introduced. The sharp drop in vapor flow at the top confirms total condensation (*Appendix J, Figure J7*), and the overall profile suggests the column is operating as expected. The EB liquid composition (*Appendix J, Figure J6*) peaks at the top and decreases downward, while the ST rises steadily and dominates at the bottom, showing expected volatility behavior. Light components (benzene, toluene) remain minimal in the liquid phase, indicating they leave as distillate. High reflux ensures EB's sharp decrease in liquid phase and lighter components move upward, while the reboiler drives separation by keeping styrene in the bottoms.

Following this, we specified the packing material geometry and additional design parameters to finalize the packed column configuration. The resulting design conditions were:

1) Number of stages (N): 100;
2) Reflux ratio (RR): 10;
3) Column diameter (d): 4.3 m;
4) Feed stage location: 37 above stage.

These values were subsequently utilized for cost estimation and material selection to ensure an optimized and economically viable design.

3.4.5. Construction material selection and overall sizing

Stainless steel 316L is well-suited for a styrene distillation column due to its excellent corrosion resistance, particularly against organic acids and high-temperature process conditions, which are common in styrene separation [40]. Its low carbon content minimizes carbide precipitation, reducing the risk of sensitization and ensuring long-term durability in the presence of heat and trace impurities. Additionally, 316L provides mechanical strength and oxidation resistance, making it ideal for vacuum and low-pressure distillation systems [49].

Mellapak Plus 252Y was selected as suitable packing for styrene production because it operates effectively under vacuum to moderate pressure conditions, which aligns with the typical operating range of styrene distillation. Its low-pressure drop per theoretical stage (0.3–1.0 mbar) helps minimize energy consumption, making it efficient for large-scale separation. Additionally, its ability to handle a wide range of liquid loads ensures flexibility in managing the varying flow rates encountered in styrene purification [50].

More detailed calculations on the material's mechanical properties and sizing are provided in *Appendix J*. A summary of the general design data for unit T-101 is presented in the specification sheet below (**Table 22**), while the complete specification sheet can be found in the Appendix J.

Table 22. Specification sheet for T-101 unit

DATA SHEET FOR DISTILLATION COLUMN T-101

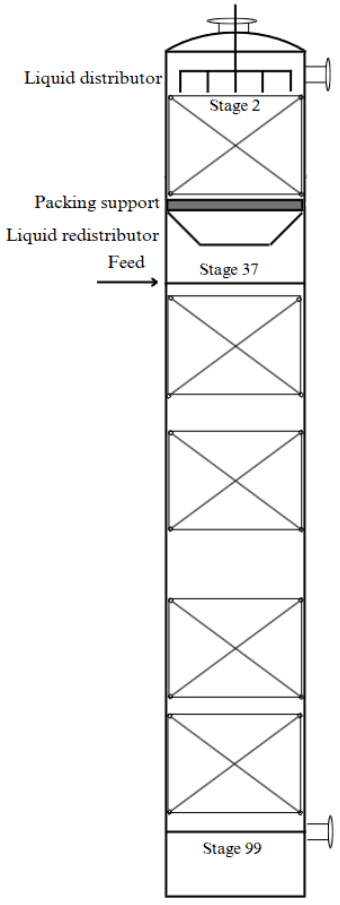

Operating & Mechanical data		
	Operating	**Design**
Column type	Packed bed	
Packing type	Structured	
Pressure (atm)	0.5/0.51	0.165
Temperature (℃)	70/120	150
# of stages	100	
Actual reflux ratio	10	
Reboiler	Kettle	
Reboiler heat duty, MW	21	
Condenser type	Total	
Condenser heat duty, MW	-20.9	
Column inside diameter (m)	4.3	
HETP (m)	0.5	
Height of column (m)	50	
Shell wall thickness (mm)	6	
Shell head thickness (mm)	5	
Packing material	MellapakPlus 252Y	
Material of Construction		
Shell	SA 240 (316L)	
Head	SA 240 (316L)	
Packing material	SA 240 (304SS) [12G]	

3.5 Distillation Column T-102 design

3.5.1 Brief Description

Tray distillation column is employed for ethylbenzene (EB) and toluene separation due to the close boiling points of these components and the necessity to achieve high-purity separation efficiently. The sieve tray type distillation column is selected for this separation process as it offers effective vapor-liquid contact, high mass transfer efficiency, and better handling of varying liquid loads. The separation mechanism relies on the relative volatility of EB and toluene, where toluene, being more volatile, is recovered as the distillate, while EB is collected as the bottom product [40].

During the separation process, vapor generated from the reboiler passes through perforated trays, where it interacts with the descending liquid phase. This staged contact ensures efficient phase equilibrium, enhancing the separation of EB and toluene. The tray design,

including hole diameter, weir height, and tray spacing, plays a crucial role in optimizing performance [40]. Unlike packed columns, which rely on continuous contact, sieve trays allow for precise stage-wise separation, making them suitable for mixtures with close-boiling components [40]. A critical factor influencing performance is the reflux ratio, which regulates separation efficiency by altering equilibrium conditions at each stage. The optimal reflux ratio, coupled with proper column design, including tray type, column diameter, feed stage location, and temperature control, ensures high-purity ethylbenzene recovery for the recycle. The predetermined purity constraints and impurity limits dictated key design parameters, such as the number of trays, reflux ratio, and pressure profile across the column. Furthermore, component volatility data, derived from saturation pressure correlations, were essential in determining relative volatilities and optimizing the separation efficiency of the ethylbenzene-toluene system. All the detailed calculations are given in the Excel file.

3.5.2 Column operating design

The distillation column T-102 was designed to separate ethylbenzene from other components, namely toluene, benzene for further recycling . After the majority of styrene is extracted in the first distillation (T-101), the top product (stream 17) is fed to the distillation column (T-102) at 1.4 atm and 70C with a flow rate of 148.98 kmol/h and a composition of 72.4 mol% EB, 1.25 mol% water, 5 mol% of styrene, 18.7 mol% toluene, 2.61 mol% benzene, and negligible amount of hydrogen.

The separation process primarily relies on the volatility of entered components and their relativity (shown in **Table 23**) to the reference component, which is mainly the component in a distillation process that has the highest boiling point among the desired products also known as heavy-key (HK). The more the difference between volatilities, the easier the separation will proceed. For this distillation column, ethylbenzene (EB) is selected as the heavy key (HK), while toluene is chosen as the light key (LK). The structural similarity between HK and LK allows to assume near-ideal solution behavior and use Raoult's law with Antoine's equation (*Appendix J, Equation J1*).

Table 23. The saturation pressure and relative volatility of feed components

Component	Condenser		Reboiler		Geom. Average
	P_{sat}, atm	Relative Vol.	P_{sat}, atm	Relative Vol.	Relative Vol.
EB	0.11	1	1.43	1	1
Steam/water	0.31	2.75	4.66	3.25	2.99
ST	0.08	0.72	1.13	0.79	0.76
Toluene	0.27	2.41	2.72	1.90	2.14

Benzene	0.72	6.50	5.84	4.07	5.15

Even though the volatility of the styrene is little less than the one of ethylbenzene its amount in the feed is almost negligible and in the same way the amount of benzene and water is also very small to consider them as LK components. As the relative volatility between the heavy and light keys is sufficient, the process operates efficiently, enabling the distillation column to achieve the targeted separation, with 99% of EB directed to the bottom and 99.9% of Toluene recovered in the top product.

Shortcut method for the multicomponent system (Fenske–Underwood–Gilliland–Kirkbride (FUGK) method) was used to find the number of minimum and actual theoretical number of stages, reflux ratios and feed entering stage. Later these values were optimised with ASPEN PLUS simulation to get the desired composition of both top and bottom product.

The Fenske equation was used to calculate the minimum number of stages required to separate the components at total reflux (*Appendix J, Eq. J2*). Based on the calculation the minimum number of stages required is 13.85, which is rounded up to 14 stages.

Underwood correlation is used to determine the minimum reflux ratio (*Appendix J, Eq. J3 and J4*). Since the entire feed and product streams exist in the liquid phase, the feed quality factor (q) is 1, resulting in a minimum reflux ratio (RR_{min}) of 3.75. The ratio of 1.5 was chosen as the ratio of RR_{actual} / RR_{min}, resulting in RR_{actual} 5.63. Gilliland's correlation (*Appendix J, Eq.J5-J7*) was used for preliminary column design determining the theoretical number of stages for the obtained reflux ratio. Based on the calculations, the theoretical number of stages required for the separation is determined to be 24. As selecting an appropriate feed point location is essential for achieving the highest possible separation for the calculated number of stages, the Kirkbride method for the ratio of number of stages above and below the feed point was used and the feed stage calculated to be 5 (*Appendix K, Eq. K1).*

3.5.3 Column internals

The tray distillation column was chosen due to its high efficiency in handling large feed flow rates, better vapor-liquid contact, and ease of operation for hydrocarbon separations [40].

Among all the types of trays, sieve trays were chosen due to their high efficiency, cost-effectiveness, and suitability for handling the vapor-liquid equilibrium of the toluene-ethylbenzene system. Their simple design allows for easy fabrication, installation, and maintenance, making them a preferred choice for many large-scale industrial distillations [40]. Standard tray spacing of 0.6096 m. Diameter of the column is 2 m.

3.5.4 Simulation approach using Aspen Plus

The preliminary design specifications were tested on **Aspen Plus** to evaluate their performance and optimize key parameters such as the reflux ratio, feed stage location, and number of theoretical stages for improved separation and to obtain desired composition of the products.

The DSTWU and RadFrac distillation column modules were used to analyze and optimize the column specifications. DSTWU was used for preliminary feasibility analysis, providing estimates for the number of stages and reflux ratio. RadFrac, a rigorous equilibrium-based model, was then employed for detailed optimization of the tray stage number, reflux ratio, feed stage for the target separation of the components.(Screenshots of inputs and results are shown in *Appendix K).* Reflux ratio was taken from the hand calculation ($5.63 \simeq 6$) as the value from the DSTW (1.63) was too small for the desired separation on the RadFrac column. Similarly, the number of stages were increased from 24 to 35 after conducting sensitivity analysis.

The duplicate block of the feed stream was used to ensure the same feed composition. The required compositions of ethylbenzene (EB) and toluene were specified in the DSTWU block to determine both the minimum and actual reflux ratios as well as the number of stages needed for separation. These values were then used as initial inputs for the RadFrac unit, where equilibrium-based calculations were first conducted, followed by a rate-based simulation for a more detailed and accurate analysis. Sensitivity analysis was conducted on key parameters, including the reflux ratio, feed stage location, and number of stages to determine the optimal conditions for achieving the top and bottom product(*Appendix K*).

To evaluate the feasibility of a separation system the pressure, temperature, flow rate and molar composition profiles were plotted against a number of stages. As shown in *Appendix K, Figure K7,* a linear pressure profile in the distillation column staying within operating pressure from 1.2 to 1.4 atm range is observed. A linear gradient suggests a uniform pressure drop which is 0.2 atm, indicating well-distributed vapor flow. *Appendix K, Figure K4* shows the temperature profile of the distillation column. It shows a sharp initial increase at the second stage, followed by an exponential rise until it reaches the last stage 35. This trend is due to the removal of lighter components at the top, while heavier components dominate the lower stages, requiring more heat for vaporization. The similarity in vapor and liquid phase temperatures indicates equilibrium at each stage, confirming proper separation within the column. The Flow rate graph (*Figure K8*) shows the molar flow rates of vapor and liquid across a distillation column, with a sharp increase at stage 14 indicating the feed entry, which adds mass and energy. Above this stage, the vapor and liquid flow rates remain stable, demonstrating effective rectification and reflux. Below stage 14, the liquid flow gradually decreases, while the vapor flow stays steady, suggesting consistent reboiler performance. The sharp liquid flow drop at stage 35 indicates the withdrawal of the heavier component as the bottom product. Overall, the trends confirm proper

column operation with expected phase behavior. This composition profile graphs show the separation of ethylbenzene (EB) and toluene in a distillation column (*Figure K5-K6*). The mole fractions of EB and toluene in both liquid and vapor phases have similar patterns. At the top of the column, the mole fraction of toluene is high, indicating that it is concentrated in the distillate, while EB dominates at the bottom, showing effective separation. The crossing points of the curves around the feed stage suggest where the mass transfer between the phases is most significant. All other components have lower mole fractions throughout the column, suggesting they are present in smaller amounts. Water remains at a consistently low concentration. The trends suggest effective separation, with a clear distinction between heavy and light components along the column.

Final specification were as follows:

1) Number of stages (N): 35;
2) Reflux ratio (RR): 6;
3) Column diameter (d): 2 m;
4) Feed stage location: 14 on-stage.

Transition to rate based simulation approach for sieve tray column system provided the standard design specifications like tray spacing, weir height, hole diameter etc. **Table 24** contains data with all specification data for the column.

3.5.5 Material selection

Stainless steel 316L is an ideal material for the toluene-ethylbenzene tray distillation column due to its superior corrosion resistance, mechanical strength, and suitability for operating conditions [40]. Its molybdenum content (~2-3%) enhances resistance to corrosion, particularly in chloride-containing environments, which is crucial for preventing material degradation in the presence of potential impurities [51]. Additionally, the low carbon content of 316L minimizes carbide precipitation during welding, thereby reducing the risk of intergranular corrosion and ensuring long-term durability [52].

Table 24. Specification sheet for distillation column T-102

DATA SHEET FOR DISTILLATION COLUMN	
Service: Distillation column	Project name: Industrial production of Styrene

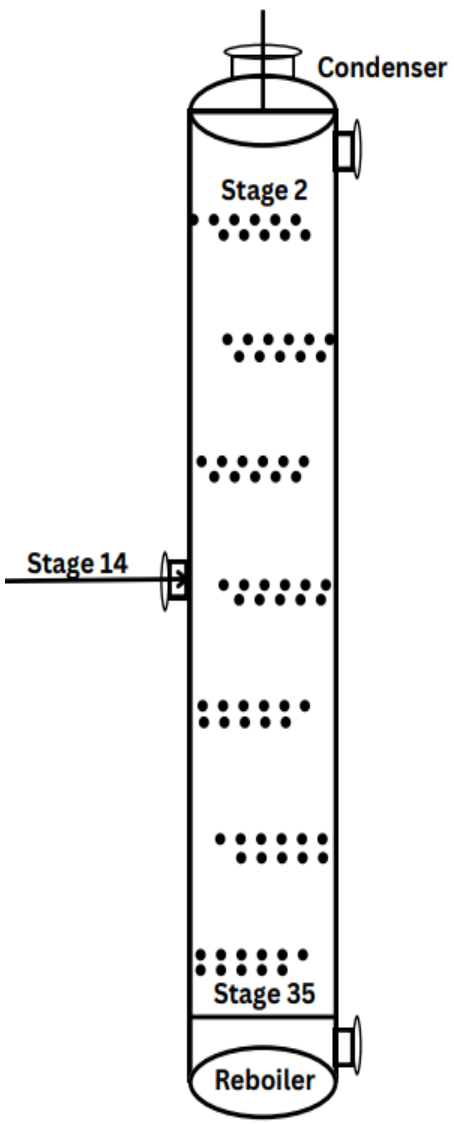

Item No.: T-102	Quantity: 1
Operating & Mechanical data	
	Operating
Column type	Tray
Tray type	Sieve
Pressure (atm)	1.2/1.4
Temperature (℃)	40/150
# of stages	35
Actual reflux ratio	6.0
Reboiler	Kettle
Reboiler heat duty, MW	3.4
Condenser type	Total
Condenser heat duty, MW	-3.1
Number of passes	1
Height of column (m)	20.12
Tray spacing (m)	0.6096
Tray diameter (m)	2
Cross-sectional area (m2)	3.14 m2
Net area (m2)	3
Hole area / Active area (m2)	0.1
Hole diameter (m)	0.0127
Weir height (m)	0.0508
Weir length (m)	1.22
Section pressure drop (atm)	0.2
Section head loss (Hot liquid height)	2.7
Section residence time	53 sec
Deck gauge thickness	10 GAUGE
Downcomer clearance	0.0381
Downcomer width top	206.45
Downcomer width bottom	206.45
Corrosion allowance (mm)	2
Material of Construction	
Wall	SA 240 316L
Head	SA 240 316L
Trays	SA 240 316L

Table 25 summarizes the simulated data for minor units in the process. The table provides the net heat duties of the minor components.

Table 25. Summary of operating conditions for minor units

Minor Unit	Outlet Temperature, ℃	Outlet Pressure, atm	Heat duty, MW
P-101 Pump	25.0	1.8	1.3×10^{-3}
E-102 Heater	500	1.8	9.5
M-101 Mixer	500	1.8	0
M-102 Mixer	625	1.8	0
E-103 Furnace	700	1.8	24.5
E-104 Furnace	620	1.8	5.4
E-106 Cooler	40	1.2	-69.7
D-101 Decanter	40	1.2	-4.8
P-102 Pump	70	1.4	9.2×10^{-4}
E-107 Heater	500	1.4	3.7

4.1 Storage tanks design

Storage tank design consists of 2 main sectors - Shell Design and Roof design. Shell Design involves calculating wall thickness, stiffener rings, stability checks for wind and seismic loads, and anchor bolt sizing. Roof Design includes stress analysis and the design of roof accessories and fittings. Both sectors ensure the tank's structural integrity, safety, and functionality [53].

Liquids are usually stored in bulk in vertical cylindrical steel tanks [40]. For storage of ethylbenzene and other volatile components, it is best to choose floating-roof tanks because it minimizes vapor loss.

In this process, fluids are stored either for use in production or for collection and eventual sale. To meet these needs, five storage tanks were designed, with some dedicated to raw materials and others to the final products (**Table 26**). The raw material storage tanks are

maintained under specific conditions for each component to ensure their purity and phase remain. The volume of the storage tanks is calculated by using the following equation:

$$V = Q * t \quad \text{(Eq. 30)}$$

For the reactants and products storage following specifications were considered:

ST-101 tank stores ethylbenzene (EB). It is constructed from stainless steel 321 (SS321), it operates at 25C and 1 bar to safely handle EB`s corrosive and flammable properties. With a 16,510 m³ capacity, it holds a two-week supply, split across three 5,000 m³ tanks for redundancy. Safety features include vapor recovery, inert gas blanketing, and leak detection. This setup ensures stable EB supply for downstream processes while mitigating operational risks [54]. The ST-102 Water Storage System provides a 2 week water supply for steam generation using one 16,000 m3 SS316L tanks. The corrosion-resistant design operates at 25°C and 1 bar with 10% extra capacity and includes safety monitoring [55].

Stream 14 from the decanter produces 4647 kmol/h of wastewater that will go back to the process after treating it from all organic compounds. The storage tank acts as a temporary reservoir that accommodates fluctuations in wastewater generation and treatment processes. The storage time considers the time needed for a 3 step treatment of wastewater, including 5-30 minutes for air stripping [56], 20-60 minutes for activated carbon adsorption [57], and continuous operation for reverse osmosis. Thus, 2 storage tanks for a 12 hour period at 25℃ is optimal, allowing accumulation and preventing the risk of microbial growth and VOC reabsorption before the treatment process begins. A closed, vertical cylindrical storage tank with a cone roof, made from corrosion-resistant material (SS316L), will be suitable for wastewater containing VOC-rich organics.

For the bottom product of the first distillation column, primarily composed of styrene with a purity of 97%, storage should be designed with an emphasis on preserving product quality while preventing polymerization. Since styrene is the main product, its storage must consider all critical factors, including material compatibility, temperature control, inhibitor addition, and safety measures. The storage will be designed for a one-month duration, requiring a total volume of 23.16 m³. Atmospheric storage tanks made of stainless steel (316) will be used, to ensure safety and quality, as these materials prevent corrosion and polymerization [40]. The storage system will incorporate nitrogen blanketing to prevent oxygen entering, reducing the polymerization. Additionally, tert-butylcatechol (TBC) will be added at a concentration of 50 ppm as a polymerization inhibitor [58]. As its weight is negligible compared to the weight of the styrene product, the mass and volume of the inhibitor was not included in the density and volume calculations. Temperature control is also critical, thus storage conditions should be maintained below 40°C to prevent thermal degradation.

For the top product of the second distillation product, primarily composed of toluene, storage must be designed to ensure stability and safety. The storage is chosen to be vertical or horizontal atmospheric storage tanks made of stainless steel 316 that ensures resistance to corrosion due to having some amount of water.

Additional storage tank units were incorporated to ensure operational continuity during cleaning or maintenance activities.

Table 26. Summary of the storage tanks used in the system

Storage tank (ST)	ST-101	ST-102	ST-103	ST-105	ST-106
Stored material	EB	Water	Wastewater	Styrene	Toluene
State	Liquid	Liquid	Liquid	Liquid	Liquid
Temperature, ℃	25	25	25 [59]	25 [59]	25 [59]
Pressure, atm	1	1	1	1	1
Flow rate, m3 /year	276,240	672,388	677,179	245,440	28105
Storage time	2 weeks	1 week	12 hours	1 month	1 month
Volume, m3	16,510	15,409	1005	21850	2133.2
Volume of 1 tank with 10% Safety Margin, m^3	5,000	16,000	1000	5,000	2500
Number of tanks	4	1	2	6	2
Material of tank	SS321	SS316L	SS316L	SS316L	SS316L

4.2 Heaters and condenser design

E-102 Furnace is required in the design to further heat ethylbenzene feed after it leaves **E-101** heat exchanger. The temperature of the stream has to match the temperature of the recycled ethylbenzene flow temperature, which is 500 °C. **E-102** is heated by combusting either purchased natural gas or waste gases from the process.

The **E-103** furnace is designed to produce from medium pressure steam of 200 °C supercritical steam at a temperature of 700 °C. The purpose of this equipment piece is to mix very high temperature steam with ethylbenzene feed to further heat reactor feed to 620 °C. The furnace utilizes combustion of purchased natural gas or waste gases from the process to achieve the high temperatures. Key design features include special heat exchanger materials to endure extreme temperatures, efficient combustion systems to minimize energy loss, and precise temperature control to ensure consistent steam output at 700°C.

The **E-104** furnace is designed to reheat the process stream between two adiabatic fixed bed reactors in series, ensuring the stream reaches the optimal reaction temperature of 620°C before entering the second reactor. As the stream exits the first reactor, its temperature drops due to the endothermic or nature of the reaction, making reheating necessary to maintain reaction efficiency and conversion rates in the second reactor. The heating is achieved by combusting either purchased natural gas or waste gases from the process.

The **E-106** cooler is designed to condense and cool the outlet stream from the **E-105** heat exchanger down to 40°C, ensuring the product stream from **R-102** is prepared for **D-101** decanter. The cooling process is critical to stabilize the product and meet the required specifications for the next stage of the process.

The E-107 heater is designed to heat a recycle stream to 500°C, ensuring it meets the required temperature for reintroduction into the process. This heating step is critical to maintain process efficiency and optimal reaction conditions, particularly when the recycled stream is fed back into a reactor or another high-temperature unit. Heat is supplied by combusting natural gas or waste gases from the process.

4.3 Decanter design

Decanter is used to separate water from the organic styrene-rich phase. The presence of water results from reaction byproducts and steam usage. To enhance separation efficiency, the decanter operates at 40℃, as indicated by a heat duty of -4.8 MW, which signifies heat removal for cooling. This cooling process helps prevent excessive styrene solubility in water and minimizes the risk of polymerization. The decanter produces a water phase, which is removed or recycled, and an organic phase, which undergoes further purification to obtain high-purity styrene. On **Table 5G** molar flow rates of stream 12 containing mostly water, stream 11 lights, and stream 13 containing mostly organic phase.

4.4 Pumps design

The pipe design for the system connecting **P-101** and **P-102** pumps must account for the operational parameters of each pump to ensure efficient and safe fluid transport. The **P-101** Pump delivers fluid at 25.09°C and 1.8 atm with a network of 1.325 kW to increase pressure before feeding into a reactor, requiring pipe materials that can handle moderate pressure and temperature, with considerations for thermal expansion. The **P-102** Pump outputs a higher temperature of 70.11°C and a slightly lower pressure of 1.4 atm, with a network of 0.92 kW, necessitating pipes that can withstand increased temperatures and minimize heat loss.

CHAPTER V. Plant Location and Layout

5.1 Plant site location

The choice of a plant site location depends on several factors such as (1) proximity to raw materials, (2) petrochemical infrastructure, (3) logistics and transportation, (4) market access, (5)

skilled labor availability, (6) economic and regulatory support, (7) environmental considerations, and finally, (8) natural hazards in the area.

In Kazakhstan, the best city for building a styrene production plant seems to be Atyrau, as it satisfies all of the above factors. All the factors are discussed in **Table 27**.

Table 27. Location justification summary

Factor	Justification
Proximity to raw materials	A new butadiene plant (340,000 t/year) by Butadien LLP will produce butadiene and derivatives like styrene-butadiene-styrene, ensuring demand and supply chain integration [60]. Atyrau is located near major oil and gas fields such as Tengiz, Kashagan, and Karachaganak (supply of feedstocks like ethane and benzene) [61].
Petrochemical infrastructure	The "National Industrial Petrochemical Technopark" (NIPT) fosters interconnected petrochemical industries, encouraging business collaboration and supply chain efficiencies [61].
Logistics and transportation	**Roads**: 3,051.6 km road network. **Railways**: 664.9 km of railway lines with 24 train services at Atyrau station (the railroad density is illustrated in *Figure 6*). **Air Transport**: International connections to Almaty, Nur-Sultan, Amsterdam, Istanbul. **Water Transport**: River port with Caspian Sea access [61].
Market access	Atyrau is located at the crossroads of Europe and Asia, thus, offers access to major markets like Russia and China [61].
Skilled labor availability	Atyrau has a skilled petrochemical workforce. The 2022 average monthly wage was 523,210 tenge, reflecting a 28.8% increase, indicating a competitive labor market [62].
Economic and regulatory support	Special Economic Zone (SEZ) NIPT provides tax benefits and reduced bureaucracy for investors [63].
Environmental considerations	While Atyrau's semi-arid climate may limit the availability of water resources for cooling, the city already hosts multiple industrial facilities, meaning that environmental monitoring systems and pollution control measures are in place.

Natural hazards	On a scale of 1 to 10, hazards and exposure index is 3.9 (low); vulnerability index is 3.7 (medium); lack of coping capacity index is 3.7 (very low) [64]. Seismic activity and landslide hazard risk is very low in Atyrau compared to other cities; for other types of hazards, the majority of the cities is more or less at the same risk [64].

For natural hazards, hazards and exposure risk describe events that might occur (riverflood, earthquake, wildfire, extreme heat, urban flood, landslide, water scarcity, and cyclone) and the exposure to them; vulnerability index – the susceptibility of communities to those hazards; lack of coping capacity index – lack of available resources that can alleviate the impact.

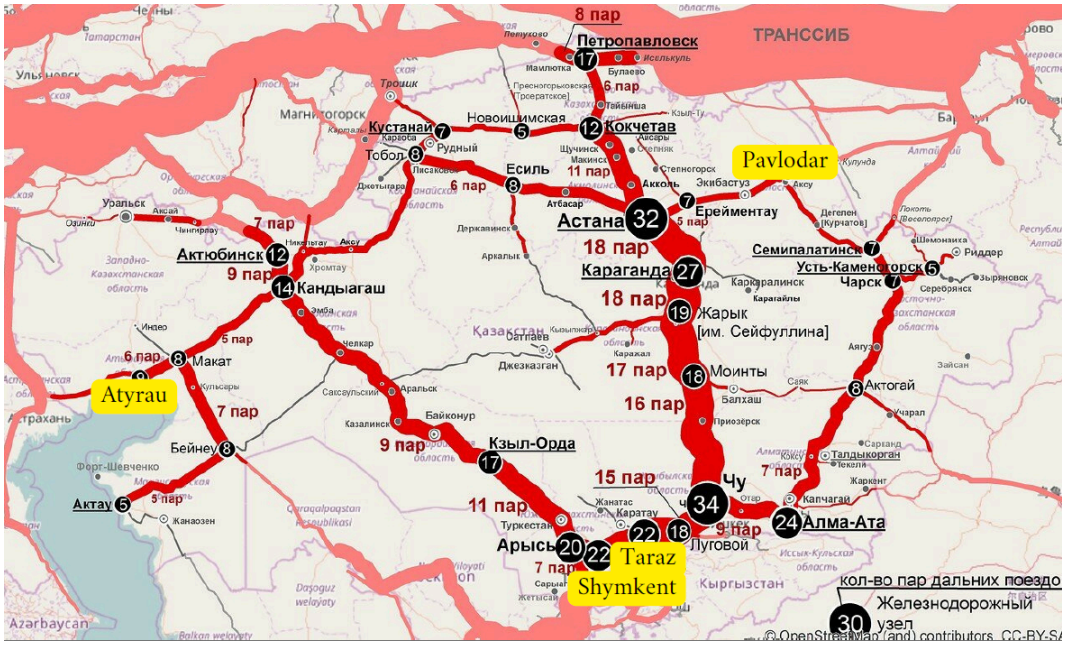

Figure 6. The map density of railroad transportation in Kazakhstan [65]

5.2 Plant layout

The styrene production plant is structured around three key stages: feed preparation, reaction, and separation. All major equipment is centrally located in a dedicated process area to minimize piping distances, reduce heat losses, and streamline operations. The layout has been optimized for efficient material and energy flow between units, with feedstock storage tanks placed near the preheating systems and product storage facilities located close to the distillation area for easy handling (*Figure 7*).

To ensure operational safety, the plant is divided into risk-based zones [66]:

1) Red zones indicate high-risk areas, including reactor systems and ethylbenzene handling zones;
2) Orange zones denote equipment, storage rooms and utility areas with moderate mechanical or thermal hazards;
3) Green zones represent safe zones equipped with emergency response facilities, such as first aid stations, offices and fire-fighting systems.

A control room with integrated instrumentation and monitoring systems is located adjacent to the reactor and separation units to enable real-time supervision. Utilities such as cooling water, steam supply, and instrument air are co-located to ensure reliable service to all process units. Cooling units are placed in different areas from the heating units.

Support facilities include maintenance workshops, spare parts stores, and a quality control lab for analyzing raw materials, intermediates, and final products. Administrative buildings, canteens, changing rooms, and parking areas are placed in designated safe zones away from the high-risk operational areas, ensuring personnel safety and comfort. The plant layout also incorporates open space adjacent to the processing area and within tank farms to accommodate future expansions, such as additional separation units, waste treatment systems, or capacity upgrades.

Strategically located emergency exits are installed around all major processing zones, with clear signage and direct access to designated evacuation routes. These exits lead toward green zones and ultimately to the main assembly area located in the safe zone of the plant.

Additionally, to enhance the logistics efficiency and streamline the transportation of raw materials and final products, a private railway line will be integrated with the public railway network.

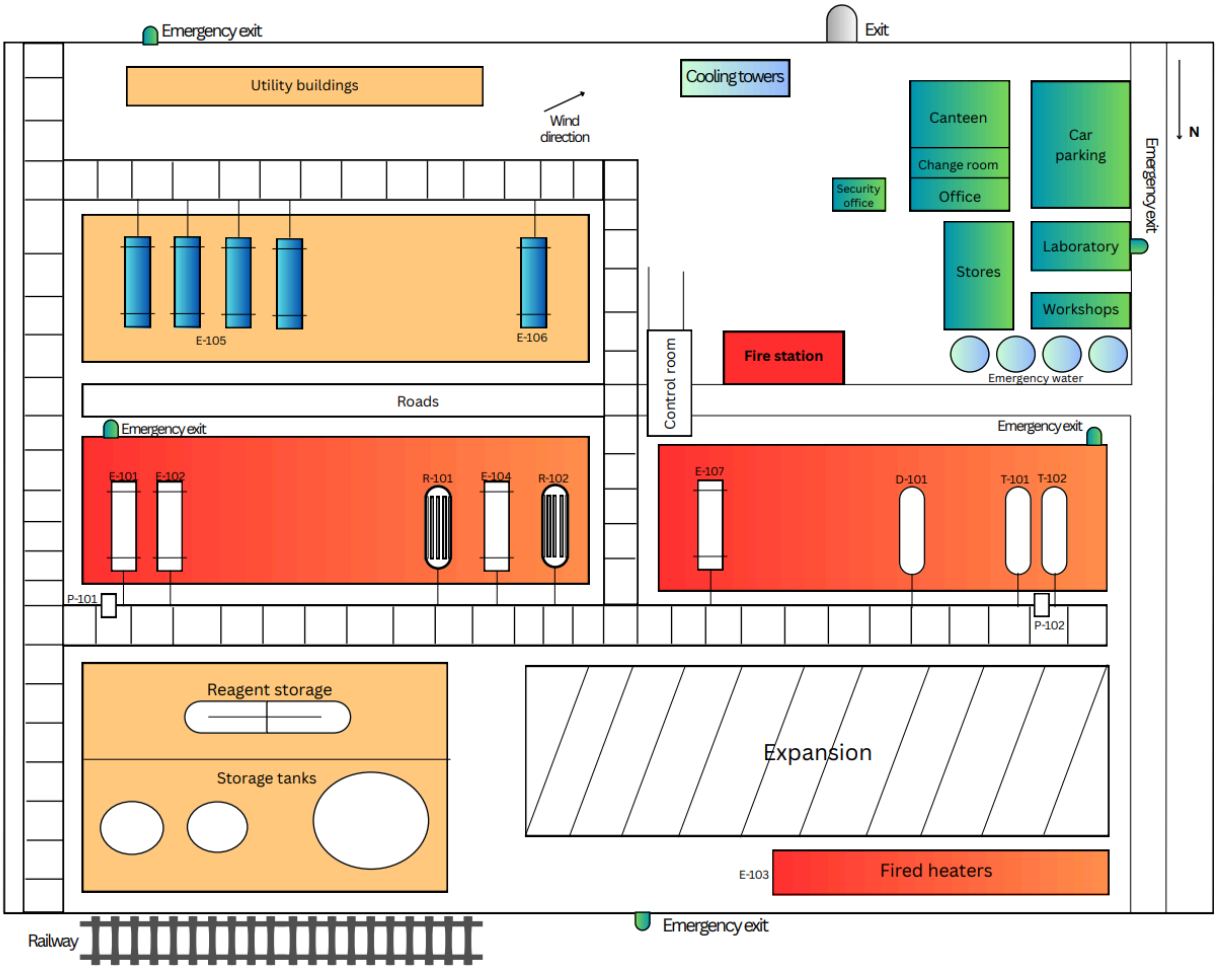

Figure 7. Styrene production plant layout

Based on the industry examples, a rough estimate for the land area required for a chemical plant producing 200,000 tons per year would be 10-20 hectares. This estimate accounts for production facilities, storage, utilities, and safety zones [67]. The exact area depends on factors such as the type of chemicals produced, the complexity of the processes, and the level of automation.

CHAPTER VI. Environment and Waste Streams

The waste streams from the process flow diagram contain light gases and wastewater that are separated in a decanter, as well as aromatic compounds and hydrocarbons, which are the top product of the T-102 distillation column. On top of it, the emissions from heat furnaces (E-103 and E-104) and catalyst should be treated after usage (**Table 28**).

Table 28. Flow rates of the waste streams in kmol/hr

	13	**14**	**18**
Ethylbenzene	1.8	0.61	1.08
Steam/water	16.3	4647.3	1.86
Styrene	2.7	0.2	0
Hydrogen	212.9	0.3	0
Toluene	1.3	1.26	27.88
Benzene	0.39	0.015	3.90
Ethylene	3.5	0.79	0
Methane	29	1.39	0
Total	**267.85**	**4651.92**	**34.72**

6.1 Light gases treatment

Stream 18 is directed to a distillation column, where toluene is recovered as the bottom product. The toluene will be collected and sent for sale. The top product, which contains a mixture of benzene, ethylbenzene (EB), steam and light gases from stream 13 is redirected as fuel for the heat furnaces. This approach maximizes energy efficiency, reduces the need for external fuel sources, and supports overall process integration within the plant [40].

The E-103 and E-104 mainly emit CO2, CO, and steam gases. While the amount of CO gas can be reduced by combustion optimization to achieve full combustion, carbon dioxide emissions from the heat furnace will be captured using a post-combustion carbon capture system. The resulting steam from combustion can be released into the air. In this process, the flue gas exiting the furnace, which mainly contains CO_2 with steam and CO, is first cooled and cleaned to remove particulates and acidic gases. The cleaned gas is then directed into an absorber column where it comes into contact with an amine-based solvent that selectively reacts with and absorbs the CO_2. Once the solvent becomes saturated with carbon dioxide, it is pumped into a regeneration column where it is heated. This step releases the CO_2 from the solvent, allowing it to be collected in a concentrated form while the regenerated solvent is recycled back to the absorber for reuse. The captured CO_2 can then be compressed and either stored in geological formations or transported to other plants to be used in downstream processes, such as enhanced oil recovery or chemical production. This integrated approach reduces the overall carbon footprint of the operation while maintaining continuous furnace performance [68].

6.2 Wastewater treatment

The wastewater from a styrene plant primarily produced from the decanter consists of water for 99.9% with a trace of some hydrocarbons like methane and toluene. Due to the

presence of toxic organic compounds, particularly benzene and styrene, that cause significant hazards to aquatic ecosystems, comprehensive wastewater treatment is necessary to meet environmental safety standards. According to Kazakhstan's national discharge regulations, the maximum allowable concentration (MAC) for benzene in wastewater is 0.05 mg/L, and 0.1 mg/L for toluene [69]. However, despite the relatively low molar concentrations, calculated concentrations of benzene (13.8 mg/L), toluene (1384.6 mg/L), ethylbenzene (777.1 mg/L), and styrene (253.8 mg/L) exceed Kazakhstan's environmental discharge limits, thus requiring special treatment. After the treatment, the water can be recycled back to the process for the generation of steam or cooling, reducing freshwater intake and fostering a more eco-friendly and cost-efficient operation.

6.2.1 Air Stripping

Air stripping eliminates VOCs (benzene, toluene, ethylbenzene, styrene) and dissolved gases (hydrogen, ethylene, methane) by volatilization. Wastewater flows through a packed tower, where countercurrent air transfers contaminants to the vapor phase. Off-gases are treated via carbon adsorption or incineration to meet air quality standards. Air stripping removes the majority of the VOCs and gases to 1 mg/L, preparing the wastewater for further treatment.

6.2.2 Activated Carbon Adsorption

Activated carbon adsorption polishes the wastewater by removing residual VOCs to meet discharge standards. The wastewater passes through granular activated carbon (GAC) beds, which adsorb organic compounds like benzene and toluene. This process reduces VOCs to be less than 0.1 mg/L ensuring compliance to the regulations. Spent carbon is regenerated or disposed of as hazardous waste, and the treated wastewater proceeds to final treatment.

6.2.3 Reverse Osmosis (RO)

Reverse osmosis (RO) ensures ultra-low contaminant levels for discharge by removing trace organics and salts. Wastewater is forced through semi-permeable membranes, removing up to 99% of remaining contaminants, meeting EPA standards. The concentrate stream is disposed of as hazardous waste, while the permeate is recycled back to the process.

6.3 Catalyst treatment

The styrene production process uses an iron oxide-based catalyst, Fe_2O_3 doped with potassium, in reactors R-101 and R-102 to facilitate ethylbenzene dehydrogenation. Even though catalysts do not directly participate in the reaction, their activity gradually declines over time due to coke formation and hydrocarbon adsorption. As a result, they need to be replaced every 2–3 years, leading to the generation of significant amounts of spent catalyst waste. This waste, containing metals and organic residues, poses environmental risks and is classified as hazardous under Kazakhstan's Ecological code and the Basel Convention [70].

The catalyst management process begins with thermal regeneration to restore the activity of the spent catalyst. In this step, the catalyst is heated at 500 to 700°C under a controlled, oxygen-lean atmosphere to burn off adsorbed hydrocarbons and coke without degrading the Fe_2O_3 structure. Released gasses of volatile organic compounds will be treated through carbon adsorption to meet Kazakhstan's air quality standards, as outlined in Safety requirements for toxic and highly toxic substances [71]. Thermal regeneration can restore up to 70% of the catalyst's activity, allowing approximately 35,000 kg of the annual catalyst waste to be reused in reactors R-101 and R-102, significantly extending the catalyst's lifespan by one to two cycles. For catalysts that are too degraded for regeneration, typically up to 30% of the total catalyst amount, metal recovery is used to extract valuable iron and potassium compounds. This involves hydrometallurgical leaching, where the spent catalyst is treated with alkali solutions to dissolve metal oxide and potassium compounds, followed by p by precipitation techniques to selectively recover target components [72]. This process achieves up to 80% recovery of iron and potassium, yielding around 8,000 to 12,000 kg of Fe_2O_3 and 2,000 to 3,000 kg of potassium salts annually. Residual solids, constituting about 10% of the waste are encapsulated with cement to immobilize metals, preventing leaching in accordance with standards, and then disposed of in a licensed hazardous waste landfill compliant with Kazakhstan's regulations and the Basel Convention [73].

Beyond catalyst resynthesis, Fe_2O_3 is highly suitable for use in construction materials, a sector with significant demand in Kazakhstan due to ongoing infrastructure projects in cities like Nur-Sultan. Iron oxide can serve as a colorant in cement production, imparting red or brown hues to concrete and masonry products, or as a fluxing agent to enhance clinker formation during cement manufacturing. The construction industry accepts Fe_2O_3 with 60 to 90% purity, making the recovered material an ideal candidate.

Spent catalyst must be stored in sealed, fire-resistant containers and handled with dry absorbents to manage spills.

CHAPTER VII. Total Investment and Profitability

7.1 Price of Raw Materials and Final Product

An evaluation of the prices of raw materials through regions before the start of economic assessment is crucial since it directly impacts the plant`s financial viability. Given the direct correlation between hydrocarbon prices and raw material costs, we conducted a comprehensive regional market analysis to identify the most economically advantageous procurement strategy. **Table 29** demonstrates the significant geographical price disparities for ethylbenzene. And in table it can be seen that it is beneficial to buy ethylbenzene in China, particularly in Career henan chemical co [74].

Table 29. The global prices of raw materials

Seller country or region	Price, USD per ton	Source

China	1,000	[74]
Czech Republic	1,070	[75]
Germany	1,060	[75]
France	1,090	[75]

All the calculations are shown in Excel sheet. It is also important to consider the selling price of the final product. Styrene is considered the main product, while toluene is treated as a valuable by-product of the production process. For the economic evaluation, we assume that styrene will be sold at a market price of $1.5000 per kilogram, based on current global pricing trends and historical averages [76]. Meanwhile, toluene, which is recovered during the separation stage, will be sold at $0.6530 per kilogram [77]. These selling prices are used to estimate annual revenues and calculate key financial indicators such as ROI, NPV, and payback period.

7.2 Fixed Capital Investment Estimation

The fixed capital investment is the total cost of designing, constructing, and installing a plant and the associated modifications needed to prepare the plant site. The fixed capital investment is made up of Inside battery limits (ISBL), offsite investment (OSBL), engineering and construction costs and contingency charges.

(Note: All cost references are based on 2024 pricing and economic conditions.)

7.2.1 Inside battery limits (ISBL)

To get ISBL minor equipments such as decanter, 4 fired heaters capital costs were retrieved from ASPEN economic analyzer, while the cost of the major equipment pieces that were taken into account are 2 reactors, 2 distillation columns and 2 heat exchangers were calculated by hand (**Table 31**).

To estimate the cost of equipment, we will use the cost correlation formula provided [78]:

$$C_e = a + bS^n \quad \text{(Eq. 31)}$$

Where, C_e = purchased equipment cost on a U.S. Gulf Coast basis, Jan. 2010, a = constant value 1, b = constant value 2, S = size parameter, n = exponent for type of equipment.

Table 30. Preliminary purchase price for several equipment pieces

Equipment	Size parameter	a	b	n	S	Cost
R-101	**Surface Area,** m^2	28000	54	1.2	37.647	64,000
R-102	**Surface Area,** m^2	28000	54	1.2	37.647	64,000
T-101	**Shell mass,kg**	17400	79	0.85	34015	579,200
	Kettle reboiler	29000	400	0.9	822.245	256,000
	304ss structured packing, m^3	0	7600	1	4.12	31,300
T-102	**Shell mass, kg**	17400	79	0.85	4847.39	124,000
	Trays, m	130	440	1.8	2	58,200
	Kettle reboiler	29000	400	0.9	398.22	116,500
E-101	**Area of heat exchanger**	28000	54	1.2	36.16	32,000
E-105	**Area of heat exchanger**	29000	400	0.6	3884.8	708,000

The inside battery limits (ISBL) investment—the cost of the plant itself, the cost of which directly depends on the technical characteristics and configuration of the equipment. This investment category covers all the installation and construction work required to put the equipment into operation at the production facility. It includes several essential components that combine to transform individual pieces of equipment into a fully functional production system. These components include the installation of pipeline networks connecting technological nodes (f_p), the proper installation and placement of all major equipment elements (f_{er}), as well as the implementation of instrumentation and control systems for monitoring and automating processes (f_i). In addition, the investment covers the installation of an electrical system to power the equipment (f_{el}), as well as all necessary construction work to prepare and maintain the infrastructure of the site. Other elements of the FCI include the construction of auxiliary buildings and structures (f_s), as well as necessary protective measures such as painting and insulation (f_l). Together, these complex installation works represent the complete material base necessary for the implementation of the project from design to operation.

The calculation for all equipment is shown below and coefficients are provided at the **Table 31**:

$$C = \sum_{i=1}^{M} C_{e,i,CS}[(1 + f_p)f_m + (f_{er} + f_{el} + f_i + f_C + f_s + f_l)] \qquad \text{(Eq. 32)}$$

Table 31. Typical Factors for Estimation of Project Fixed Capital Cost [78]

	Process Type		
Item	**Fluids**	**Fluids–Solids**	**Solids**
Major equipment, total purchase cost	C_e	C_e	C_e
f_{er} Equipment erection	0.3	0.5	0.6
f_p Piping	0.8	0.6	0.2
f_i Instrumentation and control	0.3	0.3	0.2
f_{el} Electrical	0.2	0.2	0.15
f_c Civil	0.3	0.3	0.2
f_s Structures and buildings	0.2	0.2	0.1

f_l Lagging and paint	0.1	0.1	0.05

Additionally, The cost estimation model incorporates three precise adjustment factors to enhance accuracy. First, the material factor (f_m) applies a 1.3 multiplier specifically for stainless steel components, accounting for their 30% cost increase compared to standard carbon steel alternatives. This adjustment ensures proper budgeting for corrosion-resistant materials essential in process equipment.

The location factor is based on 2003 data and can be updated by dividing by the ratio U.S. dollar/local currency in 2003 and multiplying by the ratio U.S. dollar/local currency in 2024. Location factor for China (indigenous) is 0.61. The exchange rate in 2003 averaged about 1 yuan = 0.137 USD and in 2024 1 yuan = 0.1426 [79]. Additionally, we add 10% for every 1000 miles from the nearest major industrial center (Xinjiang province, China). The driving distance from Xinjiang to Atyrau is approximately 1,729 miles. The 2024 location factor for Atyrau:

$$Location\ factor\ =\ 0.61\ *\ \frac{0.1426}{0.137} * (1 + \frac{10\%}{100\%} * \frac{1{,}729\ miles}{1000\ miles}) = 0.745 \quad \text{(Eq. 33)}$$

As for the time factor, CEPCI in 2010 is 532.9 and in 2024 is approximately 798.9, as a result by division we get 1.5 time factor [80].

7.2.2 Total fixed Capital Investment Calculation

The whole calculation of fixed investment capital can be seen in EXCEL. The capital cost estimations are provided at **Table 32**. We estimated offsite (OSBL) costs at 40% of ISBL investment, following standard industry practice for preliminary budgeting. This percentage represents a typical mid-range value for chemical plants where site-specific infrastructure details are not yet available. It covers essential support infrastructure for plant operations, including utilities (power, steam, cooling water), storage (tank farms, warehouses), and environmental systems (wastewater treatment, fire protection).

Engineering costs cover detailed design, procurement, construction supervision, and project management services required to execute a project. These expenses include process engineering, equipment procurement, administrative overheads, and contractor profits, typically outsourced to specialized engineering firms. Costs are estimated at 30% of ISBL+OSBL for small projects.

Contingency charges are incorporated into project budgets to account for cost estimation uncertainties and unforeseen expenses. These reserves address potential variations such as design changes, material price fluctuations, currency risks, labor issues, and subcontractor challenges.

Typically set at a minimum of 10% of ISBL plus OSBL costs, contingency fees protect contractors from budget overruns, particularly in fixed-price bids.

Table 32. Total Fixed Capital Investment

Equipment	ID	Total cost of equipments, USD
Reactors	**R-101**	263,000
	R-102	263,000
Distillation columns	**T-101**	3,010,000
	T-102	1,250,000
Heat exchangers	**E-101**	134,000
	E-105	2,970,000
Minor equipments		18,400,000
ISBL = Total cost of equipments		26,400,000
OSBL		10,550,000
Engineering Costs		11,078,000
Contingency		5,540,000
Total Fixed Capital Investment		53,500,000

7.3 Operating Costs (OPEX)

7.3.1 Variable Costs of Production

Variable production costs are expenses that change in direct proportion to the plant's output. This category includes costs of raw materials as well as utilities, consumable materials, in this process catalyst. Production of styrene requires a large amount of the ethylbenzene as well as investments in the FE(III) oxide doped with K catalyst. Capital investment of the catalyst is 100 tons for 1,000 $/ton, resulting in 100,000$ annually and as the lifetime of the catalyst is assumed to be 2 years, regeneration or purchase of new has to be considered. The identified utilities for this process design are cooling water, steam, natural gas and electricity.

The price of natural gas was taken as the current world price of 3.245 $/MMBTU [81], however it is worth mentioning that Kazakhstan has one of the world's lowest natural gas prices for households of around 0.07 $ per cubic meter or around 2.03 $/MMBTU [82]. Even though businesses typically pay more for the same amount of energy in Kazakhstan, it is still well below global price, but global price is still taken, since the natural gas market is volatile and future fluctuations have to be considered. Also, heat removed from E-104 unit is regenerated to heat distillation column reboilers. It is also worth mentioning that burning by-product gases releases 33.64 MW of heat that can be used to reduce purchase of natural gas.

The price of saturated 160 °C steam and saturated 110 °C steam as well as cooling water were taken from ASPEN economic analyzer. The electricity price is 0.071 $/kWh for businesses, which is ~25% more expensive for businesses than for households [83]. Cooling water is used for Heat removal from E-106 and condensers of distillation columns. Average sewage services for special economic zones is 212.4 KZT or ~0.41$ per cubic meter [84].

Overall utility expenses are 5,432,857.735 $/operating year. The utilities rates and prices are presented in **Table 33**. Also, ASPEN economic analyzer's results are available in the economic analysis spreadsheet. The difference betweens it and provided results account to waste heat regeneration and requirements of condensers of the distillation columns.

Table 33. Utilities summary

Utility	Rate	Rate Unit	Price ($)	Price Unit	Cost per 1 hour ($/hour)	Annual Cost ($/ year)
Electricity	54.9	kW	0.0775	$/kWh	4.26	34,000
Gas	$48.1 \cdot 10^6$	BTU/hr	$3.245 \cdot 10^{-6}$	$/BTU	372.6	2,980,000
Steam (1 bar)	$59.08 \cdot 10^6$	BTU/hr	$1.9 \cdot 10^{-6}$	$/kJ	178.6	1,428,000
Steam (6 bar)	$6.24 \cdot 10^6$	BTU/hr	$1.9 \cdot 10^{-6}$	$/kJ	12.51	100,000
Wastewater	$0.084 \cdot 10^6$	kg/hr	0.41	$/m^3	34.44	275,500
Cooling water	$343.2 \cdot 10^6$	BTU/hr	$0.212 \cdot 10^{-6}$	$/kJ	76.77	614,00
Total					679.12	5,431,500

7.3.2 Fixed Cost of Production

Labor costs were identified using the assumption of 15 workers per shift and 8 hour, 5 working day week and 49 operating weeks per year, the overall number of operators is estimated

to be 62 with pay of 1000$/month. Supervisions expenses are expected to be around 25% of operating labor cost, direct salary overhead, which includes employee insurance and other required benefits, is 45% of combined operating labor cost and supervisions. These costs are combined to the cost of labor.

Assumption was made that maintenance expenses are 3% of ISBL investment and property taxes and insurance were assumed to be 2% of ISBL investment. General plant overhead is estimated to be 65% of labor cost and maintenance sum. Interest on debit financing is 6% of working capital.

Depreciation was calculated using the MACRS tax tool for 10 years, which is a reduction of assets monetary value and decrease of taxable income, but is still an expense worth taking into account. The value of depreciation is expressed in percentage of total fixed capital cost.

Table 34. Depreciation Calculation

Year	**Depreciation(%)**	**Value($/operating year)**
3	10	5,354,000
4	18	9,638,000
5	14.4	7,710,000
6	11.5	6,157,000
7	9.22	4,926,000
8	7.4	3,962,000
9	6.6	3,534,000
10	6.6	3,534,000
11	6.6	3,534,000
12	6.6	3,534,000
13	3.33	1,767,000

Table 35. Fixed costs of production

Fixed cost	**Value ($/operating year)**
Labor	1,800,000
Supervisions	450,000

Direct salary overhead	1,010,000
Maintenance	617,000
Property taxes and insurance	412,000
Plant overhead	2,500,000
Interest on Debit Financing	838,000
Total	7,627,000

7.4 Cash Flow

The styrene production plant will be entirely self-funded, meaning all capital expenditures, including construction, equipment, and working capital, are financed through internal equity and retained earnings, without debt or government subsidies. Since Atyrau is located in an industrial zone the tax will be 0%. This funding approach provides complete control over financial planning, eliminates debt service obligations, and accelerates capital recovery reinvestment of operating profits.

In **Table L1** *in appendix L*, the total capital expenditure (CapEx) for the project is estimated at $53 million USD which will be spent during first two years of development:

1) Year 1: $21.4 million is allocated to basic infrastructure, civil works, and partial equipment procurement;
2) Year 2: $32.1 million is covering remaining equipment, installation, automation systems, and commissioning.

These investments are aimed at establishing a high-efficiency, continuous-process technological process, designed for a production capacity of approximately 200,720 tons of styrene per year.

In the third year preceding the full-scale launch of production, an additional $15.1 million is allocated to meet the working capital needs. This one-time investment ensures smooth growth in operating activities and includes the purchase of sufficient raw materials for the first two weeks of production; covering utility costs, labor and basic supplies; reserve capital to manage cycles of settlements with creditors and debtors and stabilize initial cash flow.

In figure 8, starting from year 4, the curve shows a steady and consistent upward trend, indicating positive annual cash flows resulting from profitable operations. Over the remaining years, cash flow inflows continue to accumulate, eventually reaching nearly 260 MM$ by year 13. This steady increase demonstrates the project`s strong profitability and sustainability, with a fast payback period and substantiation return on investment.

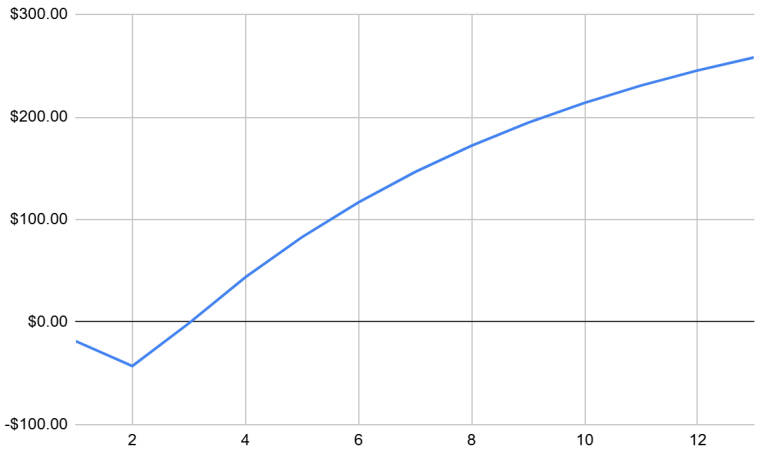

Figure 8. Cumulative Cash Flow Diagram (Present Value)

7.5 Discounting, Depreciation and Analysis Period

For all financial projections, a discount rate of 12% has been applied. This reflects the company's internally set cost of capital, capturing the opportunity cost of investing in this project relative to alternative ventures of similar risk. The period of economic analysis was taken as 13 years since in the first 2 years construction was done and there was no operating of the plant, and extra 11 years were taken because 10 year MACRS depreciation was earlier assumed for chemical technology equipment, which splits up to 11 years because of the assumption that assets start service halfway through the first year of production and depreciation value of first year of operation is divided between first and 11th years of plant production time.

7.6 Profitability Analysis

The project's profitability has been evaluated using standard financial indicators, including Net Present Value (NPV), Internal Rate of Return (IRR), Return on Investment (ROI), and payback period.

Table 1 in Appendix L highlights excellent financial viability. IRR was calculated through excel formula and shows that the project generates strong returns with the higher IRR over 13 years indicating that the longer time horizon allows for greater cumulative returns due to compounding and extended revenue generation the 58% over 5 years is already very high suggesting the project is highly profitable in the short term while the increase to 70% over 13 years reflects additional value from sustained performance and potentially lower annual capital expenditures spread over a longer period both figures demonstrate that the investment is financially attractive with the extended timeframe further enhancing its profitability.

Return on Investment (ROI) was calculated using the standard formula applied in chemical process economic evaluations, where cumulative net profit is divided by the product of the project duration and initial investment:

$$Annualized\ ROI\ = \frac{Cumulative\ Net\ profit}{plant\ live\ x\ initial\ investment} x100\% \qquad \text{(Eq. 34)}$$

In this approach, cumulative net profit refers to the total accumulated cash flow over the project period minus the initial investment (capital expenditure and working capital from Years 1–3). The plant life refers to the number of operational years considered in the evaluation. The 7-year ROI was found to be 53%, indicating that the project generates, on average, a profit equal to 53% of the initial investment per year over its first seven operational years. The 13-year ROI was calculated to be 81%, reflecting continued profit accumulation beyond the payback period, and suggesting strong long-term project sustainability.

Table 36. Main economic indicators of the production plant

Payback Period	3.09 years		
Internal Rate of Return (IRR)	58% over 5 years	70% over 13 years	
Net Present Value (NPV)	226.2 million USD		
Annual ROI (7 years)	53%	Annual ROI (13 years)	81%

The high ROI figures obtained in this analysis are primarily attributed to the project's self-funded nature and its strong operational profitability. Since the project does not rely on external financing or debt, there are no interest payments or loan servicing costs, which significantly improves net cash flow and accelerates capital recovery. All generated profits are retained by the company, contributing directly to ROI without deductions from debt obligations.

Furthermore, the process design ensures stable, high-value product output (i.e., styrene and toluene) while maintaining relatively low operational costs, especially due to the strategic location in Kazakhstan with access to low-cost utilities, raw materials and no tax. The capital investment was also optimized through efficient equipment selection and waste heat integration, leading to lower-than-average CAPEX for a plant of this capacity.

These factors in Table 37 combined with consistent annual revenue, rapid payback of 3 years, and the absence of financial liabilities enable the plant to achieve an exceptionally high return on each dollar invested, both during the first seven years of operation (ROI = 53%) and over the full 13-year evaluation period (ROI = 81%).

CHAPTER VIII. Conclusions and future work

In conclusion, the project successfully designed and assessed a complete industrial process for the styrene production in Atyrau, Kazakhstan, integrating both technical and economic aspects. To meet this objective, the work involved evaluating reaction pathways, conducting kinetic modeling, simulating the process in Aspen Plus, sizing equipment, planning the plant layout, and estimating financial feasibility. The report outlines the production pathway,

major and minor equipment designs, and addresses environmental considerations alongside an initial cost analysis.

The selected production method, ethylbenzene dehydrogenation, was chosen due to its industrial maturity and high efficiency, offering over 90% selectivity and 70% conversion under optimized conditions. The reaction is carried out in two adiabatic plug flow reactors, with intermediate reheating using fired heaters. The downstream section of the process involves product purification through distillation and recovery of unreacted feedstock. The plant is designed for an output capacity of approximately 200k tons of styrene annually, with toluene recovered as a marketable by-product.

Following the establishment of mass balances, detailed mechanical and thermal designs were completed for key process units, such as reactors, distillation columns, and heat exchangers. Supplementary equipment, including pumps and condensers, was also specified using both shortcut design methods and Aspen simulations. The process was compiled into a PFD and a comprehensive plant layout developed with attention to operational safety and efficiency.

Following, the Atyrau region was selected for plant construction based on favorable industrial conditions including access to feedstock, utilities, and transportation networks. Environmental factors were taken into account, and provisions for managing waste heat, wastewater, and emissions were included in the plant concept.

The last part was capital cost estimation and it revealed a total fixed investment of $53 million USD across two years, with an additional $15.1 million allocated in Year 3 to cover startup and working capital. Using global pricing benchmarks for styrene and toluene, and applying a 12% discount rate, the financial evaluation demonstrated promising results, including an NPV of $226 million, an IRR of 69%, and a payback period of 3.08 years.

While the current design focuses exclusively on styrene and toluene, future development may consider integrating by-product recovery such as hydrogen and benzene, improving energy efficiency through heat integration, or expanding into the production of value-added derivatives like styrene oxide. Further work should also focus on minimizing emissions and reducing the environmental footprint of the facility. Strategies could include CO_2 capture from combustion units, use of low-emission catalysts, or even partially replacing fossil fuel-based utilities with renewable energy sources where feasible. Moreover, condensers and reboilers operate independently, resulting in high utility consumption. Integrating the heat duties of condensers with fired heaters or other reboiler systems could significantly reduce steam and fuel usage. This heat exchange strategy would not only lower operating costs but also decrease the plant's environmental footprint by minimizing excess heat discharge and fossil fuel dependency. Additionally, the distillation section presents a major energy burden. The current column designs operate with very high reboiler duties and significant column heights, which not only consume large amounts of steam but also create structural and maintenance challenges. To address this, the distillation column heights could be split into two sequential columns. This approach, known

as column sectioning or “split distillation,” reduces the operational load per column, allows better temperature control, and can improve overall separation efficiency while making maintenance safer and more manageable.

From an environmental perspective, wastewater and catalyst treatment strategies are already well integrated but can be further enhanced. Real-time control of VOC stripping and adsorption systems would optimize performance under varying load conditions. Moreover, exploring advanced oxidation processes or biological polishing steps could reduce long-term reliance on activated carbon and membrane systems. In catalyst handling, while thermal regeneration already recovers up to 70% of spent catalyst, future efforts could include on-site in-situ regeneration methods to reduce downtime, and more efficient metal recovery technologies to reclaim iron and potassium from the remaining unusable portions.

Nevertheless, the project confirms the technical validity and economic feasibility of constructing a styrene plant in Kazakhstan. It provides a strong foundation for further development and could significantly contribute to the national petrochemical industry by enhancing self-sufficiency and enabling future innovation.

REFERENCES

[1] PubChem, "Styrene," *pubchem.ncbi.nlm.nih.gov*, Sep. 16, 2004. https://pubchem.ncbi.nlm.nih.gov/compound/Styrene

[2] R. R. Miller, R. Newhook, and A. Poole, "Styrene Production, Use, and Human Exposure," *Critical Reviews in Toxicology*, vol. 24, no. sup1, pp. S1–S10, Jan. 1994, doi: https://doi.org/10.3109/10408449409020137.

[3] "U.S. Synthetic Rubber Program - National Historic Chemical Landmark," American Chemical Society. https://www.acs.org/education/whatischemistry/landmarks/syntheticrubber.html

[4] I. W. G. on the E. of C. R. to Humans, *Styrene*. International Agency for Research on Cancer, 1994. Available: https://www.ncbi.nlm.nih.gov/books/NBK507533/

[5] Stéphane, C., Margaux, D., Maria, F., Gilles, J., Amaury, L., Thibault, P., Mateo, T., & Yifan, W. (2023). "Process design of styrene monomer production". *ULiège, FSA, Chemical Engineering*. 2023 [Online]. Available: https://www.chemeng.uliege.be/upload/docs/application/pdf/2024-06/final_article_eu_group.pdf

[6] PubChem, "Ethylbenzene," *Nih.gov*, 2025. https://pubchem.ncbi.nlm.nih.gov/compound/Ethylbenzene#section=Chemical-and-Physcal-ProErties.

[7] NOAA Office of Response and Restoration, US GOV, "STYRENE MONOMER, STABILIZED |CAMEO Chemicals | NOAA," *Noaa.gov*, 2010. https://cameochemicals.noaa.gov/chemical/4553

[8] PubChem, "Styrene," *pubchem.ncbi.nlm.nih.gov*, Sep. 16, 2004. https://pubchem.ncbi.nlm.nih.gov/compound/Styrene

[9] "STYRENE STY." Available: https://cameochemicals.noaa.gov/chris/STY.pdf

[10] PubChem, "Hydrogen," *Nih.gov*, 2019. https://pubchem.ncbi.nlm.nih.gov/compound/Hydrogen

[11] NOAA, "The Atmosphere," *National Oceanic and Atmospheric Administration*, Apr. 14, 2023. https://www.noaa.gov/jetstream/atmosphere

[12] E. D. de M. Sobrinho *et al.*, “From Waste to Styrene–Butadiene (SBR) Reuse: Developing PP/SBR/SEP Mixtures with Carbon Nanotubes for Antistatic Application,” *Polymers*,vol.16, no. 17, p. 2542, Sep. 2024,. doi:https://doi.org/10.3390/polym16172542

[13] “Styrene Butadiene Rubber (SBR) market Insights, Trends, Analysis, and Forecast, 2034,” *Prismane Consulting*, 2022. https://prismaneconsulting.com/report-details/global-styrene-butadiene-rubber-sbr-marke-study

[14] Shrine Chemicals, "Styrene Monomer," *Shrine Chemicals*, [Online]. Available: https://shrinechemicals.com/product/styrene-monomer/

[15] ASTM International, *ASTM D2827-13: Standard Specification for Styrene Monomer*, West Conshohocken, PA, USA, 2013. [Online]. Available: https://standards.iteh.ai/catalog/standards/astm/2c24afa0-ef45-4942-85a3-34e1d716a6b2/astm-d2827-13.

[16] C. Nederlof, Güliz Talay, Freek Kapteijn, and Michiel Makkee, “The role of RWGS in the dehydrogenation of ethylbenzene to styrene in CO2,” *Applied Catalysis A General*, vol. 423–424, pp. 59–68, Feb. 2012, doi: https://doi.org/10.1016/j.apcata.2012.02.019.

[17] L. Buchori and F. M. Y. Putri, “Pinch Analysis For Styrene Production With Lummus/UOP Smart SM Technology,” *IOP Conference Series: Materials Science and Engineering*, vol. 1053, no. 1, p.012105, Feb. 2021, doi: https://doi.org/10.1088/1757-899x/1053/1/012105.

[18] W. L. Luyben, “Design and Control of the Styrene Process,” Industrial & Engineering Chemistry Research, vol. 50, no. 3, pp. 1231–1246, Feb. 2011, doi: https://doi.org/10.1021/ie100023s.

[19] S.-S. Chen and Updated by Staff, “Styrene,” *Kirk-Othmer Encyclopedia of Chemical Technology*, Sep. 2006, doi: https://doi.org/10.1002/0471238961.1920251803080514.a01.pub2.

[20] “US3326996A - Dehydrogenation of ethylbenzene to styrene - Google Patents,”*Google.com*, May 06, 1964. https://patents.google.com/patent/US3326996A/en.

[21] Nurul Sabaruddin, “Faculty of Biochemical and Chemical Engineering Styrene Production from Ethylbenzene,” *Academia.edu*, May 18, 2017. https://www.academia.edu/33068026/Faculty_of_Biochemical_and_Chemical_Engineer

ng_Styene_Production_from_Ethylbenzene

[22] E. H. Lee, “Iron Oxide Catalysts for Dehydrogenation of Ethylbenzene in the Presence of Steam,” *Catalysis Reviews*, vol. 8, no. 1, pp. 285–305, Jan. 1974, doi:https://doi.org/10.1080/01614947408071864.

[23] H. F. Rase, *Handbook of Commercial Catalysts*. Informa, 2016. Doi:https://doi.org/10.1201/b21367.

[24] “Encyclopedia of Chemical Processing and Design,” *Google Books*, 2025. https://books.google.kz/books/about/Encyclopedia_of_Chemical_Processing_and.html?id=DKNfx4efDQC&redir_esc=y.

[25] D. H. James and W. M. Castor, “Styrene,” *Ullmann’s Encyclopedia of Industrial Chemistry*, Jun. 2000, doi: https://doi.org/10.1002/14356007.a25_329.

[26] M. Imanari and M. Takiguchi, “Catalyst for the production of styrene.” https://patents.google.com/patent/US4460706A/en.

[27] N. Dulamiţă *et al.*, “Ethylbenzene dehydrogenation on Fe2O3-Cr2O3-K2CO3 catalysts promoted with transitional metal oxides,” *Applied Catalysis A: General*, vol. 287, no. 1, pp. 9–18, Jun. 2005, doi: https://doi.org/10.1016/j.apcata.2005.02.037.

[28] H.-G. Franck and J. W. Stadelhofer, *Industrial Aromatic Chemistry*. Berlin, Heidelberg: Springer, 1988. doi: https://doi.org/10.1007/978-3-642-73432-8.

[29] “US3326996A - Dehydrogenation of ethylbenzene to styrene - Google Patents,” *Google.com*, May 06, 1964. https://patents.google.com/patent/US3326996A/en.

[30] J. Lee and G. F. Froment, “Ethylbenzene dehydrogenation into styrene: Kinetic modeling and reactor simulation,” *Chem. Eng. J.*, vol. 136, no. 2-3, pp. 294–301, 2008, doi: 10.1016/j.cej.2007.04.017.

[31] M. Boudart, “Classical Catalytic Kinetics: A Placebo or the Real Thing?” *Top. Catal.*, vol. 21, no. 1-3, pp. 111–119, 2002, doi: 10.1023/A:1014591406226.

[32] R. Tang, Y. Zhou, and L. Xie, “Experimental, kinetics, and reactor modeling studies of the direct dehydrogenation of ethylbenzene to styrene in the Fixed-Bed reactor,” *Industrial & Engineering Chemistry Research*, Jun. 2024, doi: 10.1021/acs.iecr.4c01175.

[33] P. Sharma, R. Dwivedi, R. Dixit, M. Batra, and R. Prasad, “Mechanism evolution for the oxidative dehydrogenation of ethylbenzene to styrene over V2O5/TiO2 catalyst: computational and kinetic approach,” *RSC Advances*, vol. 5, no. 50, pp. 39635–39642, Jan. 2015, doi: 10.1039/c5ra00446b.

[34] Z. Lian, C. Si, F. Jan, M. Yang, and B. Li, “Resolving the mechanism complexity of oxidative dehydrogenation of hydrocarbons on nanocarbon by microkinetic modeling,” *ACS Catalysis*, vol. 10, no. 23, pp. 14006–14014, Nov. 2020, doi: 10.1021/acscatal.0c02952.

[35] S. S. E. H. Elnashaie, B. K. Abdallah, S. S. Elshishini, S. Alkhowaiter, M. B. Noureldeen, and T. Alsoudani, “On the link between intrinsic catalytic reactions kinetics and the development of catalytic processesCatalytic dehydrogenation of ethylbenzene to styrene,” *Catalysis Today*, vol. 64, no. 3–4, pp. 151–162, Jan. 2001, doi: 10.1016/s0920-5861(00)00520-4.

[36] N. Dulamiţă *et al.*, “Ethylbenzene dehydrogenation on Fe2O3-Cr2O3-K2CO3 catalysts promoted with transitional metal oxides,” *Applied Catalysis a General*, vol. 287, no. 1, pp. 9–18, May 2005, doi: 10.1016/j.apcata.2005.02.037.

[37] K. Zha *et al.*, “Insights into promotional effects for ethylbenzene dehydrogenation to styrene with steam over fe-K, fe-K-ce and fe-K-ce-mo mixed oxide catalysts,” *Applied Catalysis A: General*, vol. 666, p. 119372, Sep. 2023. doi:10.1016/j.apcata.2023.119372

[38] W. J. Lee and G. F. Froment, "Ethylbenzene Dehydrogenation into Styrene: Kinetic Modeling and Reactor Simulation," *Industrial & Engineering Chemistry Research*, Feb. 6, 2008. [Online]. Available: https://pubs.acs.org/doi/full/10.1021/ie071098u

[39] A. C. Dimian and C. S. Bildea, "Energy Efficient Styrene Process: Design and Plantwide Control," *Ind. Eng. Chem. Res.*, vol. 58, no. 12, pp. 4890–4905, 2019, doi: 10.1021/acs.iecr.8b05560.

[40] Sinnott, R. K. & Towler, G. P. (2020). *Chemical Engineering Design* (6th ed.).

[41] C. Hu, “Reactor design and selection for effective continuous manufacturing of pharmaceuticals,” *Journal of Flow Chemistry*, vol. 11, no. 3, pp. 243–263, May 2021, doi: 10.1007/s41981-021-00164-3

[42] C. L. Cozadd, “Optimization and cost comparison of reactor types in a styrene production process,” 2019.

[43] Froment, G. F., Bischoff, K. B., & De Wilde, J. (2011). *Chemical Reactor Analysis and Design* (3rd ed.).

[44] Moulijn, J. A., Makkee, M., & van Diepen, A. (2013). *Chemical Process Technology*.

[45] Andrew. (2022, January 6). SS 304 Properties - SS304 Density, composition, tensile yield strength. *304 Stainless Steel*. https://304stainlesssteel.org/ss-304/

[46] D. Dr. Lausberg, M. Lieb, H. Moeckel, H. Uhr, and B. Se, “EP0222248B1 - Method for the distillation of styrene - Google Patents,” Nov. 09, 1985. https://patents.google.com/patent/EP0222248B1/en

[47] H. Z. Kister, *Distillation design*. New York, N.Y.: Mcgraw-Hill, 1992. https://aussiedistiller.com.au/books2/Distillation%20Design.pdf

[48] J. D. Seader, E. J. Henley, and D Keith Roper, *Separation process principles with applications using process simulators*. Hoboken, Nj: John Wiley & Sons, Inc,2016. https://studylib.net/doc/25894930/seader---separation-process-principles--with-applications…

[49] A. Bahadori, *Corrosion and Materials Selection*. John Wiley & Sons, 2014

[50] “40 years of experience in packing styrene columns | Sulzer,” *Sulzer.com*, 2020. https://www.sulzer.com/en/shared/stories/40-years-of-experience-in-packing-styrene-cons

[51] Szewczyk-Nykiel, “The influence of molybdenum on corrosion resistance of sintered austenitic stainless steels,” Czasopismo Techniczne. Mechanika, vol. 2015, pp. 131–142, Sep. 2016, doi:10.4467/2353737xct.15.344.4865.

[52] “EFFECT OF CARBIDE PRECIPITATION ON 316L AUSTENITIC STAINLESS STEEL WELDED JOINTS INVESTIGATING THE METALLURGICAL & TENSILE PROPERTIES,”ResearchGate.https://www.researchgate.net/publication/355443625_EFFECT_OF_CARBIDE_RECIPITATION_ON_316L_AUSTENITIC_STAINLESS_STEEL_WELDED_JOINTS_INVETIGATING_THE_METALLURGICAL_TENSILE_PROPERTIES

[53] S. Y. Kuan, “Design, construction and operation of the floating roof tank,” 2009. [Online]. Available: http://eprints.usq.edu.au/8503/

[54] Sigma-Aldrich Chemie GmbH, "Safety Data Sheet: Ethylbenzene," *Merck*, Version 6.9, Dec. 18, 2024. [Online]. Available: www.sigma-aldrich.com.

[55] A. Albertin and T. Obreza, “SL220/SS439: Preparing and Storing an Emergency Safe Drinking Water Supply,” edis.ifas.ufl.edu, Aug. 13, 2020. https://edis.ifas.ufl.edu/publication/SS439

[56] U.S. Environmental Protection Agency, *Community Guide to Air Stripping*, EPA-542-F-21-001, Office of Land and Emergency Management, 2021. [Online]. Available: https://semspub.epa.gov/work/HQ/401577.pdf

[57] Donau Carbon US LLC, *Activated Carbon for Waste Water Treatment*, Donau Carbon US LLC, Dunnellon, FL, [Online]. Available: https://www.donau-carbon-us.com/Downloads/Waste-Water-E.aspx.

[58] U.S. Environmental Protection Agency, "Holding Time & Preservation," EPA, Oct. 2024. [Online]. Available: https://www.epa.gov/hw-sw846/holding-time-preservation

[59] U.S. Environmental Protection Agency, *Estimating Air Emissions from Wastewater Collection and Treatment*, vol. II, ch. 5, Emission Inventory Improvement Program, Mar. 1997. [Online]. Available: https://www.epa.gov/sites/default/files/2015-08/documents/ii05.pdf

[60] JSC NC KazMunayGas, “Implementation of the Joint Kazakh-Russian Project ‘Production of Butadiene and Its Derivatives,’” *Www.kmg.kz*, Nov. 15, 2022. https://www.kmg.kz/en/press-center/press-releases/implementation-of-the-joint-kazakh-russia-projec-production-of-butadiene-and-its-derivatives//

[61] “Petrochemical industry,” *Invest.gov.kz*, 2023. https://atyrau.invest.gov.kz/doing-business-here/regulated-sectors/oil/.

[62] “Key labor indicators in the Republic of Kazakhstan (2022),” *stat.gov.kz*. https://stat.gov.kz/en/industries/labor-and-income/stat-wags/publications/56840/

[63] “The special economic zone ‘National Industrial Petrochemical Technopark,’” *Westdala.kz*, 2018. https://westdala.kz/en/project/sez-nipt-45/ .

[64] "[file] Country Disaster Risk Profile of the Republic of Kazakhstan (98474)," *Preventionweb.net*, 2025. https://www.preventionweb.net/media/98474/download?startDownload=20250417.

[65] "Казахстанские железные дороги," *@livejournal*, 2017. https://ru-railway.livejournal.com/3137242.html.

[66] J. C. Mecklenburgh and J. C. Mecklenburgh, "Process Plant Layout," *Journal of Pressure Vessel Technology*, vol. 108, no. 2, pp. 245–246, May 1986, doi: https://doi.org/10.1115/1.3264778.

[67] "Invest 1.1 billion! The integrated project with an annual output of 240,000 tons of Luxi Chemical is about to start construction," *Soviek-chemical.com*, 2023. https://www.soviek-chemical.com/news/news3.html?utm.

[68] "Amine-based post-combustion capture," *GCCA*. https://gccassociation.org/cement-and-concrete-innovation/carbon-capture-and-utilisatio/amne-based-post-combustion-capture/

[69] "Об утверждении технического регламента 'Требования к безопасности токсичных и высокотоксичных веществ' - ИПС 'Әділет,'" *Adilet.zan.kz*, 2025. https://adilet.zan.kz/rus/docs/P1000001219 .

[70] "ECOLOGICAL CODE OF THE REPUBLIC OF KAZAKHSTAN - 'Adilet' LIS," *adilet.zan.kz*. https://adilet.zan.kz/eng/docs/K2100000400

[71] "Об утверждении технического регламента 'Требования к безопасности токсичных и высокотоксичных веществ' - ИПС 'Әділет,'" *Adilet.zan.kz*, 2025. https://adilet.zan.kz/rus/docs/P1000001219.

[72] Jong Hyuk Jeon, A. Belén, J. Lee, and Rajesh Kumar Jyothi, "Hydrometallurgical process development to recycle valuable metals from spent SCR deNOX catalyst," *Scientific Reports*, vol. 11, no. 1, Nov. 2021, doi: https://doi.org/10.1038/s41598-021-01726-0.

[73] Basel Convention, *Technical Guidelines on the Environmentally Sound Management of Spent Catalysts from Petroleum Refining Industries*, United Nations Environment Programme, 2003.

[74] "Ethylbenzene | China | Manufacturer | career henan chemical co," *chemicalbook*, 2019. https://www.chemicalbook.com/ProductDetail_EN_620351.htm.

[75] "Ethylbenzene exports by country |2023," *Worldbank.org*, 2023. https://wits.worldbank.org/trade/comtrade/en/country/ALL/year/2023/tradeflow/Exports/parner/WLD/product/290260.

[76] "CAS No. 100-42-5 Polystyrene Raw Material High Quality Fast Delivery Factory Supply Styrene," *Made-in-China.com*, 2025. https://nearchem.en.made-in-china.com/product/xFKfolaDCSpB/China-CAS-No-100-45-Polyst
rene-Raw-Material-High-Quality-Fast-Delivery-Factory-Supply-Styrene.html.

[77] "Toluene Price List in Global Market - ECHEMI," *www.echemi.com*.https://www.echemi.com/pip/toluene-temppid160704000607.html

[78] G. Towler and R. Sinnott, "Chapter 7 - Capital Cost Estimating," *ScienceDirect*, Jan. 01, 2013. https://www.sciencedirect.com/science/article/pii/B9780080966595000079?via%3Dihub

[79] "Chinese Yuan to US Dollar History: 2024," *Exchangerates.org.uk*, 2024. https://www.exchangerates.org.uk/CNY-USD-spot-exchange-rates-history-2024.html.

[80] C. Maxwell, "Cost Indices – Towering Skills," *toweringskills.com*, May 28, 2020. https://toweringskills.com/financial-analysis/cost-indices/

[81] Trading Economics, "Natural Gas – Price – Chart – Historical Data – News," Trading Economics. [Online]. Available: https://tradingeconomics.com/commodity/natural-gas.

[82] Daryo News, "Kazakhstan leads with lowest global natural gas prices: $0.07 per cubic meter," *Daryo News*, May 28, 2024. [Online]. Available: https://daryo.uz/en/2024/05/28/kazakhstan-leads-with-lowest-global-natural-gas-prices-07-per-cubic-meter

[83] GlobalPetrolPrices.com, "Kazakhstan electricity prices, September 2024," GlobalPetrolPrices.com. [Online]. Available: https://www.globalpetrolprices.com/Kazakhstan/electricity_prices/.

[84] Invest.gov.kz, "Special Economic Zones," Invest in Kazakhstan. [Online]. Available: https://invest.gov.kz/doing-business-here/fez-and/the-list-of-sez-and/.

[85] National Center for Biotechnology Information, "Toluene," *PubChem*, CID 1140. [Online]. Available: https://pubchem.ncbi.nlm.nih.gov/compound/Toluene.

[86] National Center for Biotechnology Information, "Benzene," *PubChem*, CID 241. [Online]. Available: https://pubchem.ncbi.nlm.nih.gov/compound/Benzene.

[87] W. M. Haynes, *CRC Handbook of Chemistry and Physics*, 95th ed., CRC Press LLC, Boca Raton, FL, 2014-2015.

[88] W. M. Haynes, *CRC Handbook of Chemistry and Physics*, 94th ed., CRC Press LLC, `Boca Raton, FL, 2013-2014, pp. 3-34.

[89] International Labour Organization (ILO), "Hydrogen," *ICSC 0001*, April 2014. [Online]. Available: https://www.ilo.org/dyn/icsc/showcard.display?p_version=2&p_card_id=0001.

[90] R. H. Perry, D. W. Green, and J. O. Maloney, *Perry's Chemical Engineers' Handbook*, 9th ed. New York, NY: McGraw-Hill, 2008.

[91] S. C. Pak and W. B. Kay, "Gas-liquid critical temperatures of mixtures. Benzene + n-alkanes and hexafluorobenzene + n-alkanes," *Industrial & Engineering Chemistry Fundamentals*, vol. 11, p. 255, 1972.

[92] D. M. VonNiederhausern, G. M. Wilson, and N. F. Giles, "Critical Point and Vapor Pressure Measurements at High Temperatures by Means of a New Apparatus with Ultralow Residence Times," *Journal of Chemical & Engineering Data*, vol. 45, pp. 157-160, 2000.

[93] H. K. Onnes, C.-A. Crommelin, and P. G. Cath, "Isothermals of diatomic substances and their binary mixtures. XIX. A preliminary determination of the critical point of hydrogen," *Proceedings of the Royal Netherlands Academy of Arts and Sciences*, vol. 20, pp. 178-184, 1917.

[94] A. S. Teja and D. J. Rosenthal, "The critical pressures and temperatures of twelve substances using a low residence time flow apparatus," *AIChE Symposium Series*, vol. 86, no. 279, pp. 133-137, 1990.

[95] M. B. Ewing, M. L. McGlashan, and P. Tzias, "Phase equilibria, and critical temperatures and pressures, of fluid (benzene + hexafluorobenzene)," *Journal of Chemical Thermodynamics*, vol. 13, p. 527, 1981.

[96] M. D. Larranaga, R. J. Lewis Sr., and R. A. Lewis, *Hawley's Condensed Chemical Dictionary*, 16th ed., p. 576. Hoboken, NJ: John Wiley & Sons, 2016.

[97] J. A. Riddick, W. B. Bunger, and T. K. Sakano, *Techniques of Chemistry*, 4th ed., vol. II, *Organic Solvents*, New York, NY: John Wiley and Sons, 1985, p. 187.

[98] Engineering Toolbox, "Gases - Dynamic Viscosities," [Online]. Available: https://www.engineeringtoolbox.com/gases-absolute-dynamic-viscosity-d_1888.html.

[99] H. Watanabe, "Further examination of the transient hot-wire method for the simultaneous measurement of thermal conductivity and thermal diffusivity," *Metrologia*, vol. 39, pp. 65-81, 2002.

[100] T. E. Daubert, R. P. Danner, H. M. Sibul, and C. C. Stebbins, *Physical and Thermodynamic Properties of Pure Compounds: Data Compilation, extant 1994 (core with 4 supplements)*, Taylor & Francis, Bristol, PA, 1994. [Online]. Available: https://chemistry.mdma.ch/hiveboard/rhodium/pdf/chemical-data/thermcond_liquids.pdf

[101] Engineering Toolbox, "Hydrogen - Thermal conductivity vs. temperature and pressure," [Online]. Available: https://www.engineeringtoolbox.com/hydrogen-H2-thermal-conductivity-temperature-pressure-d_2106.html.

[102] D. T. Jamieson and J. S. Tudhope, "A simple device for measuring the thermal conductivity of liquids with moderate accuracy," *J. Inst. Pet.*, vol. 50, pp. 150-153, 1964.

[103] The thermal conductivity of liquids - IV. Temperature dependence of thermal conductivity, "The thermal conductivity of liquids - IV. Temperature dependence of thermal conductivity," *Int. J. Heat Mass Transfer*, vol. 10, pp. 1075-1088, 1967.

[104] J.-L. Fortier and G. C. Benson, "Heat capacities of some binary aromatic hydrocarbon mixtures containing benzene or toluene," *Journal of Chemical & Engineering Data*, vol. 24, no. 1, pp. 34-37, 1979.

[105] Regional Activity Centre for Cleaner Production (REMPEC), "Styrene monomer (inhibited)," [Online]. Available: https://midsis.rempec.org/en/find-chemical/styrene-monomer-inhibited.

[106] M. W. Chase, Jr., *NIST-JANAF thermochemical tables* (4th ed.), *Journal of Physical and Chemical Reference Data*, Monograph 9, pp. 1-1951, 1998.

[107] R. Paramo, M. Zouine, and C. Casanova, "Saturated heat capacities of some linear and branched alkyl-benzenes between 288 and 348 K," *Int. J. Thermophys.*, vol. 24, pp. 185-199, 2003.

[108] H. Kawaji, "Study of molecular dynamics in some crystals using calorimetry," M.Sc. thesis, Graduate School of Science, Osaka University, 1986.

[109] J. A. Dean, *Lange's Handbook of Chemistry*, 17th ed. New York: McGraw-Hill, 1999.

[110] N. S. Osborne and D. C. Ginnings, "Measurements of Heat of Vaporization and Heat Capacity for a Number of Hydrocarbons," *Journal of Research of the National Bureau of Standards (U.S.)*, vol. 39, pp. 453, 1947.

[111] K. S. Pitzer, L. Guttman, and E. F. Westrum, "The Heat Capacity, Heats of Fusion and Vaporization, Vapor Pressure, Entropy, Vibrational Frequencies, and Barrier to Internal Rotation of Styrene," *Journal of the American Chemical Society*, vol. 68, pp. 2209-2212, 1946.

[112] R. Jochems, H. Dekker, C. Mosselman, and G. Somsen, "The Use of the LKB 8721-3 Vaporization Calorimeter to Measure Enthalpies of Sublimation: The Enthalpies of Sublimation of Bicyclo[2.2.1]hept-2-ene (Norbornene), Bicyclo[2.2.1]heptane (Norbornane), and Related Compounds," *Journal of Chemical Thermodynamics*, vol. 14, pp. 395-398, 1982.

[113] R. Sabbah, I. Antipine, M. Cotten, and L. Davy, "Some Reflections on the Calorimetric Measurement of the Enthalpy of Sublimation or Vaporization," *Thermochimica Acta*, vol. 115, pp. 153-165, 1987.

[114] R. B. Scott and F. G. Brickwedde, "Thermodynamic properties of solid and liquid ethylbenzene from 0 to 300K," *Journal of Research*, vol. NBS 35, pp. 501-512, 1945.

[115] Cheméo, "Styrene (CAS 100-42-5) - Chemical & Physical Properties," [Online].

Available: https://www.chemeo.com/cid/24-192-2/Styrene.

[116] D. R. Lide, Ed., *CRC Handbook of Chemistry and Physics*, 80th ed., CRC Press, Boca Raton, FL, 1999.

[117] D. W. Scott, G. B. Guthrie, J. F. Messerly, S. S. Todd, W. T. Berg, I. A. Hossenlopp, and J. P. McCullough, "Toluene: Thermodynamic Properties, Molecular Vibrations, and Internal Rotation," *Journal of Physical Chemistry*, vol. 66, pp. 911-914, 1962.

[118] G. D. Oliver, M. Eaton, and H. M. Huffman, "The heat capacity, heat of fusion, and entropy of benzene," *Journal of the American Chemical Society*, vol. 70, pp. 1502-1505, 1948.

[119] T. S. Akhundov, S. Y. Imanova, and N. N. Bairamova, "Ortobaric Specific Volumes and Heat Vaporizations of Ethylbenzene and Para-xylene," *Izvestiya Vysshikh Uchebnykh Zavedenii, Neft i Gaz*, vol. 19, pp. 38-74, 1976.

[120] E. G. Konakbaeva, Z. K. Anisimova, and M. I. Shakhparonov, "High-Precision Measurements of the Vapour Pressures of Binary Nonelectrolyte Solutions," *Vestnik Moskovskogo Universiteta, Series 2: Khimiya (Chemistry)*, vol. 15, pp. 30-36, 1974.

[121] F. Hovorka and D. Dreisbach, "Vapor Pressure of Binary Systems: I. Benzene and Acetic Acid," *Journal of the American Chemical Society*, vol. 56, pp. 1664-1666, 1934.

[122] C. Lopez-Lazaro, P. Bachaud, I. Moretti, and N. Ferrando, “Predicting the phase behavior of hydrogen in NaCl brines by molecular simulation for geological applications,” *BSGF - Earth Sciences Bulletin*, vol. 190, p. 7, 2019, doi: https://doi.org/10.1051/bsgf/2019008.

[123] A. Aucejo, S. Loras, V. Martínez-Soria, N. Becht, and G. Del Río, “Isobaric Vapor−Liquid Equilibria for the Binary Mixtures of Styrene with Ethylbenzene, o-Xylene, m-Xylene, and p-Xylene,” Journal of Chemical & Engineering Data, vol. 51, no. 3, pp. 1051–1055, Mar. 2006, doi: https://doi.org/10.1021/je050523s.

[124] Roshi Dahal, Petri Uusi-Kyyny, Juha-Pekka Pokki, and Ville Alopaeus, “Isobaric Vapor–Liquid Equilibrium of the Binary Mixtures Toluene + Styrene and Styrene + α-Methylstyrene,” Journal of Chemical & Engineering Data, vol. 68, no. 3, pp. 654–663, Feb. 2023, doi: https://doi.org/10.1021/acs.jced.2c00662.

[125] H. L. Clever and M. E. Battino, "IUPAC-NIST Solubility Data Series. 5/6. Krypton,

Xenon and Radon - Gas Solubilities," *NIST Standard Reference Database*, 1979. [Online]. Available: https://srdata.nist.gov/solubility/IUPAC/SDS-5-6/SDS-5-6.pdf.

[126] J. L. Lane, "IUPAC-NIST Solubility Data Series. 38. Hydrocarbons with Water and Seawater - Part 1," *NIST Standard Reference Database*, 1995. [Online]. Available: https://srdata.nist.gov/solubility/IUPAC/SDS-38/SDS-38-pages_1.pdf.

[127] R. A. Meyers, *Handbook of petrochemical production processes*. United States: The McGraw-Hill Companies, 2005.

[128] P. Sharma, R. Dwivedi, R. Dixit, M. Batra, and R. Prasad, "Mechanism evolution for the oxidative dehydrogenation of ethyl benzene to styrene over V2O5/TiO2 catalyst: computational and kinetic approach," *RSC Advances*, vol. 5, no. 50, pp. 39635–39642, Jan. 2015, doi: 10.1039/c5ra00446b.

[129] D. E. Collins and F. A. Richey, "Synthetic Organic Chemicals," *Springer eBooks*, pp. 800–862, Jan. 1992, doi: https://doi.org/10.1007/978-94-011-7691-0_22.

[130] J. A. Sidwell and B. G. Willoughby, "Examination of styrene-divinylbenzene ion-exchange resins, used in contact with food, for potential migrants," *Food Additives and Contaminants*, vol. 23, no. 7, pp. 726–737, Jul. 2006, doi: https://doi.org/10.1080/02652030600576189.

[131] R. Canterel, J. Lalevée, E. Bourgeat‐Lami, E. Lacôte, and M. Lansalot, "Visible‐Light Initiated Dispersion Photopolymerization of Styrene," *Angewandte Chemie International Edition*, vol. 62, no. 47, Oct. 2023, doi: https://doi.org/10.1002/anie.202309674.

[132] ResearchInChina, "China Styrene Market Report, 2014." [Online]. Available: http://www.researchinchina.com/Htmls/Report/2014/7941.html

[133] ICIS, "Chemical profile: Europe styrene," *ICIS Chemical Business*, Feb. 12, 2021. [Online]. Available: https://www.icis.com/subscriber/icb/2021/02/12/10605927/chemical-profile-europe-styrene/

[134] Plastinfo.ru, "Company profile of Rosneft Polymers," Plastinfo.ru. [Online]. Available: https://plastinfo.ru/com/17972/.

[135] OAO "Plastic", "English version," OAO "Plastic." [Online]. Available:

https://oaoplastic.ru/english-version.

[136] Plastinfo.ru, "Company profile of Nizhnekamskneftekhim," Plastinfo.ru. [Online]. Available: https://plastinfo.ru/com/5189/.

[137] "Career Henan Chemical Co," ChemicalBook. [Online]. Available: https://www.chemicalbook.com/manufacturer/coreychem/.

[138] "Ethylbenzene CAS100-41-4 | China | Manufacturer | Zhuozhou Wenxi import and Export Co., Ltd," *Chemicalbook*.

[139] "Polymers of styrene, in primary forms, nes imports by country |2023." https://wits.worldbank.org/trade/comtrade/en/country/ALL/year/2023/tradeflow/Imports partner/WLD/product/390390#

[140] A. C. Dimian and C. S. Bildea, "Energy Efficient Styrene Process: Design and Plantwide Control," *Ind. Eng. Chem. Res.*, vol. 58, no. 12, pp. 4890–4905, 2019, doi: 10.1021/acs.iecr.8b05560.

[141] Atlas Steels, *Stainless Steel Grade Datasheets*, Aug. 2013. [Online]. Available: https://www.atlassteels.com.au/documents/Atlas%20Grade%20datasheet%20-%20all%0datasheets%20rev%20Aug%202013.pdf.

[142] Special Metals Corporation, *INCOLOY® Alloy 800 Technical Bulletin*, [Online]. Available: https://www.specialmetals.com/documents/technical-bulletins/incoloy/incoloy-alloy-800.pdf.

[143] Editor Engineeringtoolbox, "Process Pipes - Allowable Stress vs. Temperature," Apr. 08, 2024. https://www.engineeringtoolbox.com/temperature-allowable-stresses-pipes-d_1338.html

[144] X. L. I. & E. Co. Ltd, "Joint Efficiency Or Joint Quality Factor - News - News - XI'AN LINHUI IMPORT & EXPORT CO., LTD," Aug. 04, 2022. https://www.lksteelpipe.com/news/joint-efficiency-or-joint-quality-factor-59777852.html

[145] "Pipe Thickness Calculator as per ASME B31.3," *The Piping Engineering World*, Jun. 29, 2023. https://www.pipingengineer.org/pipe-thickness-calculator/

APPENDICES

Appendix A

A.1 Pure component properties

Table A1. Pure component physical and thermodynamic properties under standard conditions

		Ethylbenzene	**Styrene**	**Hydrogen**	**Toluene**	**Benzene**
Molecular weight (g/mol)	**Literature**	106.16 [6]	104.15 [1]	2.016 [10]	92.14 [85]	78.11 [86]
	Aspen	106.1674	104.15152	2.01588	92.141	78.114
Density (kg/m3)	**Literature**	862.6 [87]	901.6 [87]	0.082 [87]	862.3 [87]	875.6 [88]
	Aspen	862.2703	901.3944	0.0823583	863.9338	872.073
Boiling point (°C)	**Literature**	136.2 [87]	145.3 [87]	-253 [89]	110.6 [87]	80.08 [88]
	Aspen	136.16	145.16	-252.76	110.63	80.09
Melting point (°C)	**Literature**	-94.95 [87]	-30.65 [87]	-259 [89]	-94.9 [87]	5.558 [88]
	Aspen	-94.95	-30.61	-259.2	-94.97	5.53
Critical temperature (°C)	**Literature**	344 [90]	362.85 [90]	-239.96 [90]	318.6 [94]	288.9 [90]
	Aspen	344.11	362.85	-239.96	318.6	288.9
Critical pressure (Pa)	**Literature**	3.65×10^{6} [91]	3.87×10^{6} [92]	1.3×10^{6} [93]	$4.11\times$ [94]	4.89×10^{6} [95]

	Aspen	3.6×10^{6}	3.87×10^{6}	1.3×10^{6}	4.1×10^{6}	4.8×10^{6}
Viscosity (Pa*s)	**Literature**	6.4×10^{-4} [96]	6.96×10^{-4} [97]	8.9×10^{-6} [98]	5.6×10^{-4} [87]	6.04×10^{-4} [88]
	Aspen	6.35×10^{-4}	7.023×10^{-4}	8.91×10^{-6}	5.54×10^{-4}	5.99×10^{-4}
Thermal conductivity (W/(m*K)	**Literature**	0.13 [99]	0.137 [100]	0.185 [101]	0.1302 [102]	0.1422 [103]
	Aspen	0.128974374	0.136527	0.1781205	0.1307867	0.14259
Specific heat capacity (J/(kg*K)	**Literature**	1756.44 [104]	1747.5 [105]	14305 [106]	1707.18472 [107]	1739.0859 [108]
	Aspen	1749.29	1740.75	14271.13	1707.1	1736.45
Enthalpy of formation (kJ/mol)	**Literature**	29.92 [90]	147.4 [90]	0 [119]	50.17 [90]	82.88 [90]
	Aspen	29.921	147.2	0	50.17	82.88
Gibbs free energy of formation (kJ/mol)	**Literature**	130.73 [90]	213.9 [90]	0 [109]	122.2 [90]	129.6 [90]

	Aspen	130.73	213.9	0	122.2	129.6
Enthalpy of vaporization (kJ/mol)	**Literature**	42.25 [110]	43.9 [111]	N/A	37.79 [112]	33.8 [113]
	Aspen	42.32	44.419	N/A	37.932	33.871
Enthalpy of fusion (kJ/mol)	**Literature**	9.18 [114]	10.955 [115]	0.11736 [116]	6.636 [117]	9.8663 [118]
	Aspen	9.173	10.950	0.117	6.636	9.866
Vapor pressure (Pa)	**Literature**	1268.4 [119]	841.26 [111]	N/A	3800 [120]	12650 [121]
	Aspen	1279.488	830.9172	N/A	3803.901	12640

A.2 Temperature-dependant properties plots

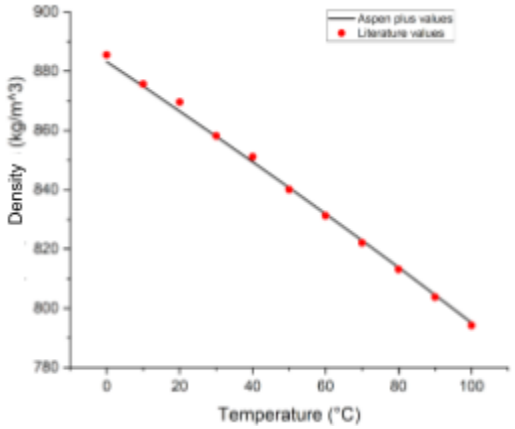

Figure A1. Density vs Temperature plot for Ethylbenzene

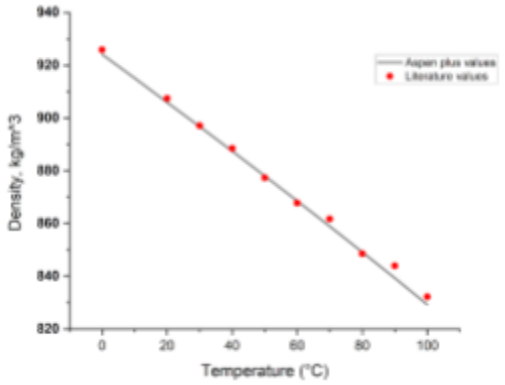

Figure A2. Density vs Temperature plot for Styrene

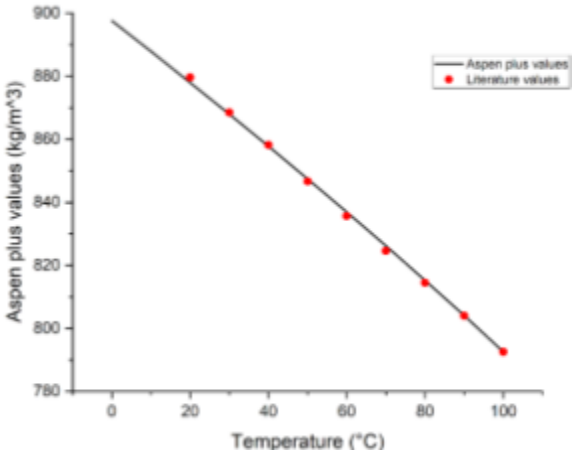

Figure A3. Density vs Temperature plot for Benzene

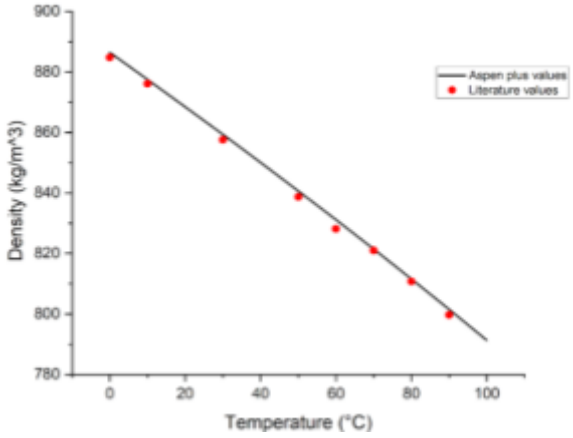

Figure A4. Density vs Temperature plot for Toluene

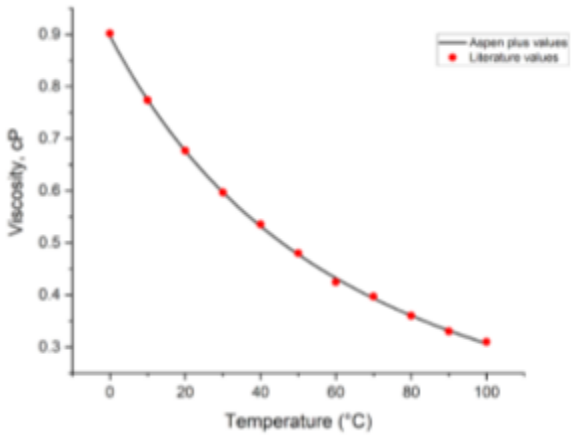

Figure A5. Viscosity vs Temperature plot for Ethylbenzene

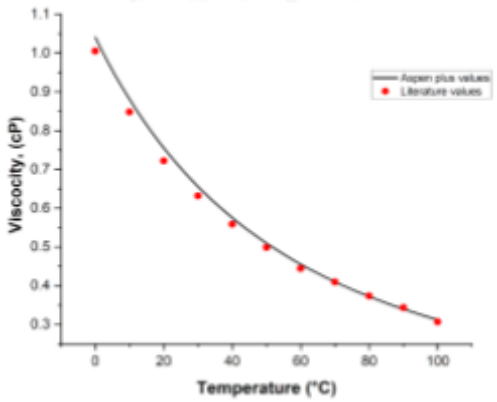

Figure A6. Viscosity vs Temperature plot for Styrene

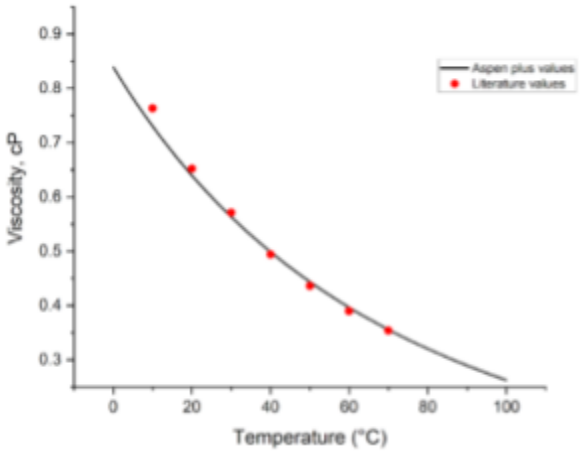

Figure A7. Viscosity vs Temperature plot for Benzene

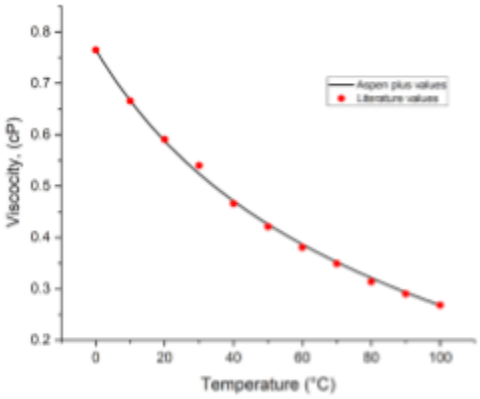

Figure A8. Viscosity vs Temperature plot for Toluene

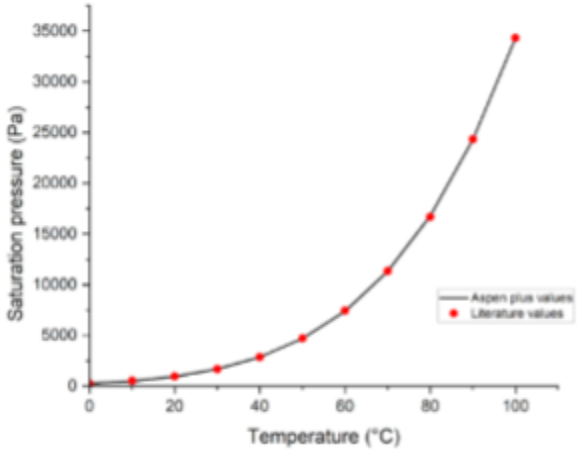

Figure A9. Saturation pressure vs Temperature plot for Ethylbenzene

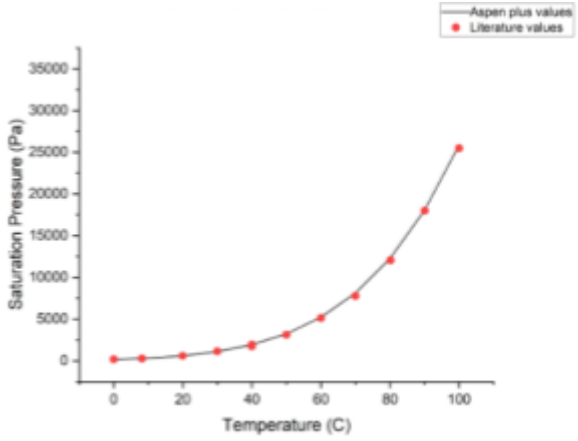

Figure A10. Saturation pressure vs Temperature plot for Styrene

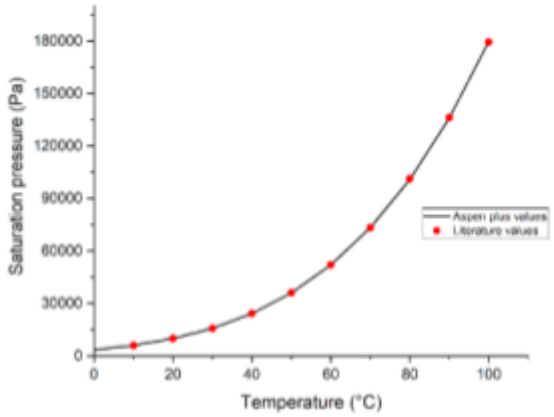

Figure A11. Saturation pressure vs Temperature plot for Benzene

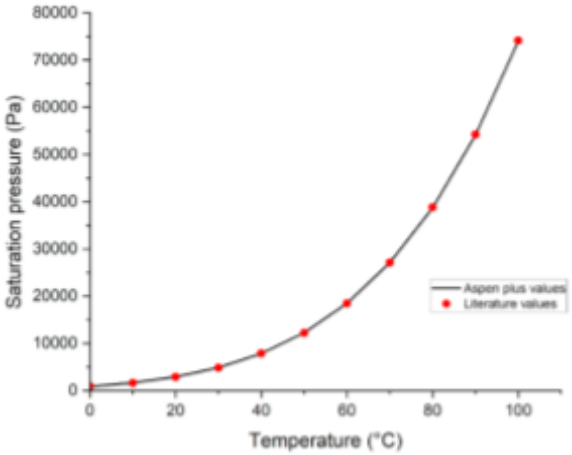

Figure A12. Saturation pressure vs Temperature plot for Toluene

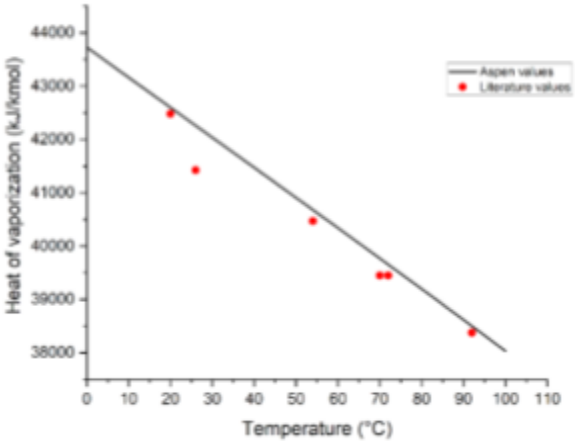

Figure A13. Heat of vaporization vs Temperature plot for Ethylbenzene

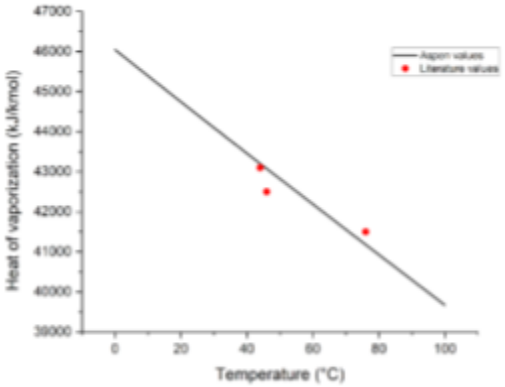

Figure A14. Heat of vaporization vs Temperature plot for Styrene

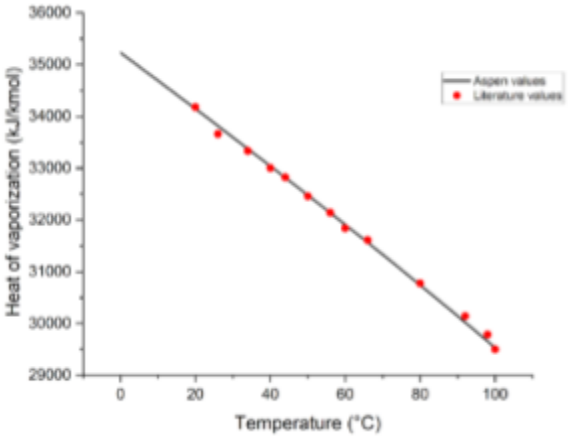

Figure A15. Heat of vaporization vs Temperature plot for Benzene

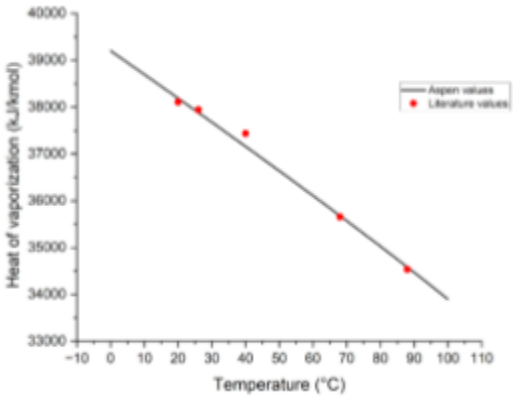

Figure A16. Heat of vaporization vs Temperature plot for Toluene

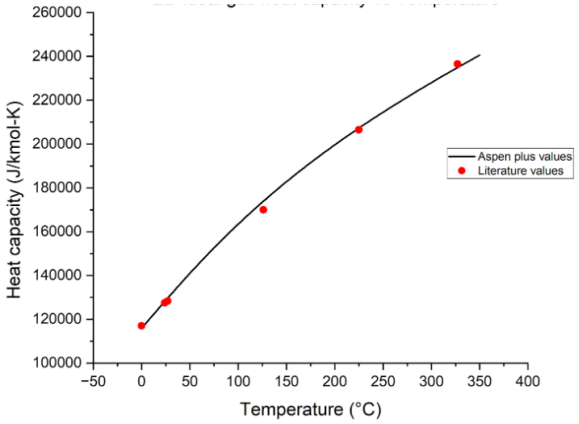

Figure A17. Ideal gas heat capacity vs Temperature plot for Ethylbenzene

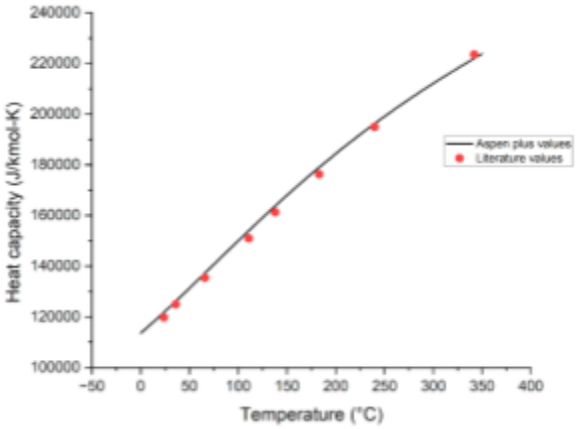

Figure A18. Ideal gas heat capacity vs Temperature plot for Styrene

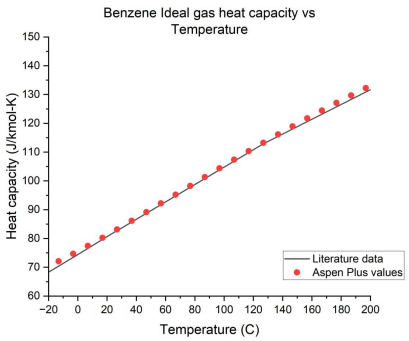

Figure A19. Ideal gas heat capacity vs Temperature plot for Benzene

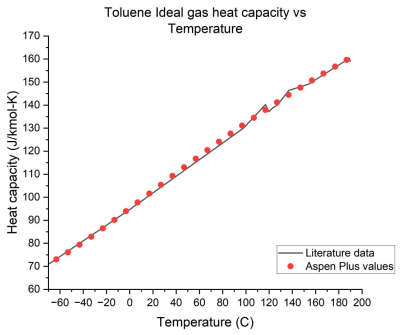

Figure A20. Ideal gas heat capacity vs Temperature plot for Toluene

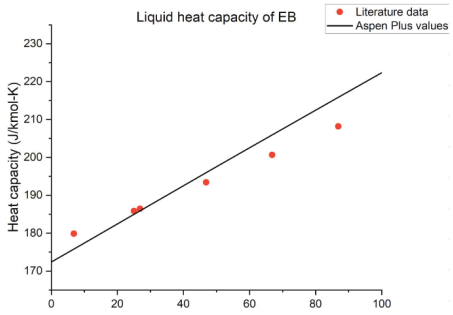

Figure A21. Liquid heat capacity vs Temperature plot for EB

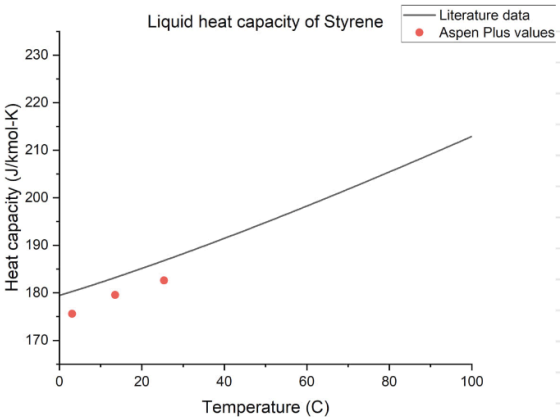

Figure A22. Liquid heat capacity vs Temperature plot for Styrene

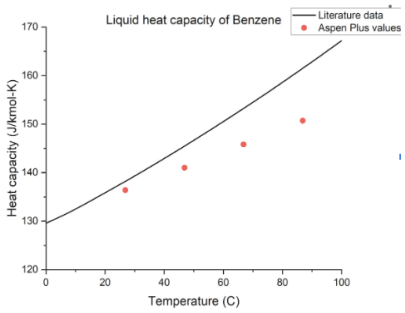

Figure A23. Liquid heat capacity vs Temperature plot for Benzene

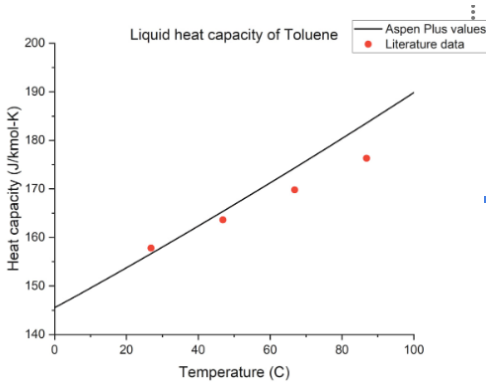

Figure A24. Liquid heat capacity vs Temperature plot for Benzene

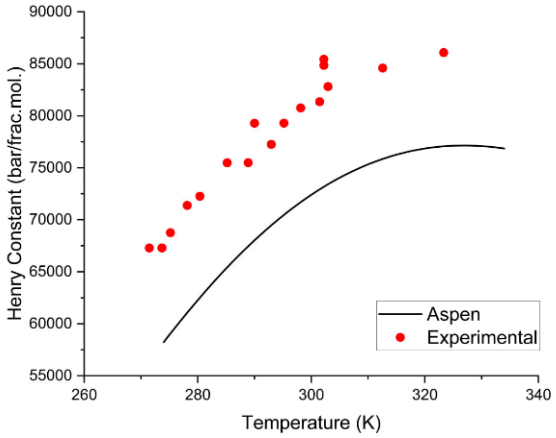

Figure A25. Henry constant vs Temperature plot for H2/H2O system [122]

Appendix B

B.1 Validation of the thermodynamic model

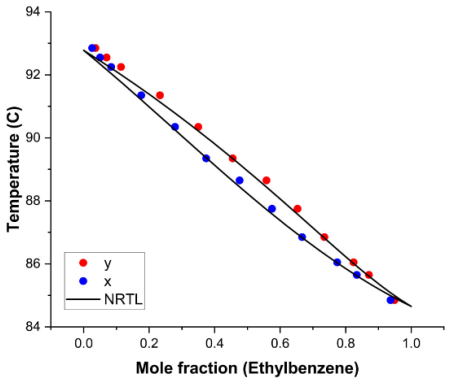

Figure B1. VLE for EB/ST binary mixture for NRTL method at 20 kPA

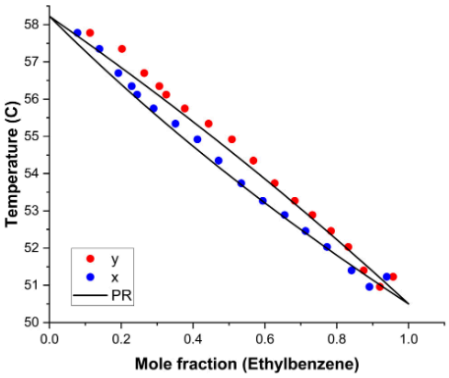

Figure B4. VLE for EB/ST binary mixture for Peng-Robinson method at 5 kPA [123]

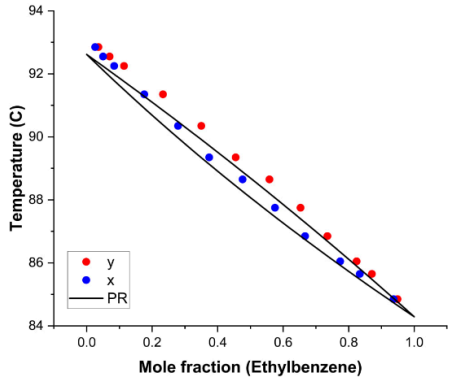

Figure B2. VLE for EB/ST binary mixture for Peng-Robinson method at 20 kPA

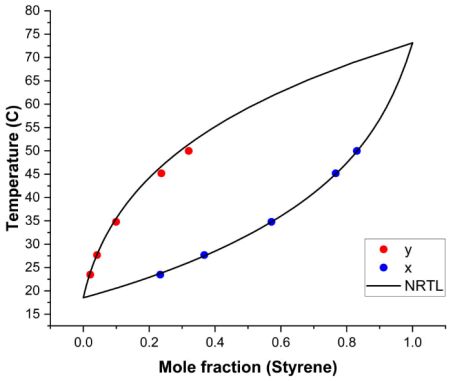

Figure B5. VLE for ST/B binary mixture for NRTL method at 9.3 kPA

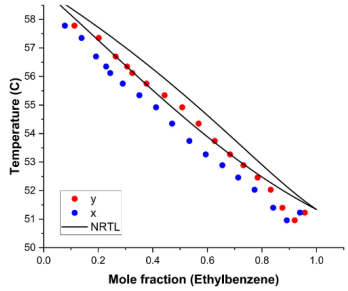

Figure B3. VLE for EB/ST binary mixture for NRTL method at 5 kPA [123]

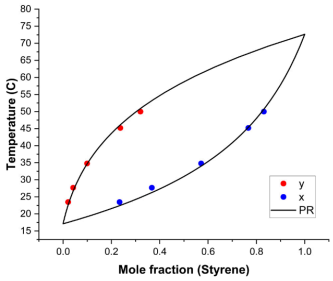

Figure B6. VLE for ST/B binary mixture for Peng-Robinson method at 9.3 kPA

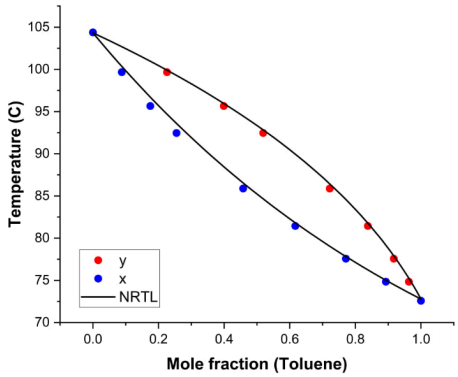

Figure B7. VLE for ST/T binary mixture for NRTL method at 30 kPA

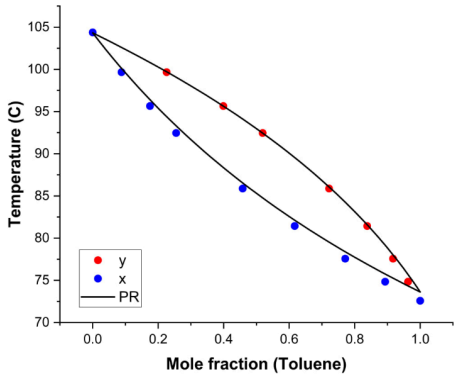

Figure B8. VLE for ST/T binary mixture for Peng-Robinson method at 30 kPA

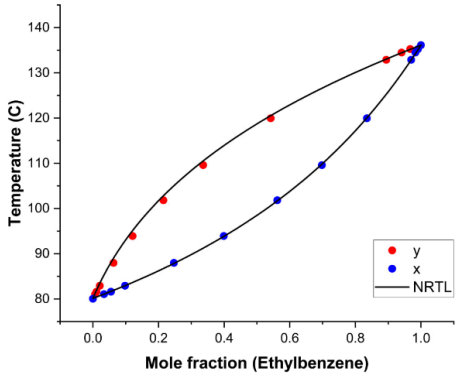

Figure B9. VLE for EB/B binary mixture for NRTL method at 101.32 kPA

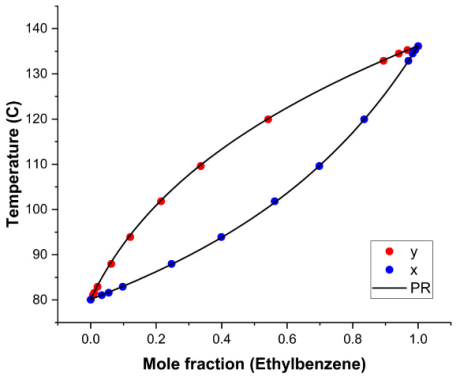

Figure B10. VLE for EB/B binary mixture for Peng-Robinson method at 101.32 kPA

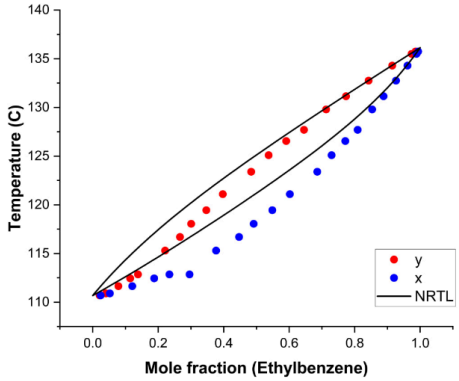

Figure B11. VLE for EB/T binary mixture for NRTL method at 101.325 kPA [124]

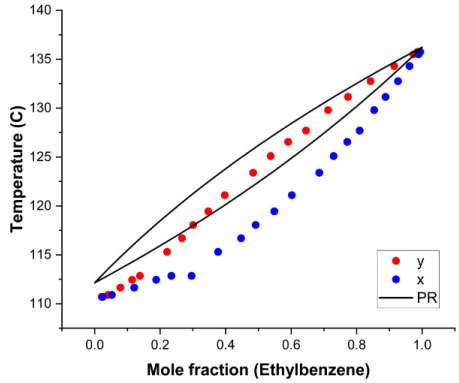

Figure B12. VLE for EB/T binary mixture for Peng-Robinson method at 101.325 kPA [124]

Appendix C

C.1 Tables with hazard profiles of benzene and toluene

Table C1. Benzene hazard profile

GHS standards [125]			
H225 (99.7%)	Highly flammable liquid and vapor		
H304 (99.3%)	Might be fatal if swallowed		
H315 (99.8%)	Causes skin irritation		
H319 (99.8%)	Causes serious eye irritation		
H340 (99.8%)	May cause genetic defects		
H350 (99.8%)	May cause cancer		
H372 (99.3%)	Repeated exposure might damage organs		
H412 (16.4%)	Harmful to aquatic life in a long term fashion		
Diamond [126]	**Hazard**	**Value**	**Description**
	Health	2	Can cause temporary incapacitation or residual injury
	Flammability	3	Can be ignited under almost all ambient temperature conditions
	Instability	0	Normally stable even under fire
	Special		
Hazard indicating pictograms [127]			
			

Table C2. Toluene hazard profile

GHS standards [128]			
H225 (98.41%)	Highly flammable liquid and vapor		
H304 (99.9%)	Might be fatal if swallowed		
H315 (98.41%)	Causes skin irritation		
H336 (100%)	Narcotic effects; may cause dizziness		
H361 (96.19%)	Might lead to fertility damage or damage the unborn child		
H373 (100%)	Repeated exposure may damage vital organs		
H412 (11.18%)	Harmful to aquatic life in a long term fashion		
Diamond [126]	**Hazard**	**Value**	**Description**
	Health	2	Can cause temporary incapacitation or residual injury
	Flammability	3	Can be ignited under almost all ambient temperature conditions
	Instability	0	Normally stable even under fire
	Special		
Hazard indicating pictograms [127]			
			

Appendix D

D.1 Table with key applications of styrene

Table D1. Summary of the major applications of styrene

Application	Styrene Composition	**KEY CONSIDERATIONS**	**MAIN USE CASES**	**REFERENCES**
Polystyrene production	Styrene	High purity for clarity and consistency, adjust viscosity and polymerization rate	Packaging, disposable housewares insulation	[2]
ABS (acrylonitrile-butadiene-styrene)	Styrene Butadiene, Acrylonitrile	Enhancев impact resistance, control polymerization for toughness and surface finish	Automotive parts, electronics housings, toys	[2]
SBR (styrene-butadiene rubber)	Styrene Butadiene	Optimize abrasion resistance, ensure proper elasticity and durability	Tires, conveyor belts, footwear soles	[3]
UPR (unsaturated polyester resin)	Styrene	Facilitate cross-linking for durability, consistency in viscosity and reactivity	Fiberglass-reinforced plastics, construction	[2]

SAN (styrene-acrylonitrile)	Styrene Acrylonitrile	Achieve chemical resistance, adjust polymerization for stiffness and transparency	Plastic lenses, windows, and transparent household items	[129]
Expanded polystyrene (eps)	pure styrene	Low-density formulation, control purity to avoid defects	Insulation, protective packaging	[2]
Ion-exchange resins	Styrene Divinylbenzene	High purity for efficient ion exchange, tailor composition for specific capacities	Water softening, demineralization,decolourization	[130]
Polystyrene peroxide	Styrene	Photoirradiation of the charge transfer complex between styrene and oxygen	coating and molding compositions	[131]

Appendix E

E.1 Lyuben's proposed design

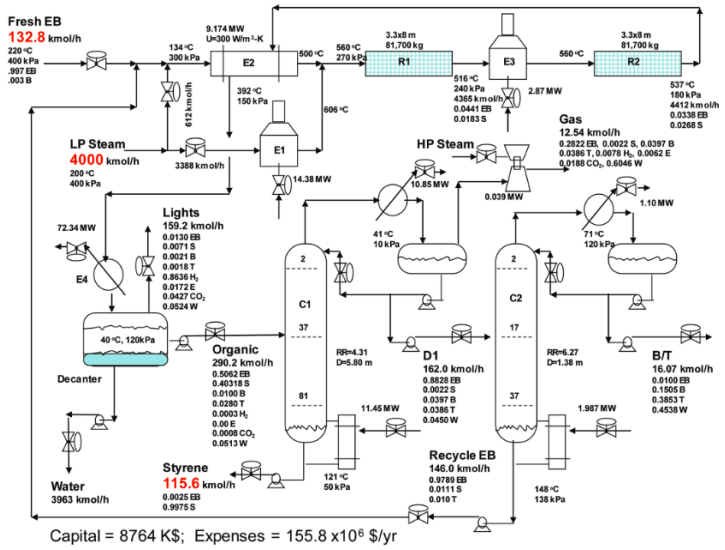

Figure E1. Luyben's proposed design [18]

E.2 Production rates of styrene by country

Table E1. Capacities of factories for styrene production around the world

Manufacturer	Location	Capacity (kt/year)
China [132]		
CSPC	Huizhou	640
ZRCC Lyondell Chemical	Ningbo	620
SECCO	Shanghai	650
Shuangliang Eco-Energy	Jiangyin	420
Jilin Petrochemical	Jilin	460
Dagu Chemical	Tianjin	500
Dushanzi Petrochemical	Karamay	320
Huajin Chemical	Panjin	232
SP Chemical	Taixing	320
Newsolar	Changzhou	250
Europe [133]		

LyondellBasell/Covestro	Maasvlakte, Netherlands	680
Total	Gonfreville, France	600
Versalis	Mantova, Italy	595
BASF	Ludwigshafen, Germany	550
ELLBA	Moerdijk, Netherlands	550
Trinseo	Terneuzen, Netherlands	500
INEOS Styrolution	Antwerp, Belgium	500
Repsol	Tarragona, Spain	450
Shell	Moerdijk, Netherlands	440
Trinseo	Boehlen, Germany	300
Russia		
SIBUR [134]	Perm	135
	Nizhnekamsk	240
JSC “Plastic” [135]	Tula	60
Gazprom [136]	Salavat	220

E.3 Cost of the components

Table E2. Costs of EB in Chinese companies

Company	Purity (%)	USD/kg (2024)	USD/kg (2027)
Career Henan Chemical Co [137]	99<	1	1.19
Zhuozhou Wenxi Import and Export Co., Ltd [138]	99<	10	11.88

Table E3. Costs of Styrene imports in CIS countries (2023) [139]

Country	**Trade Value (1000 USD)**	**Quantity (Kg)**	**Price per MT (USD) (2023)**	**Price per MT (USD) (2027)**

Kazakhstan	2,173.04	748,455	2,903.37	3,450.83
Azerbaijan	1,089.34	847,382	1,285.53	1,527.93
Armenia	263.18	158,297	1,662.57	1,976.06
Kyrgyz Republic	735.49	395,520	1,859.55	2,210.18
		Average	1,927.75	2,216.27

Appendix F

F.1 Kinetics calculations' graphs

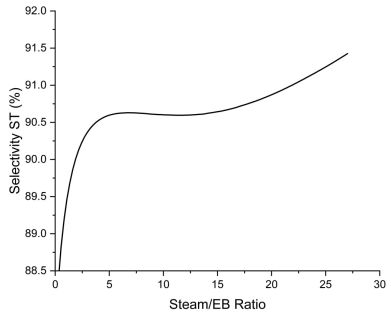

Figure F1. Effect of H2O/EB ratio on the overall selectivity of styrene. T = 620°C. P = 1 atm. W/F = 36,000 kg (1st reactor). W/F = 46,000 kg (2nd reactor)

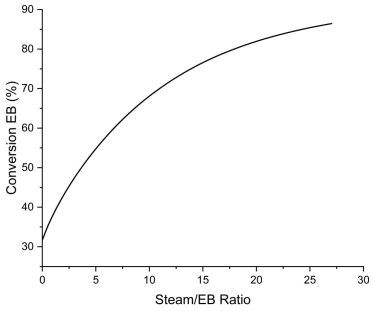

Figure F2. Effect of H2O/EB ratio on the overall conversion of EB. T = 620°C. P = 1 atm. W/F = 36,000 kg (1st reactor). W/F = 46,000 kg (2nd reactor)

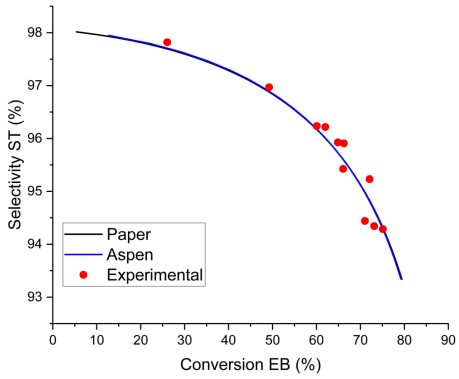

Figure F3. Selectivity of styrene over conversion of ethylbenzene. T = 620°C. Ptot = 0.612 bar. H2O/EB ratio = 11 [140]

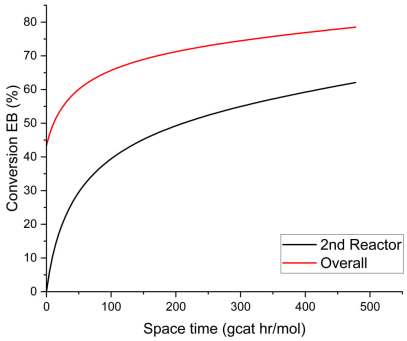

Figure F4. Conversion of the ethylbenzene with the change of catalyst weight. T = 620°C. P = 1 atm. H2O/EB ratio = 12. W/F = 36,000 kg (1st reactor)

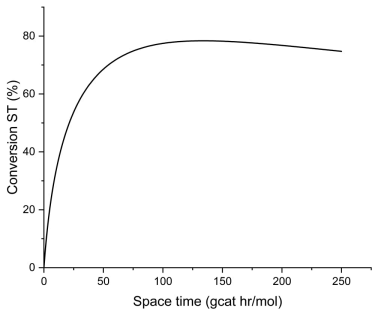

Figure F5. Conversion to the styrene with the change of catalyst weight for the first reactor. T = 620°C. P = 1 atm. H2O/EB ratio = 12

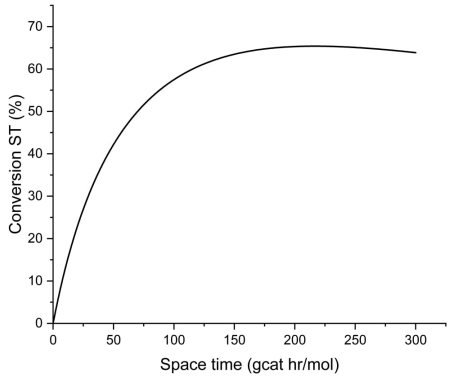

Figure F6. Conversion to the styrene with the change of catalyst weight for the second reactor. T = 620°C. P = 1 atm. H2O/EB rat io = 12. W/F=36,000kg (1st reactor)

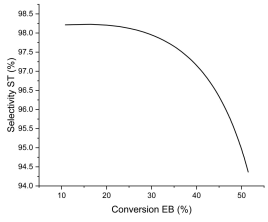

Figure F7. Selectivity of the styrene over conversion EB while changing the catalyst weight in the second reactor. T = 620°C. P = 1 atm. H2O/EB ratio = 12. W/F = 36,000kg (1st reactor)

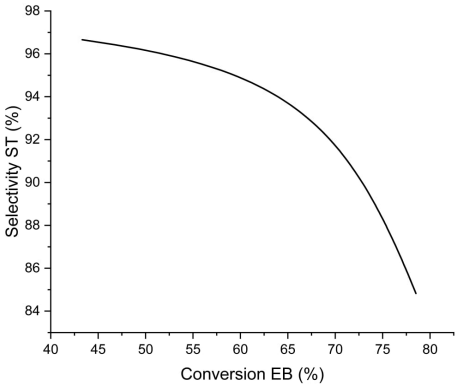

Figure F8. Selectivity of the styrene over conversion EB while changing the catalyst weight in the first reactor. T = 620°C. P = 1 atm. H2O/EB ratio = 12

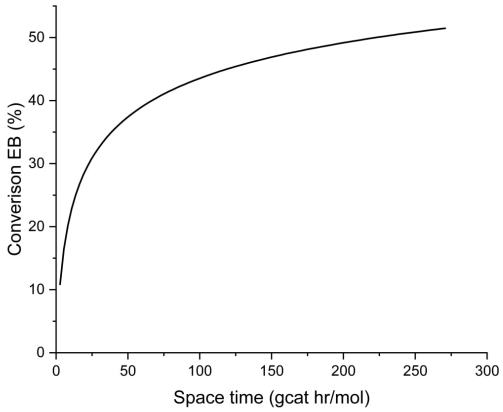

Figure F9. Conversion of the EB over the space-time in the first reactor. T = 620°C. P = 1 atm. H2O/EB ratio = 12

Appendix G

G.1 Heat exchanger design and E-101 details

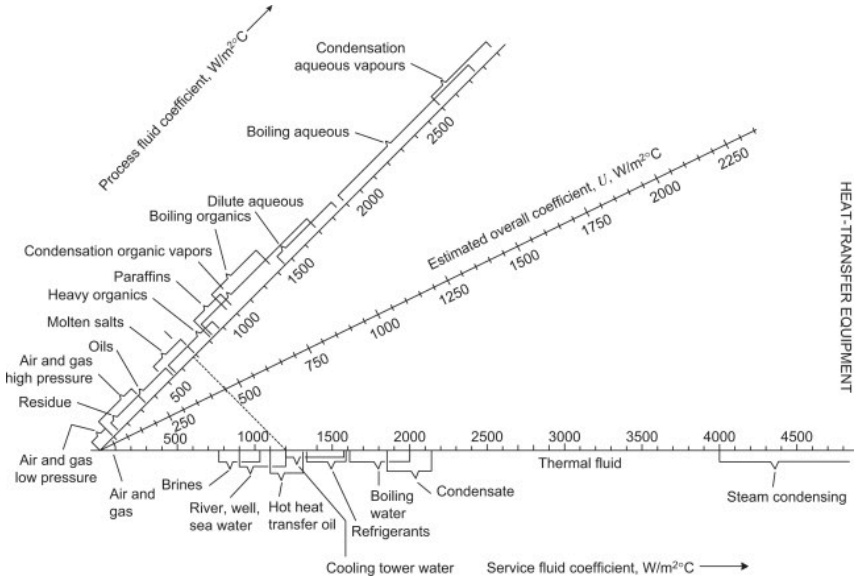

Figure G1. Assumptions of U based on physical nature of fluids.

Outside Diameter (mm)	Wall Thickness (mm)				
16	1.2	1.7	2.1	—	—
19	—	1.7	2.1	2.8	—
25	—	1.7	2.1	2.8	3.4
32	—	1.7	2.1	2.8	3.4
38	—	—	2.1	2.8	3.4
50	—	—	2.1	2.8	3.4

Figure G2. Standard tubes dimensions

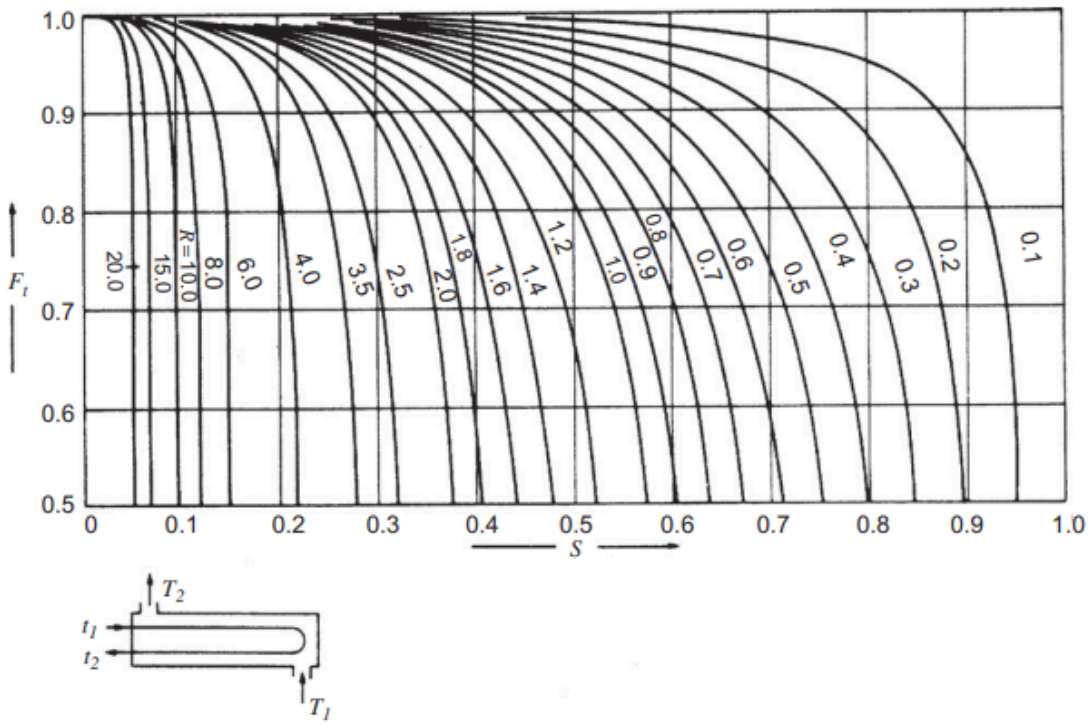

Figure G3. Temperature correction factor graph

$$R = (T_{h,in} - T_{h,out})/(T_{c,out} - T_{c,in}) = 0 \quad \text{(Eq. G.1)}$$

$$P = (T_{c,out} - T_{c,in})/(T_{h,in} - T_{c,in}) = 0.823 \quad \text{(Eq. G.2)}$$

N tubes per pass is 63.

Triangular Pitch, $p_t = 1.25d_o$					
No. Passes	**1**	**2**	**4**	**6**	**8**
K_1	0.319	0.249	0.175	0.0743	0.0365
n_1	2.142	2.207	2.285	2.499	2.675
Square Pitch, $p_t = 1.25d_o$					
No. Passes	**1**	**2**	**4**	**6**	**8**
K_1	0.215	0.156	0.158	0.0402	0.0331
n_1	2.207	2.291	2.263	2.617	2.643

Figure G4. Constants for Use in equation of bundle diameter [40]

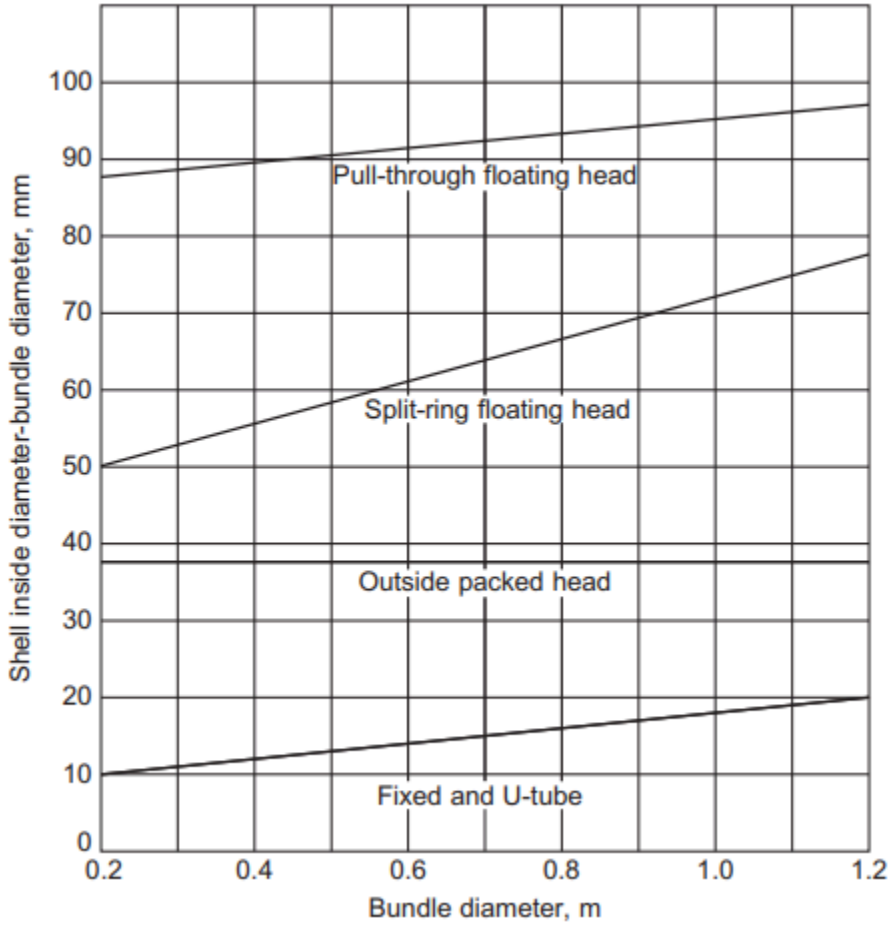

Figure G5. Shell clearances [40]

Nominal Shell Dia., mm	Carbon Steel		Alloy Steel
	Pipe	Plate	
150	7.1	—	3.2
200–300	9.3	—	3.2
330–580	9.5	7.9	3.2
610–740	—	7.9	4.8
760–990	—	9.5	6.4
1010–1520	—	11.1	6.4
1550–2030	—	12.7	7.9
2050–2540	—	12.7	9.5

Figure G6. Shell thicknesses [40]

From this graph, D_S The internal shell diameter is 0.478 m. From TEMA standards, minimal thickness for shell diameters between 330-580 mm is 3.2 mm, thus D_{Sout} is 0.4844 m.

Vibration analysis:
According to the recommendations, the velocity of tube side vapor should not exceed 30 m/s for atmospheric pressure and 10 m/s for high pressure

$$V = \frac{Q}{N\pi(0.5D_I)^2} = \frac{1.739072738*10^6}{63*3.14*(0.5*0.025)^2} = 14.29\ m/s \quad \text{(Eq. G.3)}$$

This exceeds the recommended value for high pressure vapor, but in the tubes condensation occurs and flow velocity is expected to drop and further calculations demonstrate that pressure drop is in expected range.The velocity of liquid at the shell side is expected to be in range 0.3-1 m/s The calculations are the following:

$$A_S = (p_t - D_O)D_S l_B/p_t = 0.03655744\ m^2 \quad \text{(Eq. G.4)}$$

$$G_S = W_S/A_S = 227.4868444\ kg/s\ m^2 \quad \text{(Eq. G.5)}$$

$$u_S = G_S/\rho = 0.2795510463\ m/s \quad \text{(Eq. G.6)}$$

A_S is equivalent shell area, p_t is tube pitch, in this design $p_t = 1.25 * D_O$, l_B is baffle spacings, in this design $l_B = 0.8 * D_S$, G_S is mass flux, W_S is mass flow rate, ρ is density.

This is not in the range of values provided, however moderate pressure drop requirements and guaranteed absence of flow vibrations were considered more important than high heat transfer coefficient

Heat transfer coefficient:
Shell:

$$d_e = (1.27/D_O) * (p_t^2 - 0.785 * D_0^2) = 0.024685625\ m \quad \text{(Eq. G.7)}$$

$$Re = G_s d_e/\mu = 15582.377 \quad \text{(Eq. G.8)}$$

$$Pr = C_p\mu/k = 5.864716925 \quad \text{(Eq. G.9)}$$

Where Re is Reynolds number, μ is viscosity, Pr is Prandtl number, C_p is heat capacity, k is thermal conductivity.

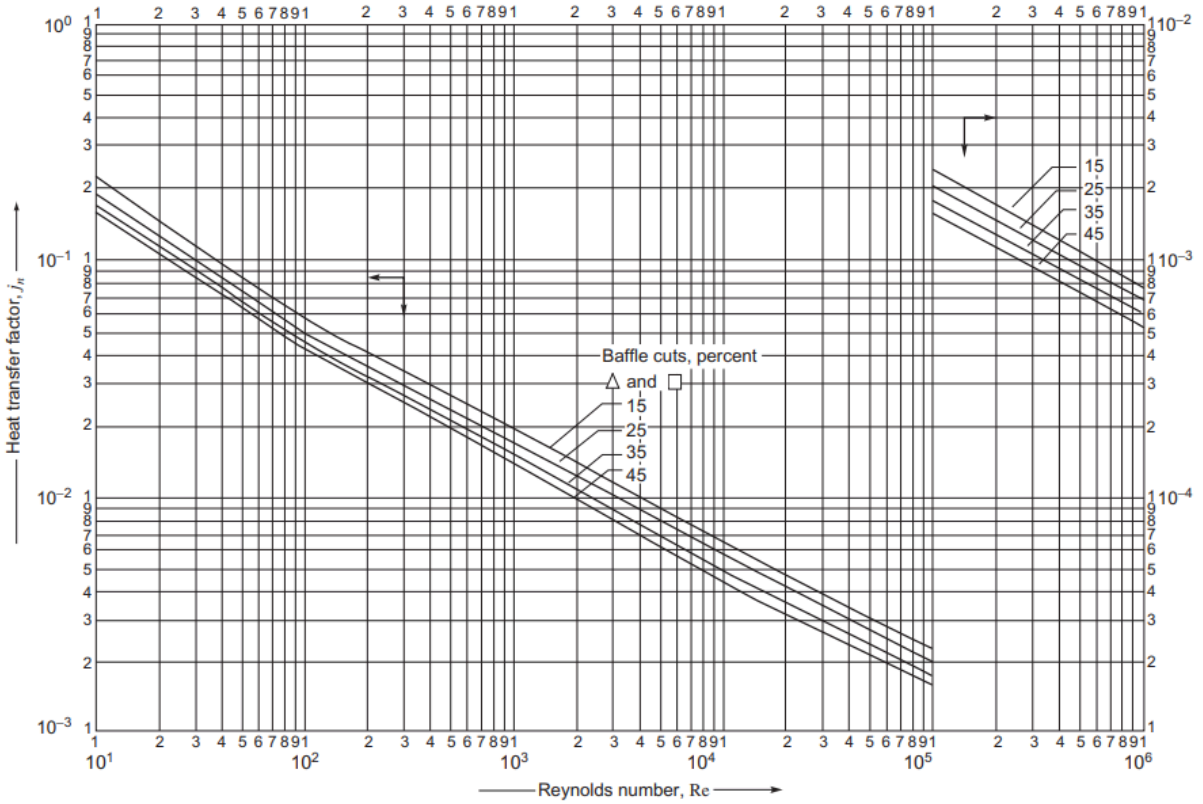

Figure G7. Heat transfer factors for shell side [40]

Pressure drop:

Tube:

Table G1. 2 phase pressure drop in tubes

Liquid	Vapor
$Re_l = (1 - x)G_S D_O/\mu_l = 2329.973$ (Eq. G.10)	$Re_g = xD_O/\mu_g = 2.63E4$ (Eq. G.11)
$f_l = 0.079Re^{-0.25}{}_l = 0.01137075631$ (Eq. G.12)	$f_g = 0.079Re^{-0.25}{}_g = 0.006202623$ (Eq. G.13)
$(dp/dl)_l = 2 * f_l * G_s{}^2/(D_I \rho_l) = 1.51$ (Eq. G.14)	$(dp/dl)_g = 2 * f_g * G_s{}^2/(D_I \rho_g) = 239.62$ (Eq. G.15)
$X = \sqrt{(dp/dl)_l/(dp/dl)_g} = 0.07954605653$ (Eq. G.16)	
$\phi^2{}_l = 1 + (20/X) + 1/X^2 = 410.465093$ (Eq. G.17)	

$$\Delta P = \phi_l^2 * (dp/dl)_l * L = 4555.552502\ Pa \qquad \text{(Eq. G.18)}$$

The calculation was carried out using Blasius correlation, Lockhart–Martinelli parameter and considering all flow as liquid

Shell:

$$\Delta P_S = 8 J_f (D_S/d_e)(L/l_b)(\rho u_s^2/2)(\mu/\mu_w)^{-0.14} = 2175.94721\ Pa \qquad \text{(Eq. G.19)}$$

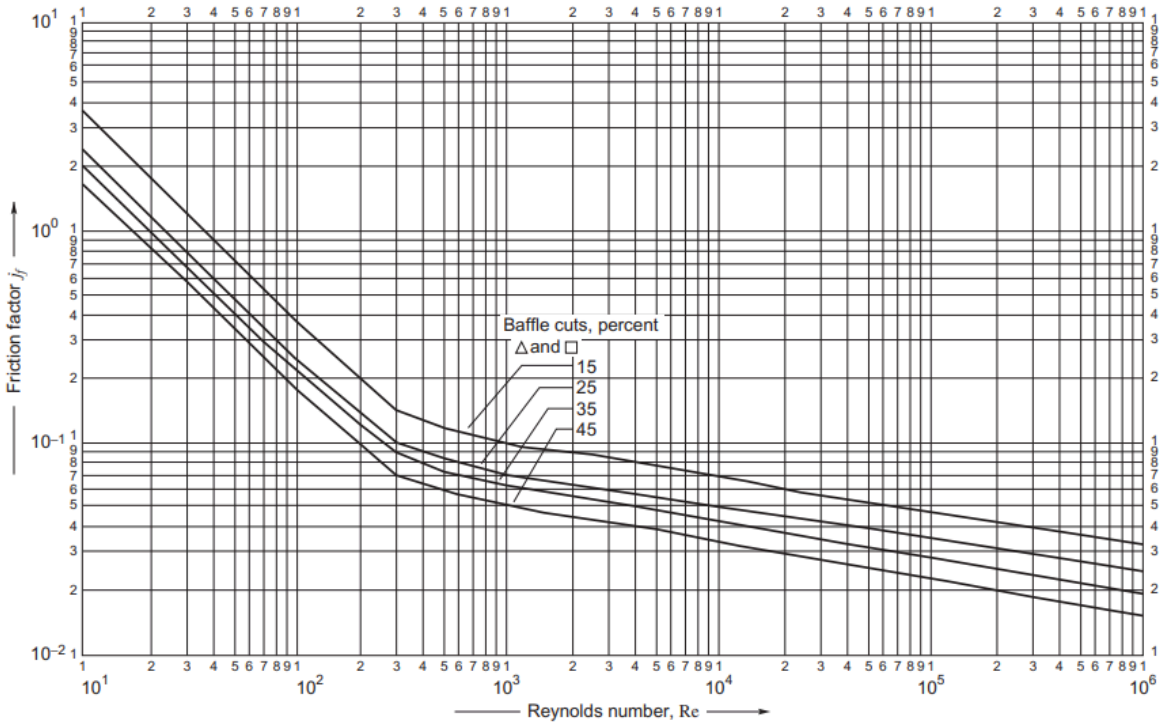

Figure G8. Friction factors for shell side [40]

After all calculations were done as visible in E-101 HE spreadsheet, validating calculated results in Aspen Plus V14 software package, specifically EDR was made use of.

The following charts summarize the finding from Simulation:

	Units	1	HOTIN1	2	HOTOUT1
Description					
From				E-101	E-101
To		E-101	E-101		
Stream Class		CONVEN	CONVEN	CONVEN	CONVEN
Maximum Relative Error					
Cost Flow	$/hr				
− MIXED Substream					
Phase		Liquid Phase	Vapor Phase	Liquid Phase	
Temperature	C	25	160	132.061	158.886
Pressure	bar	1	6.04847	0.966903	5.8754
Molar Vapor Fraction		0	1	0	0.0793151
Molar Liquid Fraction		1	0	1	0.920685
Molar Solid Fraction		0	0	0	0
Mass Vapor Fraction		0	1	0	0.0793151
Mass Liquid Fraction		1	0	1	0.920685
Mass Solid Fraction		0	0	0	0
Molar Enthalpy	cal/mol	-2666.2	-56745.4	2416.53	-65328.2
Mass Enthalpy	cal/gm	-25.1131	-3149.85	22.7615	-3626.27
Molar Entropy	cal/mol-K	-105.274	-11.2546	-90.8045	-31.0649
Mass Entropy	cal/gm-K	-0.991585	-0.624725	-0.855295	-1.72436
Molar Density	mol/cc	0.00814989	0.000174112	0.00721217	0.00205093
Mass Density	gm/cc	0.865253	0.00313667	0.765698	0.0369481
Enthalpy Flow	cal/sec	-208852	-2.63235e+06	189295	-3.0305e+06
Average MW		106.167	18.0153	106.167	18.0153
+ Mole Flows	**kmol/hr**	**282**	**167**	**282**	**167**
+ Mole Fractions					
+ Mass Flows	**kg/hr**	**29939.2**	**3008.55**	**29939.2**	**3008.55**
+ Mass Fractions					
Volume Flow	l/min	576.695	15985.9	651.676	1357.11
+ Vapor Phase					

Figure G9. Stream results in ASPEN

1	Size	16.1417	X	144.0945	in	Type	BEM	Hor		Connected in	1	parallel	1	series	
2	Surf/Unit (gross/eff/finned)			389.9	/	381.9	/		ft²	Shells/unit	1				
3	Surf/Shell (gross/eff/finned)			389.9	/	381.9	/		ft²						
4	Simulation						PERFORMANCE OF ONE UNIT								
5				Shell Side			Tube Side			Heat Transfer Parameters					
6	**Process Data**			**In**		**Out**	**In**		**Out**	Total heat load		BTU/h		5687914	
7	Total flow	lb/h		66004.6			6632.7			Eff. MTD/ 1 pass MTD		°F	122.57	/	122.24
8	Vapor	lb/h	0		0		6632.7		526.1	Actual/Reqd area ratio - fouled/clean			1	/	1.33
9	Liquid	lb/h	66004.6		66004.6		0		6106.6						
10	Noncondensable	lb/h		0				0		**Coef./Resist.**	BTU/(h-ft²-F)		ft²-h-F/BTU		%
11	Cond./Evap.	lb/h		0				6106.6		Overall fouled	121.34		0.0082		
12	Temperature	°F	77		269.15		320		317.99	Overall clean	162.18		0.0062		
13	Bubble Point	°F	276.33		274.09		320		317.99	Tube side film	2830.02		0.0004		4.29
14	Dew Point	°F	276.33		274.09		320		317.99	Tube side fouling	1064.05		0.0009		11.4
15	Vapor mass fraction		0		0		1		0.0793	Tube wall	1564.29		0.0006		7.76
16	Pressure (abs)	psi	14.5		14.02		87.73		85.22	Outside fouling	880.55		0.0011		13.78
17	DeltaP allow/cal	psi	2.9		0.48		3.77		2.51	Outside film	193.3		0.0052		62.77
18	Velocity	ft/s	0.81		0.92		37.86		3.21						
19	**Liquid Properties**									**Shell Side Pressure Drop**			psi		%
20	Density	lb/ft³	54.016		47.806				53.243	Inlet nozzle			0.11		22.81
21	Viscosity	cp	0.6347		0.2458				0.169	InletspaceXflow			0.04		7.86
22	Specific heat	BTU/(lb-F)	0.3881		0.504				1.153	Baffle Xflow			0.16		33.82
23	Therm. cond.	BTU/(ft-h-F)	0.075		0.06				0.395	Baffle window			0.12		25.18
24	Surface tension	lbf/ft							0.00136	OutletspaceXflow			0.04		8.25
25	Molecular weight		106.17		106.17				18.02	Outlet nozzle			0.01		2.09
26	**Vapor Properties**									Intermediate nozzles					
27	Density	lb/ft³					0.196		0.191	**Tube Side Pressure Drop**			psi		%
28	Viscosity	cp					0.0149		0.0149	Inlet nozzle			0.24		9.35
29	Specific heat	BTU/(lb-F)					0.4751		0.4746	Entering tubes			0.02		0.78
30	Therm. cond.	BTU/(ft-h-F)					0.017		0.017	Inside tubes			0.23		8.86
31	Molecular weight						18.02		18.02	Exiting tubes			0.01		0.31
32	**Two-Phase Properties**									Outlet nozzle			2.07		80.7
33	Latent heat	BTU/lb					929.1		930.5	Intermediate nozzles					
34	**Heat Transfer Parameters**									**Velocity / Rho*V2**			ft/s		lb/(ft-s²)
35	Reynolds No. vapor						52377.14		4166.77	Shell nozzle inlet			3.84		796
36	Reynolds No. liquid		8412.19		21739.83				4259.45	Shell bundle Xflow		0.81	0.92		
37	Prandtl No. vapor						0.99		0.99	Shell baffle window		1.11	1.25		
38	Prandtl No. liquid		8		5.01				1.19	Shell nozzle outlet			1.1		58
39	**Heat Load**				BTU/h				BTU/h	Shell nozzle interm					
40	Vapor only				0				-2				ft/s		lb/(ft-s²)
41	2-Phase vapor				0				-3392	Tube nozzle inlet			106.43		2218
42	Latent heat				0				-5677421	Tubes		37.86	3.21		
43	2-Phase liquid				0				-7098	Tube nozzle outlet			131.44		40350
44	Liquid only				5687914				0	Tube nozzle interm					
45	**Tubes**						**Baffles**			**Nozzles: (No./OD)**					
46	Type				Plain		Type	Single segmental				**Shell Side**		**Tube Side**	
47	ID/OD	in	0.8504	/	0.9843		Number		10	Inlet	in	1	/ 4.5	1	/ 4.5
48	Length act/eff	ft	12.0079	/	11.7616		Cut(%d)	26.35		Outlet		1	/ 8.625	1	/ 1.315
49	Tube passes		2				Cut orientation		H	Intermediate			/		/
50	Tube No.		126				Spacing: c/c	m	0.328	Impingement protection			None		
51	Tube pattern		90				Spacing at inlet	in	12.4596						
52	Tube pitch	m	0.0312				Spacing at outlet	in	12.4596						
53	Insert				None										
54	Vibration problem (HTFS / TEMA)		No	/						TEMA RhoV2 limit exceeded					No

Figure G10. Results summary for E-101

Simulation		Shell Side		Tube Side	
Total mass flow rate	lb/h	66004.6		6632.7	
Vapor mass flow rate (In/Out)	lb/h	0	0	6632.7	526.1
Liquid mass flow rate	lb/h	66004.6	66004.6	0	6106.6
Vapor mass fraction		0	0	1	0.0793
Temperatures	°F	77	269.15	320	317.99
Bubble / Dew point	°F	276.33 / 276.33	274.09 / 274.09	320 / 320	317.99 / 317.99
Operating Pressures	psi	14.5	14.02	87.73	85.22
Film coefficient	BTU/(h-ft²-F)	193.3		2830.02	
Fouling resistance	ft²-h-F/BTU	0.0011		0.0009	
Velocity (highest)	ft/s	1.43		37.86	
Pressure drop (allow./calc.)	psi	2.9 / 0.48		3.77 / 2.51	

Total heat exchanged	BTU/h	5687914	Unit	BEM	2 pass 1 ser 1 par
Overall clean coeff. (plain/finned)	BTU/(h-ft²-F)	162.18 /	Shell size	16.1417 - 144.0945 in	Hor
Overall dirty coeff. (plain/finned)	BTU/(h-ft²-F)	121.34 /	Tubes	Plain	
Effective area (plain/finned)	ft²	381.9 /	Insert	None	
Effective MTD	°F	122.57	No.	126 OD 0.025 Tks 0.0017	m
Actual/Required area ratio (dirty/clean)		1 / 1.33	Pattern	90 Pitch 0.0312 m	
Vibration problem (HTFS)		No	Baffles	Single segmental Cut(%d) 26.35	
TEMA RhoV2 limit exceeded		No	Total cost	30841 Dollar(US)	

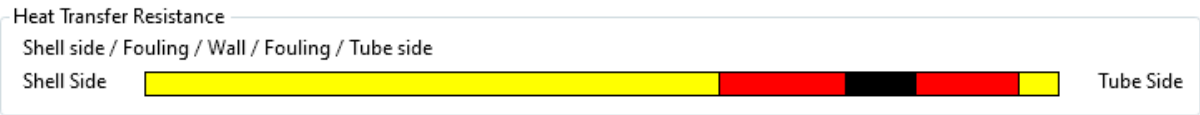

Figure G11. Heat transfer performance summary

Appendix H

H.1 Step-by-step algorithm for R-101 & R-102 design

1. Start new simulation on Aspen 14 Plus
2. Add components

Component ID	Type	Component name	Alias	CAS number
EB	Conventional	ETHYLBENZENE	C8H10-4	100-41-4
ST	Conventional	STYRENE	C8H8	100-42-5
H2	Conventional	HYDROGEN	H2	1333-74-0
WATER	Conventional	WATER	H2O	7732-18-5
BENZENE	Conventional	BENZENE	C6H6	71-43-2
TOLUENE	Conventional	TOLUENE	C7H8	108-88-3
C2H4	Conventional	ETHYLENE	C2H4	74-85-1
CH4	Conventional	METHANE	CH4	74-82-8

Figure H1. Components for Reactors

3. Define H2 as Henry Component

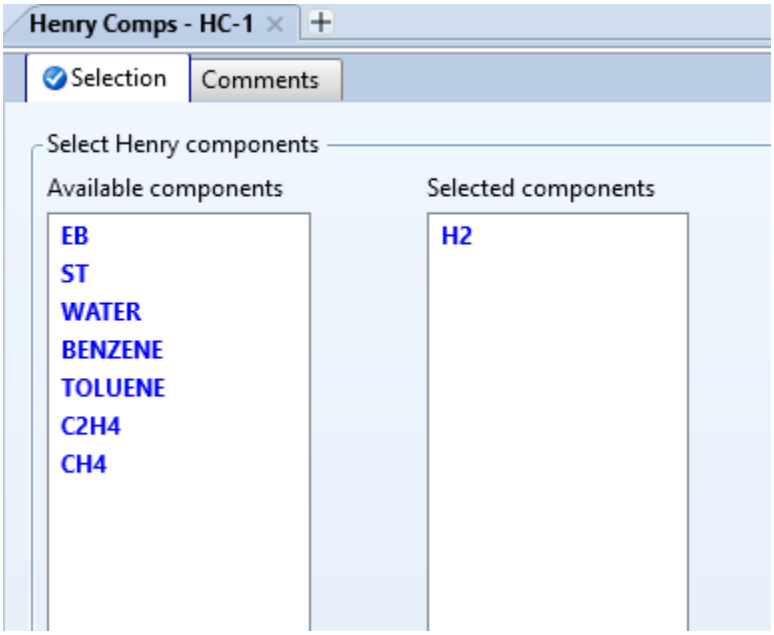

Figure H2. Defining Henry Component

4. Specify NRTL method

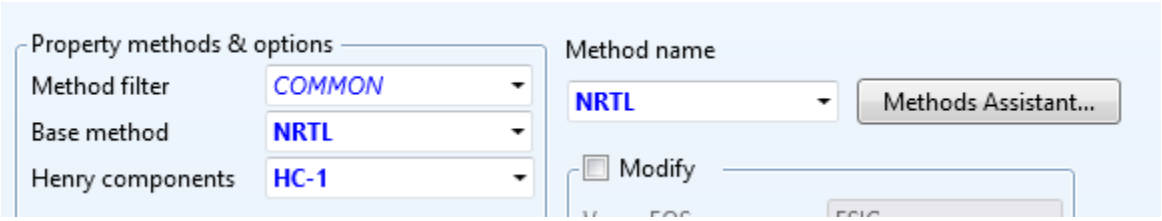

Figure H3. Setting method

5. Build main flowsheet of 2 Reactors in series

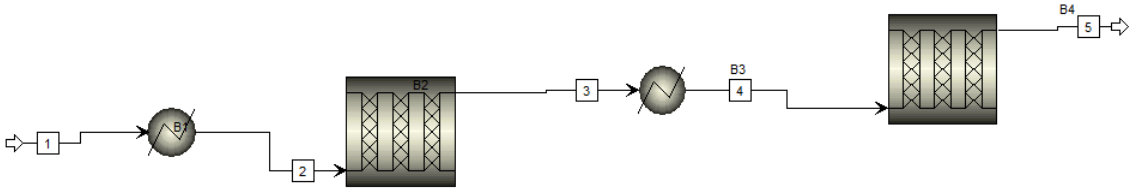

Figure H4. Reactor flow sheet

6. Create LHHW reaction

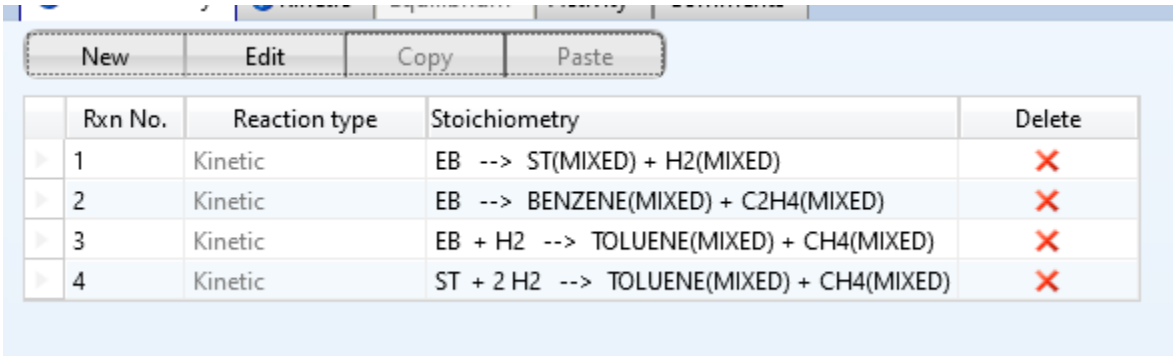

Figure H5. Kinetic reactions

7. Define Kinetic data for each reaction

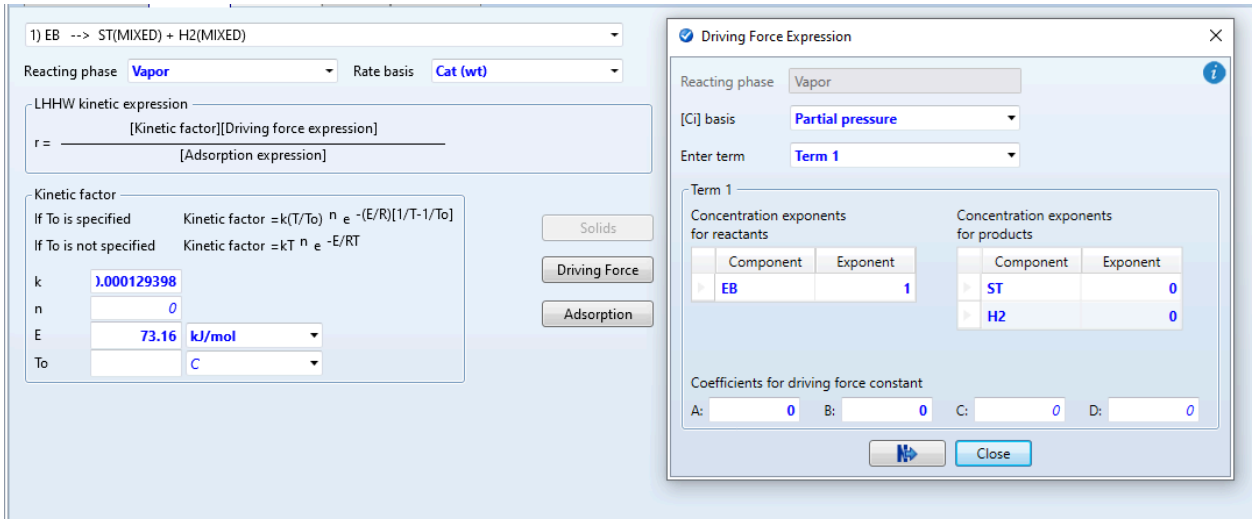

Figure H6. Setting kinetic parameters

8. Define initial flow

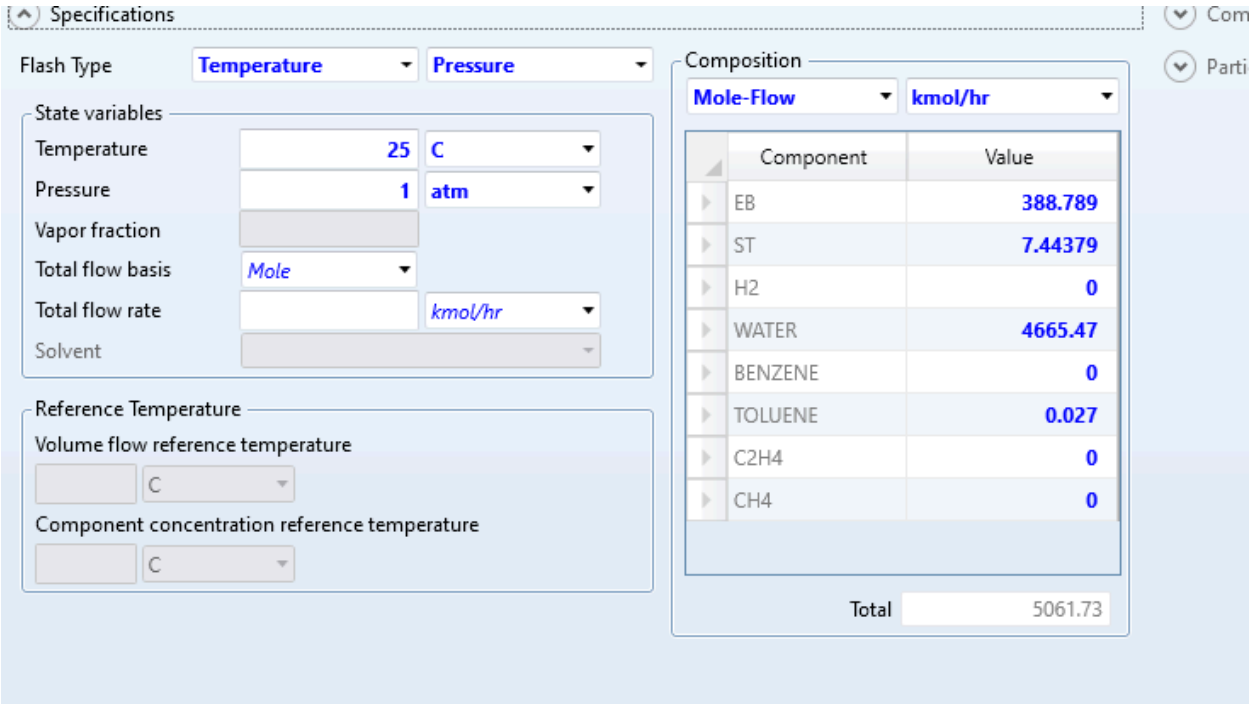

Figure H7. Defining initial flow

9. Define Heater I

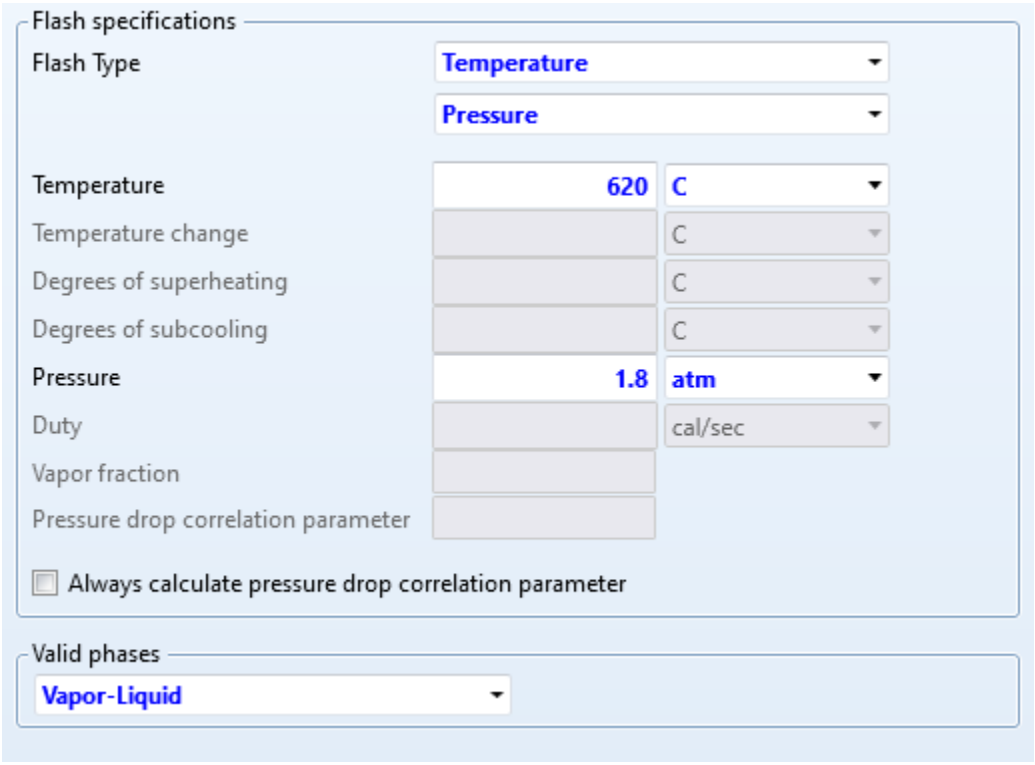

Figure H8. Heater I setup

10. Define PFR I as Adiabatic and configure it

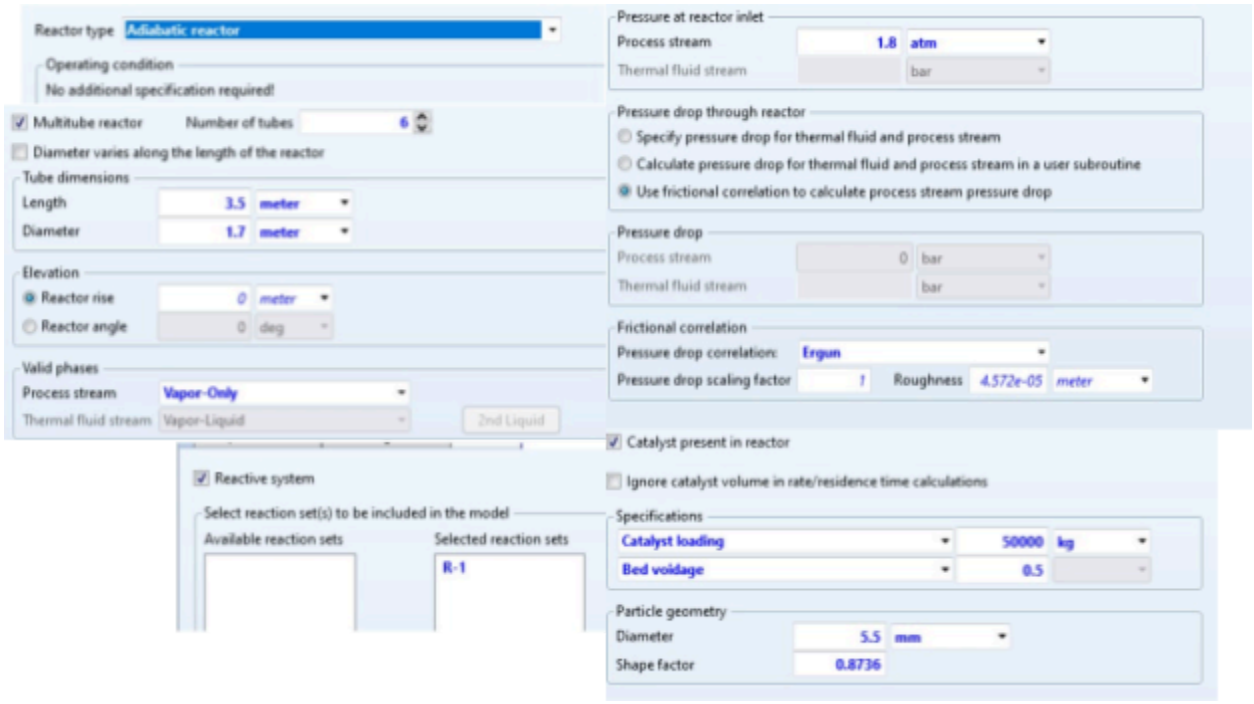

Figure H9. R-101 setup

11. Define Heater II

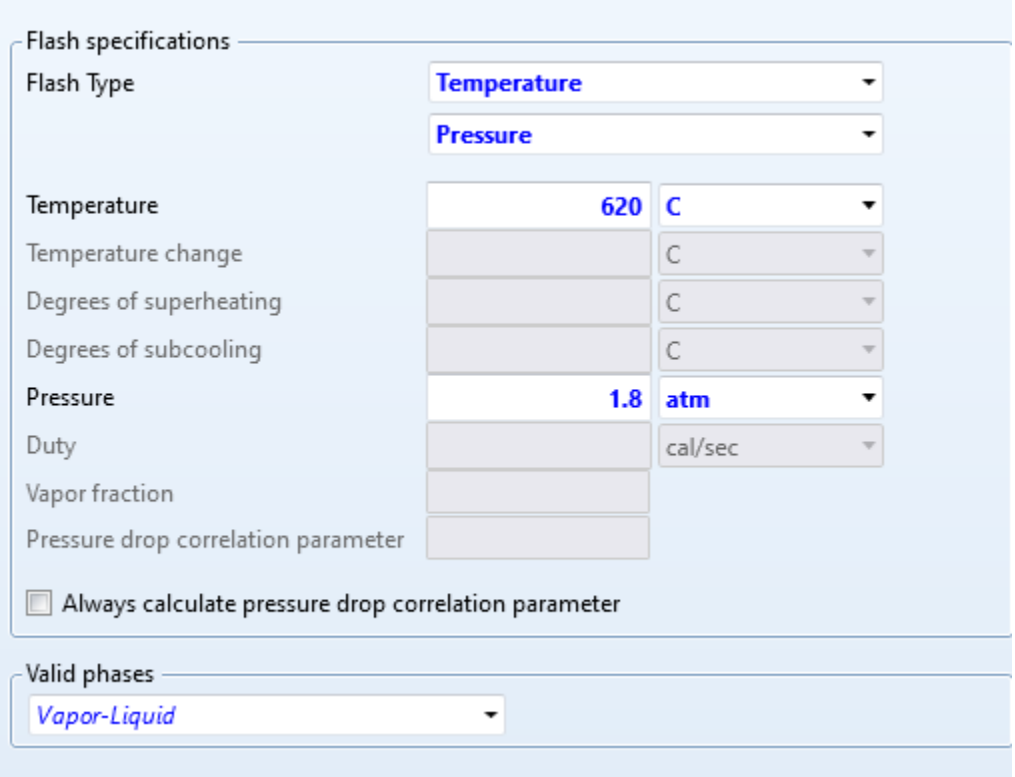

Figure H10. E-104 setup

12. Define PFR II in the same way as PFR I
13. To identify the dimensions of Reactor with relation to Pressure Drop and Velocity

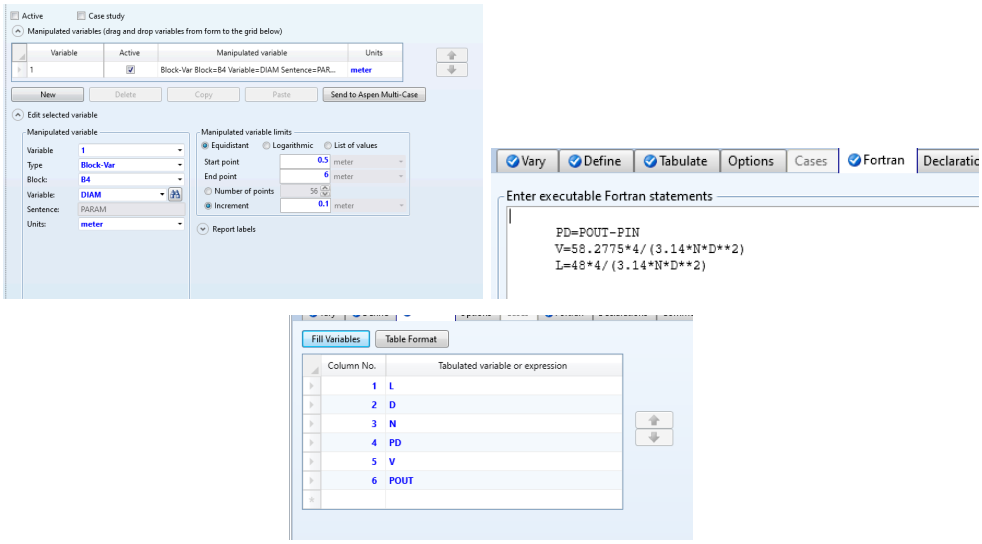

	Row/Case	Status	Description	VARY 1 B4 PARAM DIAM METER	L METER	D METER	N	PD	V	POUT BAR
	1	Errors		0.5	40.7643	0.5	6	-1.82375	49.4926	0.0001029...
	2	Errors		0.6	28.3086	0.6	6	-1.82374	34.3698	0.0001055...
	3	Errors		0.7	20.7981	0.7	6	-1.82372	25.2513	0.0001328...
	4	Errors		0.8	15.9236	0.8	6	-1.82376	19.333	9.48885e-...
	5	Errors		0.9	12.5816	0.9	6	-1.82375	15.2755	0.0001046...
	6	Warnings		1	10.1911	1	6	-1.82376	12.3731	8.84266e-...
	7	Warnings		1.1	8.42238	1.1	6	-1.8238	10.2257	4.78908e-...
	8	Warnings		1.2	7.07714	1.2	6	-1.82377	8.59246	8.49385e-...
	9	Warnings		1.3	6.03023	1.3	6	-1.82378	7.32139	7.13994e-...
	10	Warnings		1.4	5.19953	1.4	6	-1.82378	6.31283	7.37729e-...
	11	Warnings		1.5	4.52937	1.5	6	-1.82378	5.49917	6.74181e-...
	12	OK		1.6	3.98089	1.6	6	-1.17794	4.83326	0.645912
	13	OK		1.7	3.52633	1.7	6	-0.815363	4.28136	1.00849
	14	OK		1.8	3.1454	1.8	6	-0.612719	3.81887	1.21113
	15	OK		1.9	2.82301	1.9	6	-0.478609	3.42746	1.34524
	16	OK		2	2.54777	2	6	-0.383382	3.09329	1.44047
	17	OK		2.1	2.3109	2.1	6	-0.312898	2.8057	1.51095
	18	OK		2.2	2.1056	2.2	6	-0.259207	2.55643	1.56464

Figure H11. Sensitivity Setup

14. Optimal dimensions of 1.7m diameter and 3.5 m length were chosen
15. Following Results were obtained

	Units	1	2	3	4	5	
Description							
From			B1	B2	B3	B4	
To		B1	B2	B3	B4		
Stream Class		CONVEN	CONVEN	CONVEN	CONVEN	CONVEN	
Maximum Relative Error							
Cost Flow	$/hr						
− MIXED Substream							
Phase		Liquid Phase	Vapor Phase	Vapor Phase	Vapor Phase	Vapor Phase	
Temperature	C	25	620	553.834	620	590.485	
Pressure	bar	1.01325	1.82385	1.08815	1.82385	1.02772	
Molar Vapor Fraction		0	1	1	1	1	
Molar Liquid Fraction		1	0	0	0	0	
Molar Solid Fraction		0	0	0	0	0	
Mass Vapor Fraction		0	1	1	1	1	
Mass Liquid Fraction		1	0	0	0	0	
Mass Solid Fraction		0	0	0	0	0	
Molar Enthalpy	cal/mol	-62965.7	-45338.6	-43924.2	-43017	-42330.2	
Mass Enthalpy	cal/gm	-2527.39	-1819.86	-1819.86	-1782.27	-1782.27	
Molar Entropy	cal/mol-K	-44.3197	-3.67143	-2.26507	-2.23551	-0.896492	
Mass Entropy	cal/gm-K	-1.77896	-0.147368	-0.0938457	-0.0926211	-0.0377458	
Molar Density	mol/cc	0.0386415	2.45605e-05	1.58258e-05	2.45605e-05	1.43125e-05	
Mass Density	gm/cc	0.962686	0.000611883	0.000381972	0.000592794	0.000339933	
Enthalpy Flow	cal/sec	-8.8532e+07	-6.37477e+07	-6.37477e+07	-6.2431e+07	-6.2431e+07	
Average MW		24.9133	24.9133	24.1361	24.1361	23.7507	
+ Mole Flows	**kmol/hr**	**5061.73**	**5061.73**	**5224.72**	**5224.72**	**5309.49**	
− Mole Fractions							
EB		0.0768095	0.0768095	0.0420856	0.0420856	0.0208334	
ST		0.0014706	0.0014706	0.0322468	0.0322468	0.0472543	
H2		0	0	0.0296905	0.0296905	0.0401235	
WATER		0.921715	0.921715	0.892961	0.892961	0.878704	
BENZENE		0	0	0.000374122	0.000374122	0.00081082	
TOLUENE		5.33414e-06	5.33414e-06	0.00113678	0.00113678	0.00573388	
C2H4		0	0	0.000374122	0.000374122	0.00081082	
CH4		0	0	0.00113161	0.00113161	0.0057288	
+ Mass Flows	**kg/hr**	**126104**	**126104**	**126104**	**126104**	**126104**	
+ Mass Fractions							
Volume Flow	l/min	2183.2	3.43487e+06	5.50233e+06	3.54547e+06	6.1828e+06	
+ Vapor Phase							

Figure H12. Stream Results

H.2 Reactor volume calculations

To obtain the catalyst volume, the catalyst loading was divided by catalyst density:

$$V_c = \frac{M_c}{\rho_c} = \frac{50000}{2500} = 20\ m^3 \qquad \text{(Eq .H.1)}$$

To obtain the volume of reactor, the bed voidage of 0.5 and safety factor of 20% was used:

$$V = \frac{V_c}{1-\epsilon} * SF = \frac{20}{1-0.5} * 1.2 = 48\, m^3 \quad \text{(Eq .H.2)}$$

H.3 Pressure drop calculations

The pressure drop was calculated by Ergun Equation [40]:

$$\Delta P = \frac{L}{100000}\left(\frac{150\mu(1-\epsilon)^2}{d_p^2\epsilon^3\lambda^2}\nu + \frac{1.75\rho(1-\epsilon)}{d_p\epsilon^3\lambda}\nu^2\right) \quad \text{(Eq. H.3)}$$

Table H1. Ergun Equation Parameters

Parameter	**Value**	**Units**
Viscosity (μ)	3.24E-05	Pa.s
Bed voidage (ϵ)	0.5	
Particle diameter (d_p)	0.0055	m
Density (ρ)	6.12E-01	kg/m3
Velocity (ν)	4.20E+00	m/s
Length (L)	3.5	m
Shape Factor (λ)	0.8735804647	

$$\Delta P = \frac{3.5}{100000} * \left(\frac{150*3.24E-05*(1-0.5)^2}{0.0055^2*0.5^3*0.8735804647^2} * 4.2 + \frac{1.75*6.12E-01*(1-0.5)}{0.0055*0.5^3*0.8735804647} * 4.2^2\right) \quad \text{(Eq. H.4)}$$

$\Delta P = 0.613$ bar (Hand calculated)

$\Delta P = 0.72608$ bar (Aspen)

The following calculations were done for R-101. In the same procedure, the pressure drop can be calculated for R-102.

$\Delta P = 0.637$ bar (Hand calculated)

$\Delta P = 0.78572$ bar (Aspen)

Construction material calculations

Table H2. Material choice for reactor [141, 142]

	SS304L	SS316	SS321	Incoloy 800
Maximum temperature, °C	~800	~870	~900	~1100
Tensile Strength, MPa	485	515	515	600
Cr content (%)	17.5-19.5	16.0-18.0	17.0-19.0	19.0-23.0
Yield Strength (MPa)	170	205	205	310
Elongation (%)	40	40	40	40
Hardness (HB)	201	217	217	217
Thermal Expansion (10^{-6}/K)	18.4	17.5	18.6	17
Price (USD/kg)	Lower	Medium	Medium-High	High

Determining the minimum wall thickness for a specific pipe diameter and selecting the appropriate actual thickness are fundamental design steps in any project. A key formula used for calculating pipe thickness (ASME B31.3) [40]:

$$t_{wall} = \frac{P_i D}{2(SE - P_i Y)} + c \qquad \text{(Eq. H.5)}$$

Where,

P_i = Internal Design Pressure gauge, MPa with safety factor of 10%

D = Outside diameter of the tube

E = Quality factor from table (Table B14)

S = Allowable stress for material (Figure B13)

Y = Temperature coefficient (Table 15)

C = Corrosion allowance (1/16 inch)
From the figure B13, for our reactor. T=645C (1198.4ºF) with safety factor of 25C, material = SS304l, the allowable stress, S= 3000 psi (20.68 MPa).

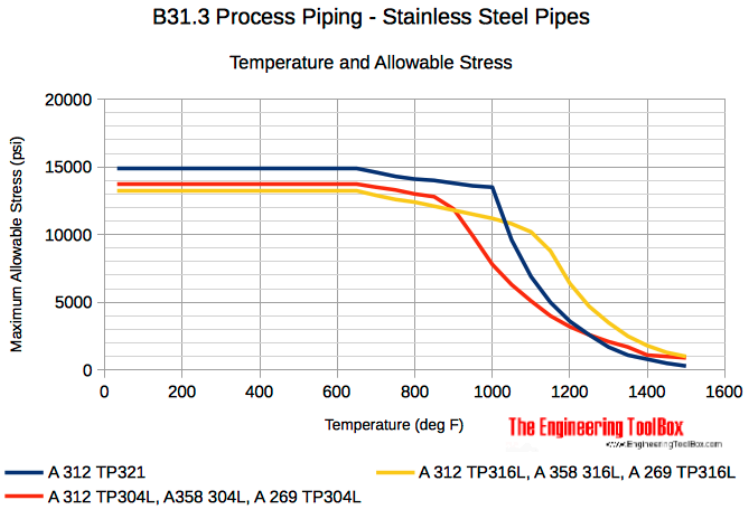

Figure H13. Temperature and Allowable Stress for different materials [25]

The maximum value of quality factors (E) is 1.0. Since our pipe is seamless without any welds, our value will be 1.

Table IX-3B Longitudinal Joints Factors for Pipeline Materials

Spec. No.	Pipe Class	*E* Factor
API 5L	Seamless	1.00
	Electric resistance welded	1.00
	Electric flash welded	1.00
	Double submerged arc welded	1.00
ASTM A53	Seamless	1.00
	Electric resistance welded	1.00
ASTM A106	Seamless	1.00
ASTM A134	Electric fusion arc welded	0.80
ASTM A135	Electric resistance welded	1.00
ASTM A139	Electric fusion welded	0.80
ASTM A333	Seamless	1.00
	Electric resistance welded	1.00
ASTM A381	Double submerged arc welded	1.00
ASTM A671	Electric fusion welded	
	Classes 13, 23, 33, 43, 53	0.80
	Classes 12, 22, 32, 42, 52	1.00
ASTM A672	Electric fusion welded	
	Classes 13, 23, 33, 43, 53	0.80
	Classes 12, 22, 32, 42, 52	1.00

Figure H14. Quality factor [144]

The factor "Y" depends on temperature. At elevated temperatures, factor Y increases leading to a decrease in the calculated required pipe wall thickness (*Figure B15*). SS304l is considered austenitic steel, therefore Y value is 0.7.

Table 304.1.1 Values of Coefficient *Y* for $t < D/6$

Material	Temperature, °C (°F)							
	482 (900) and Below	510 (950)	538 (1,000)	566 (1,050)	593 (1,100)	621 (1,150)	649 (1,200)	677 (1,250) and Above
Ferritic steels	0.4	0.5	0.7	0.7	0.7	0.7	0.7	0.7
Austenitic steels	0.4	0.4	0.4	0.4	0.5	0.7	0.7	0.7
Nickel alloys UNS Nos. N06617, N08800, N08810, and N08825	0.4	0.4	0.4	0.4	0.4	0.4	0.5	0.7
Gray iron	0.0	...	...	...	...	...	...	...
Other ductile metals	0.4	0.4	0.4	0.4	0.4	0.4	0.4	0.4

Figure H15. Values of Coefficient Y [145]

The final thickness of the wall:

$$t_{wall} = \frac{0.2*1.72}{2(20.68*1-0.2*0.7)} + 1.5875 = 9.87\ mm \cong 10\ mm \qquad \text{(Eq. H.6)}$$

Appendix I

I. 1 Design details and calculations for E-105

Tube side coefficient

$$\text{Tube cross-sectional area, } A_{cs\ tube} = \frac{\pi d_i^2}{4} = 0.000172\ m^2 \qquad \text{(Eq. G.1)}$$

$$\text{Fluid velocity, } \vartheta = \frac{\overline{m}}{\rho \times A_{cs\ tube} \times N_t} = 19.98\ \text{m/s} \qquad \text{(Eq. G.6)}$$

$$\text{Reynolds Number, } Re = \frac{\rho \times \vartheta \times d_i}{\mu} = 1.21 \times 10^4 \qquad \text{(Eq.G.8)}$$

$$\text{Prandtl number, } Pr = \frac{C_p \times \mu}{k} = 1.71 \qquad \text{(Eq.G.9)}$$

$$C = 0.021$$

$$h_{shell} = 87.55\ \text{W/m}^2\text{-K} \qquad \text{(Eq.26)}$$

Shell side coefficient

$$\text{Fluid velocity, } \vartheta = \frac{\bar{m}}{\rho \times A_{cs\ tube} \times N_t} = 38.06 \text{ m/s} \qquad \text{(Eq. G.6)}$$

$$\text{Reynolds Number, } Re = \frac{\rho \times \vartheta \times d_i}{\mu} = 2.94 \times 10^4 \qquad \text{(Eq. G.8)}$$

$$\text{Prandtl number, } Pr = \frac{C_p \times \mu}{k} = 0.935 \qquad \text{(Eq. G.9)}$$

J = 0.0021 (see *Fig. 4A*)

$$h_{tube} = 76.1 \text{ W/m}^2\text{-K} \qquad \text{(Eq. 26)}$$

Pressure drop

$$\Delta P_{tube} = N\ of\ passes \times [8 j_f \frac{L}{d_i} (\frac{\mu}{\mu_w})^{-m} + 2.5] \frac{\rho \vartheta^2}{2} = 0.006 \text{ bar} \qquad \text{(Eq. G.19)}$$

$$\Delta P_{shell} = 8 j_f (\frac{D_s}{d_e})(\frac{L}{l_b})^{-m} + 2.5] \frac{\rho \vartheta^2}{2} (\frac{\mu}{\mu_w})^{-0.14} = 0.11 \text{ bar} \qquad \text{(Eq. G.19)}$$

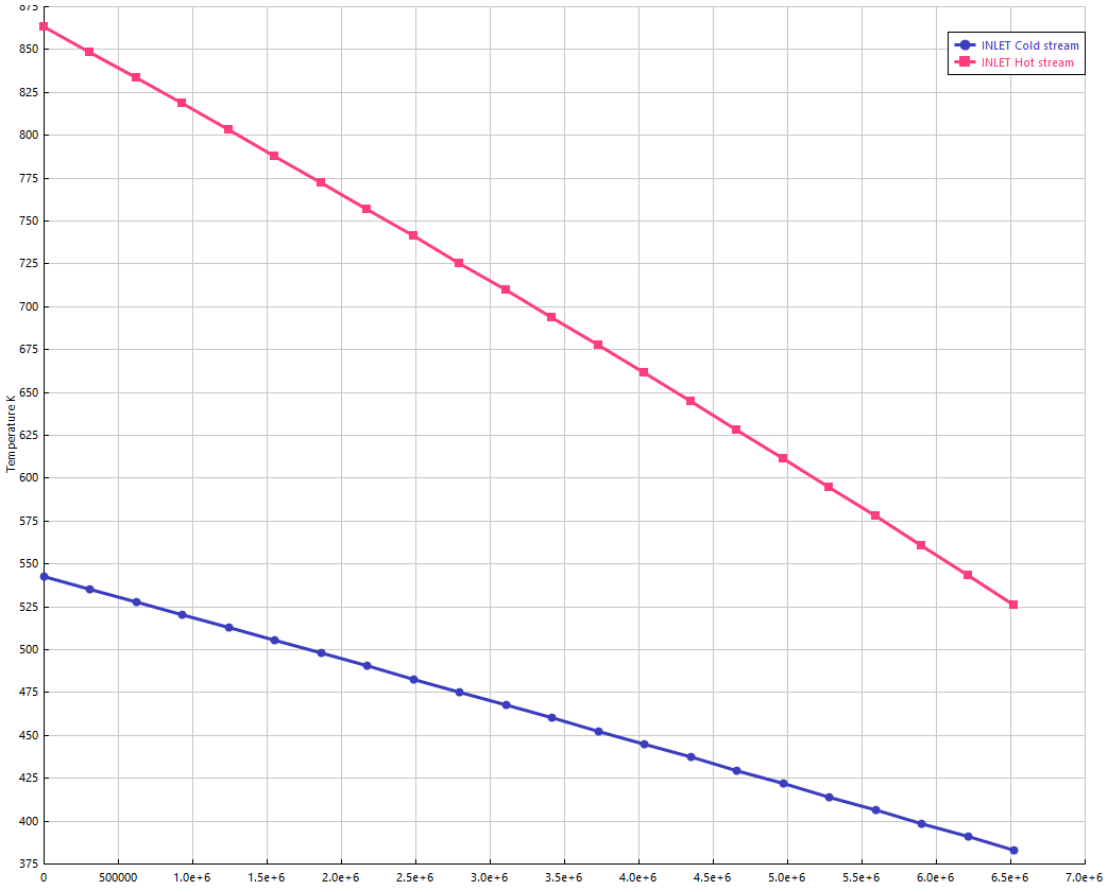

Figure I1. TQ curves for E-105 cooler

Appendix J

J.1 Design details and calculations for T-101

Table J1. Comparative analysis of column types for ST/EB separation: suitability based on operating conditions *(Gray shading indicates suitable column types for each condition)* [40]

Factor	**Packed column**	**Tray columns**
Low-pressure drop preferred	Low-pressure drop (~0.04 psi/stage for random packings, lower for structured), reducing compressor costs	Higher pressure drop (~0.15 psi/stage).
Vacuum systems required	Preferred due to lower pressure drop, better relative volatility, and energy savings.	Less suitable due to higher pressure drop.
Revamps are needed	Pressure drop reduction translates to capacity, energy, or separation improvements.	Less flexibility for revamps compared to packings.
Smaller diameter column	Relatively low diameter	In complex separation systems may lead to oversized diameter
Corrosive system	Wider range of packing materials (e.g., ceramic, plastic) available at lower cost	Limited material options; more expensive for nonmetallic trays
Prone to foaming	Less foaming due to lower vapor-liquid velocities and gentler contact	More prone to foaming due to higher velocities and violent contact
Low liquid holdup needed	Lower liquid holdup, reducing polymerization, degradation, or hazardous inventory	Higher liquid holdup, less suitable for sensitive or hazardous materials
System might have high liquid rates	Capacity drops rapidly at high liquid rates	Multipass trays handle high liquid rates more effectively
No solid system	Prone to clogging; difficult to clean (especially structured packings)	Better for solids; high velocities keep trays clear; easier to clean

Intermittent operation	Risk of crushing packings or damaging shell due to thermal expansion/contraction	Easier to accommodate thermal expansion/contraction

J.2 Height calculations

Table J2. Feed, top and bottom products' composition and flow rates

Stream #	**13**		**14**		**15**	
Compound	**Molar flow rate, kmol/h**	**Mole fraction**	**Molar flow rate, kmol/h**	**Mole fraction**	**Molar flow rate, kmol/h**	**Mole fraction**
EB	107.3	0.280	107.1	0.74	0.21	0.0009
Steam/water	1.86	0.005	1.86	0.013	0	0
ST	245.6	0.635	4.91	0.034	240.7	0.999
H2	0	0	0	0	0	0
Toluene	27.9	0.072	27.9	0.192	0	0
Benzene	3.89	0.010	3.90	0.027	0	0
Ethylene	0	0	0	0	0	0
Methane	0	0	0	0	0	0
Total	**386.6**		**145.6**		**240.9**	

Assumptions made during calculations:

- EB is a light key (LK) compound, and ST is a heavy key (HK) compound
- Packed bed column distillation with structured packing
- Packing material: Mellapak Plus 252Y
- For thickness calculations, the column is considered to be a pipe
- Reflux ratio / Min. reflux ratio = 1.5

To start calculations relative volatility of all compounds relative to HK were required. To find it, P_sat of each compound in the condenser (0.5 atm, 40℃) and reboiler (0.51 atm, 120℃) were calculated using the Antoine equation (Eq. J.1). Further two relative volatility values were obtained for different parts of the column, then geometric mean of these two were used in the following calculations (Table J2).

$$log_{10}P_{sat} = A - \frac{B}{T+C} \quad \text{(Eq. J.1)}$$

A, B, C - Antoine constants varying with temperature,
T - operating temperature

Table J3. Relative volatility of components

$\alpha_{j/HK}$	**Condenser**	**Reboiler**	**Geometric average**
eb/styrene	1.49	1.31	1.40
toluene/styrene	4.14	2.69	3.34
benzene/styrene	12.8	6.10	8.84
water/styrene	3.86	3.71	3.78

Firstly, heuristic calculations were made to find rough values for the number of stages, minimum and actual reflux ratio. To find the number of minimum stages, the Fenske equation was used:

$$N_{min} = \frac{log\left[\left(\frac{x_{D,LK}}{x_{D,HK}}\right)\left(\frac{x_{B,HK}}{x_{B,LK}}\right)\right]}{log(\alpha_{LK,HK})} \quad \text{(Eq. J.2)}$$

Where N_{min} - minimum number of stages,

$x_{D,LK}$ - fraction of LK in the distillate,

$x_{D,HK}$ - fraction of HK in the distillate,

$x_{B,LK}$ - fraction of LK in the bottom product,

$x_{B,HK}$ - fraction of LK in the bottom product,

$\alpha_{LK,HK}$ - volatility of LK relative to HK (Table A2).

Calculations showed that the minimum number of stages is 35.

Further Underwood equations were employed to estimate the minimum reflux ratio (RR_min):

$$\sum_{j=1}^{N_C} \frac{\alpha_j x_{F_j}}{\alpha_j - \theta} = 1 - q \quad \text{(Eq. J.3)}$$

$$\sum_{j=1}^{N_C} \frac{\alpha_j x_{D,j}}{\alpha_j - \theta} = 1 + RR_{min} \quad \text{(Eq.J.4)}$$

Where, x_{F_j} - feed composition of compound j.

q - feed quality = 1 as at our operating conditions the system is saturated liquid

θ - parameter found using the Goal seek function in Excel so that the underwood equation was equal to 0.

It was found that θ= 2.56781, and using Eq. 4G RR_min = 7. And RR_actual = RR_min*1.5 = 10.5. Using the reflux ratio values and Gilliland correlations (Eq. J5-7) actual number of stages were calculated:

$$X = \frac{RR - RR_{min}}{RR+1} \quad \text{(Eq. J.5)}$$

$$Y = 1 - exp\left[\left(\frac{1+54.4X}{11+117.2X}\right)\left(\frac{X-1}{X^{0.5}}\right)\right] \quad \text{(Eq. J.6)}$$

$$Y = \frac{N - N_{min}}{N+1} \quad \text{(Eq. J.7)}$$

Where N - the number of actual theoretical stages. It was calculated to be 57.

In packed bed columns, the HETP (height equivalent to theoretical plate) factor is a key factor in estimating the height of the column. According to the industry data for the packing material (Mellapak Plus 252Y), the HETP value with our system's pressure drop is about 0.5 [40]. Using the following formula:

$$H = HETP * N \quad \text{(Eq. J.8)}$$

It is possible to calculate the height of the column (H).

H = 0.5*100 = 22.8 m

As max bed height per section is 8-11 m to prevent maldistribution, the number of beds:

$$N_{bed} = \frac{H}{10} = 5 \quad \text{(Eq. J.9)}$$

J.3 Diameter calculations

Further, the inner diameter of the column was estimated using these data. Flooding conditions were used extensively to assess the flooding velocity, gas superficial velocity, pressure drop and diameter of the column. For that, the reflux ratio and individual parameters of packing material were used. As EB and ST are abundant in our system, calculations assumed a binary non-dilute system.

Flooding data for packed columns were first correlated by using a liquid-to-gas kinetic-energy ratio (F_{LV}) [40]:

$$F_{LV} = \left(\frac{L^{*}M_{L}}{V^{*}M_{V}}\right)\left(\frac{\rho_{L}}{\rho_{V}}\right)^{0.5} \quad \text{(Eq. J.10)}$$

Where L - liquid flow rate, kmol/h

V- vapor flow rate, kmol/h

M_L - molar mass of liquid, kg/kmol

M_V - molar mass of vapor, kg/kmol

ρ_L - density of liquid, kg/m^3, density of liquid leaving the top of the column. Estimated using Aspen simulation

ρ_V - density of vapor, kg/m^3, Estimated using Aspen property of mixture at 120℃ and 0.51 atm

M_L and M_V will cancel out in our case, as the distillation column uses a total condenser that liquifies all the vapor. Liquid and vapor flow rates were calculated in the distillate part using the reflux ratio definition:

$$\frac{L}{V} = RR \quad \text{(Eq. J.11)}$$

L = RR*V = 10.5*147 = 1546.7 kmol/h

And V = L+$Q_{distillate}$ = 1535.1+147 =1693.7 kmol/h

A generalized pressure-drop chart for structured packing developed by Strigle, Kister and Gill is shown in *Figure 1G*.The abscissa in the chart is F_{LV} (Eq. G9). The empirical ordinate in the chart is a modified empirical capacity factor (F_C) given by [48]:

$$F_C = u_{Vf} F_P^{0.5}\left(\frac{\rho_v}{\rho_l - \rho_v}\right)^{0.5} \upsilon_L^{0.05} \quad \text{(Eq. J.12)}$$

Where, ρ_v and ρ_L are used in lb/ft^3,

u_{Vf} - is the flooding velocity in ft/s,

F_P - packing factor for Mellapak Plus 252Y, $21 ft^{-1}$

υ_L - the kinematic viscosity in centistokes.

For modern structured packings with packing factors between 9 and 60 ft^{-1}, Kister and Gill [13] showed that the simple empirical correlation gives the specific pressure drop at flooding (units inches H_2O/ft):

$$\Delta P_{flood} = 0.115 * F_C^{0.7} \quad \text{(Eq. J.13)}$$

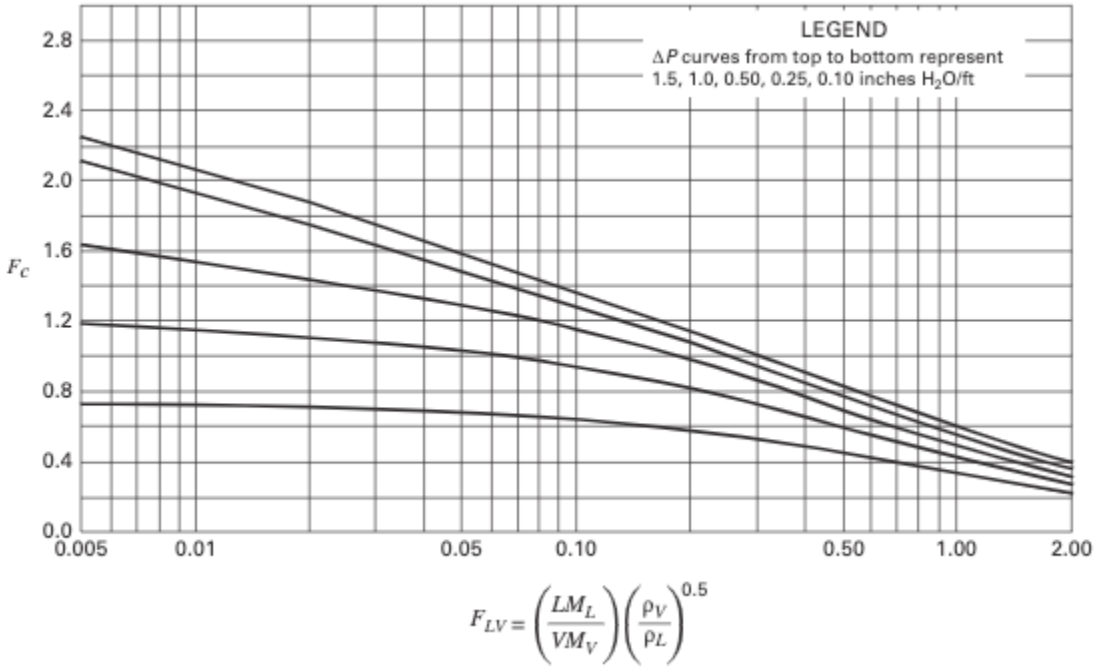

Figure J1. Generalized correlation for specific pressure drop for towers with structured packing

Using plot (Fig. J1) and F_{LV} = 0.04, ΔP_{flood} = 0.65 inches H_2O/ft capacity factor (F_C) was estimated as 1.5. Rewriting Eq. J11 for flooding velocity gives:

$$u_{Vf} = \frac{F_C}{F_P^{0.5}\left(\frac{\rho_v}{\rho_l - \rho_v}\right)^{0.5} \upsilon_L^{0.05}} \quad \text{(Eq. J.14)}$$

Thus u_{Vf} = 10.6 ft/s = 3.2 m/s. To avoid flooding in the column, vapor superficial velocity should be between 50-80% of this flooding velocity. We assumed this factor (f) was 0.7. Column (tower) diameter (D_T) equation based on a fraction (f) of flooding velocity, and the continuity equation becomes [48]:

$$D_T = \left(\frac{4VM_V}{f^* u_{Vf} \pi \rho_V}\right)^{0.5} \quad \text{(Eq. J.15)}$$

Thus, estimated D_T = 4.2 m.

J.5 Construction material calculations

For calculations, the distillation column was assumed to be a vessel. The basic data needed will be [40]:

1) Vessel function;
2) Process materials and services;
3) Operating and design temperature and pressure;
4) Materials of construction;
5) Vessel dimensions and orientation;
6) Type of vessel heads to be used;
7) Openings and connections required;
8) Specification of heating and cooling jackets or coils;
9) Specification of internal fittings.

Material data was obtained from the 2004 ASME Boiler and Pressure Vessel Code SECTION II Materials Part A Ferrous metal specifications and Part D Properties (customary or metric versions).

Material selection must consider both operating pressure and temperature. This factor is particularly critical because the distillation column operates under vacuum conditions. Extensive stress calculations were conducted to assess material compatibility and determine a reasonable wall thickness. Maximum allowable stress and nominal design strength are crucial in column design to ensure structural integrity and safety under operating conditions. They help prevent mechanical failure by accounting for material limits, pressure, temperature, and load factors. According to literature stainless steel 316L is suitable for distillation columns prone to corrosion [40]. Maximum allowable stress for this material was 115 MPa. Then minimum wall thickness (mm) of the vessel was calculated using the following equation (as specified by the ASME BPV Code (Sec. VIII D.1 Part UG-27)):

$$t_{wall} = \frac{P_i D_i}{2SE - 1.2P_i} \quad \text{(Eq. J.16)}$$

Where, P_i - internal absolute pressure of the column including safety factor +10% (HTRI data), N/mm^2

D_i - internal diameter of the column, mm

S - maximum allowable stress, N/mm^2

E - joint efficiency, for our system 0.85

Thua t_{wall} = 6 mm.

Then the top thickness of the column was calculated using an ellipsoidal top, as the column has a large diameter. Most standard ellipsoidal heads are manufactured with a major and minor axis ratio of 2:1. For this ratio, the following equation can be used to calculate the minimum thickness required (ASME BPV Code Sec. VIII D.1 Part UG-32) [40]:

$$t_{head} = \frac{P_i D_i}{2SE - 0.2P_i} = 5\ mm \quad \text{(Eq. J.17)}$$

Using these minimum thickness values we can evaluate if our material can withstand the following loads:

1) Pressure
2) Dead weight of vessel and contents
3) Wind
4) Earthquake (seismic)
5) External loads imposed by piping and attached equipment

The longitudinal and circumferential stresses due to pressure (internal or external), given by:

$$\sigma_L = \frac{PD_i}{4t} = 33\ N/mm^2 \quad \text{(Eq. J.18)}$$

$$\sigma_h = \frac{PD_i}{2t} = 65\ N/mm^2 \quad \text{(Eq. J.19)}$$

The direct stress σw due to the weight of the vessel, its contents, and any attachments:

$$\sigma_w = \frac{W_z}{\pi(D_i + t)t} = 24\ N/mm^2 \quad \text{(Eq. J.20)}$$

Where W_z = 2283 kN is the total weight of the distillation column including weights of vessel and packing material [40].

Bending stresses resulting from the bending moments to which the vessel is subjected. Bending moments will be caused by the following loading conditions:

a. The wind loads on tall self-supported vessels
b. Seismic (earthquake) loads on tall vessels

The bending stresses will be compressive or tensile, depending on location, and are given by:

$$\sigma_b = \pm \frac{M}{I_v} \left(\frac{D_i}{2} + t\right) \quad \text{(Eq. J.21)}$$

Where, M is the total bending moment at the plane being considered = $\frac{Wx^2}{2} = 6.2 * 10^6 N * m$, where x is the distance measured from the free end (height of column 44 m) and W (dynamic wind pressure as 1280 N/m2, W=1280*outer diameter) the load per unit length (Newtons per meter run) [40].

I_v the second moment of area of the vessel about the plane of bending given by:

$$I_v = \frac{\pi}{64} (D_o^4 - D_i^4) = 2.96 * 10^{11} mm^4 \quad \text{(Eq. J.22)}$$

Where, D_o - outer diameter, Di+2t, m

Thus, σ_b = 52.5 N/mm^2

The resultant longitudinal stress is:

$$\sigma_z = \sigma_L + \sigma_w \pm \sigma_b \quad \text{(Eq. J.23)}$$

$\sigma_{z,upwind}$ = 61 N/mm^2

$\sigma_{z,downwind}$ = -44 N/mm^2

The greatest difference between the principal stresses will be on the downwind side:

65 - (-44)= 109 N/mm^2, which is less than allowable 115 N/mm^2. Which justifies that the material can withstand the operating conditions of the system.

Table J4. Summary of column's accessory components [40]

Components	Illustration	Description
Packing support	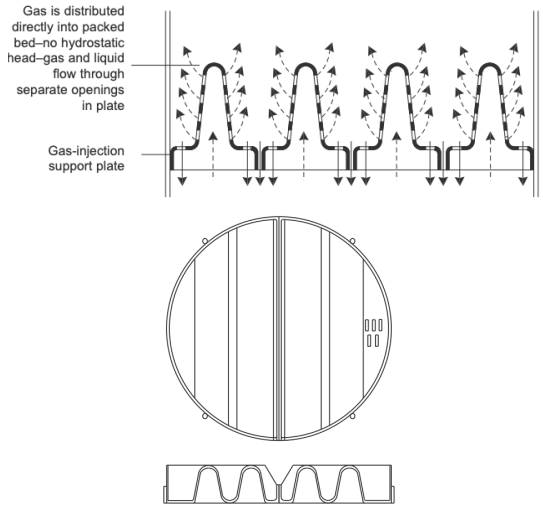	The support plate supports the wet packing while allowing gas and liquid flow. In large-diameter columns, the gas-injection type (as shown in the illustration) is ideal, with gas inlets above the fluid outflow. This design minimizes pressure drop and flooding and is available in metals, ceramics, and plastics.
Liquid distributors	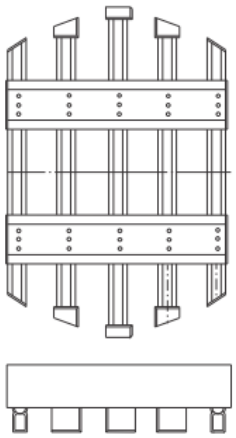	For large-diameter columns, the weir-trough-type distributor (shown in the illustration) provides good liquid distribution and a large free area for gas flow. Distributors relying on gravity flow must be installed at a level that prevents liquid maldistribution.

Liquid Redistributors	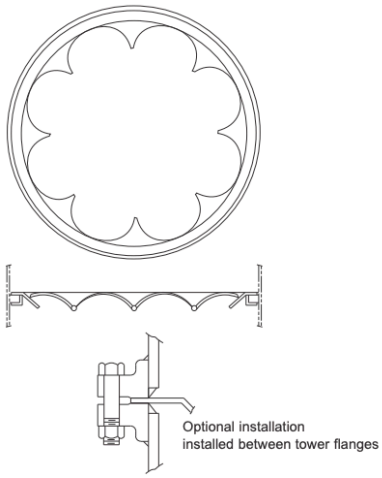	Redistributors collect liquid from the column walls and redistribute it evenly over the packing, correcting any maldistribution. A full redistributor also acts as a packing support and liquid distributor. The "wall-wiper" type, which directs collected wall liquid back to the center packing, is commonly used in large-diameter columns.

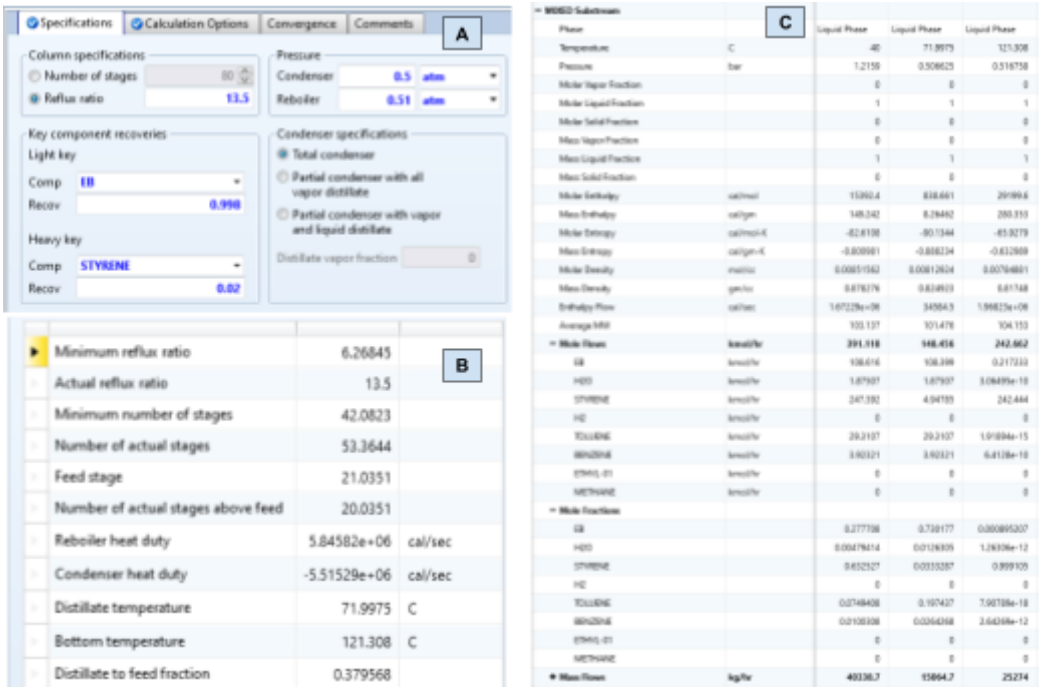

Figure J2. DSTWU: (A) Input specifications, (B) Results summary of unit, (C) Stream results

Figure J3. Input to RadFrac: (A) Configuration, (B) Streams, (C) Pressure, (D) Design and internal specifications, (E) Geometry of packing material

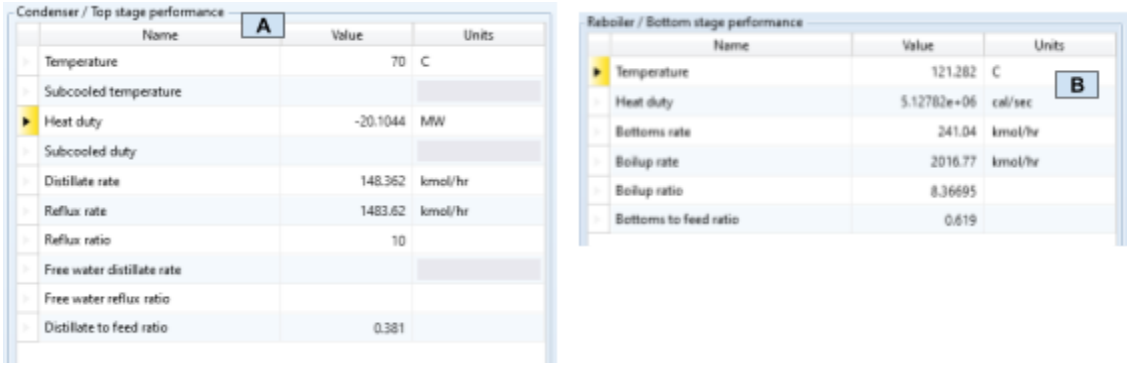

Figure J4. T-101 unit: (A) Condenser results, (B) Reboiler results

	Units	15RAD	16	17
From			RADFRAC	RADFRAC
To		RADFRAC		
Stream Class		CONVEN	CONVEN	CONVEN
Maximum Relative Error				
Cost Flow	$/hr			
− MIXED Substream				
Phase		Liquid Phase	Liquid Phase	Liquid Phase
Temperature	C	40	121.285	72.1063
Pressure	bar	1.2159	0.516758	0.506625
Molar Vapor Fraction		0	0	0
Molar Liquid Fraction		1	1	1
Molar Solid Fraction		0	0	0
Mass Vapor Fraction		0	0	0
Mass Liquid Fraction		1	1	1
Mass Solid Fraction		0	0	0
Molar Enthalpy	cal/mol	15416.3	29127.1	1119.72
Mass Enthalpy	cal/gm	149.464	279.642	11.0321
Molar Entropy	cal/mol-K	-82.6029	-65.9673	-89.852
Mass Entropy	cal/gm-K	-0.800847	-0.633336	-0.88527
Molar Density	mol/cc	0.00851545	0.00784755	0.00813091
Mass Density	gm/cc	0.878321	0.81739	0.82526
Enthalpy Flow	cal/sec	1.6773e+06	1.96162e+06	46415.6
Average MW		103.144	104.159	101.497
− Mole Flows	**kmol/hr**	**391.679**	**242.45**	**149.23**
EB	kmol/hr	108.617	0.849822	107.768
H2O	kmol/hr	1.87994	1.49553e-16	1.87994
STYRENE	kmol/hr	248.152	241.6	6.55215
H2	kmol/hr	0	0	0
TOLUENE	kmol/hr	29.126	7.11807e-14	29.126
BENZENE	kmol/hr	3.90411	3.46447e-15	3.90411
ETHYL-01	kmol/hr	0	0	0
METHANE	kmol/hr	0	0	0
+ Mole Fractions				
+ Mass Flows	**kg/hr**	**40399.5**	**25253.2**	**15146.3**
+ Mass Fractions				

Figure J5. Stream results to RadFrac

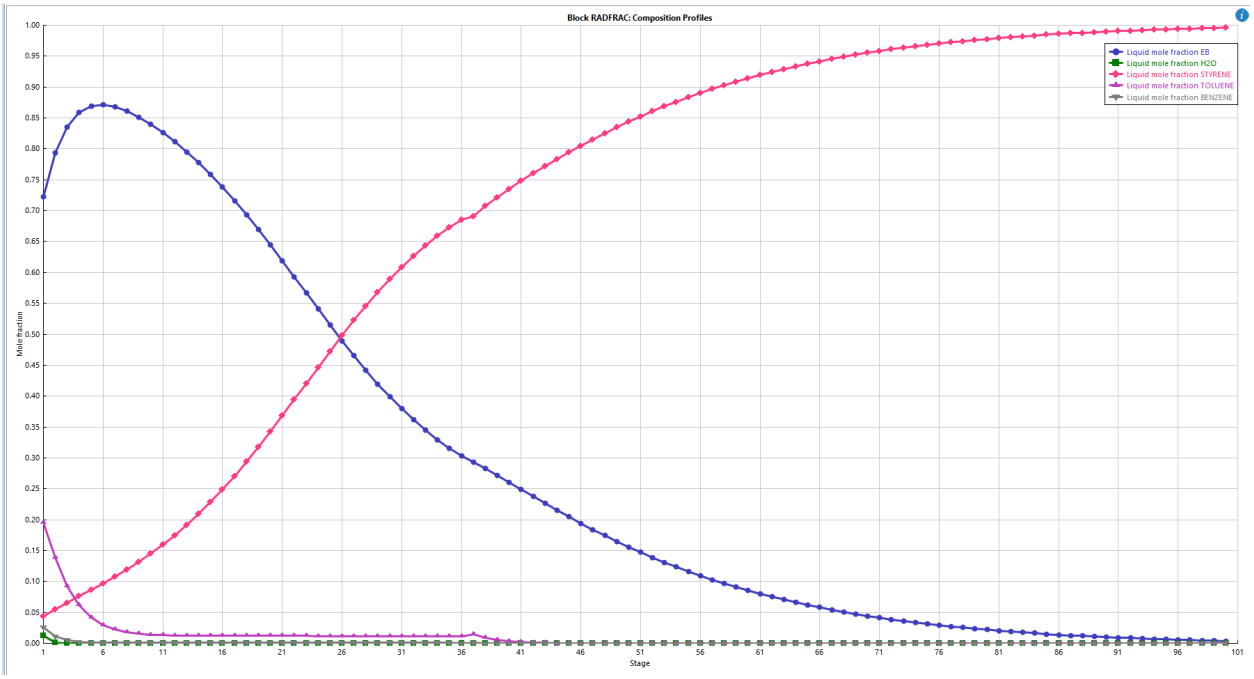

Figure J6. Liquid composition plot for RadFrac unit stream results

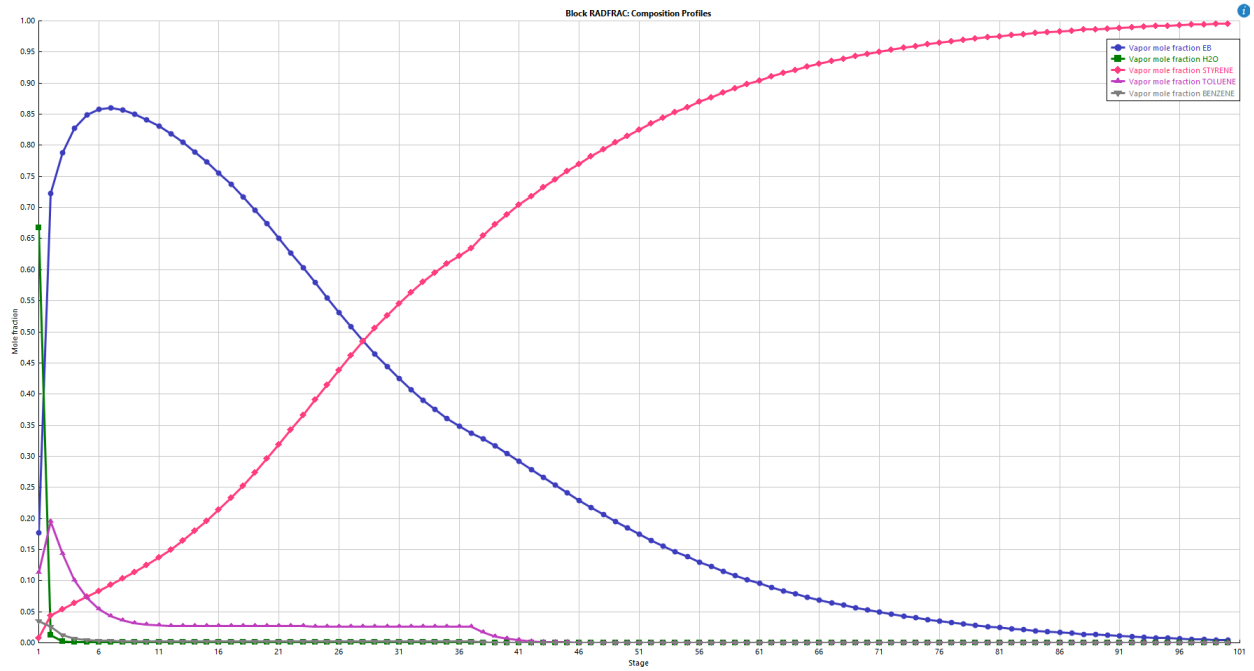

Figure J7. Vapor composition plot for RadFrac unit stream results

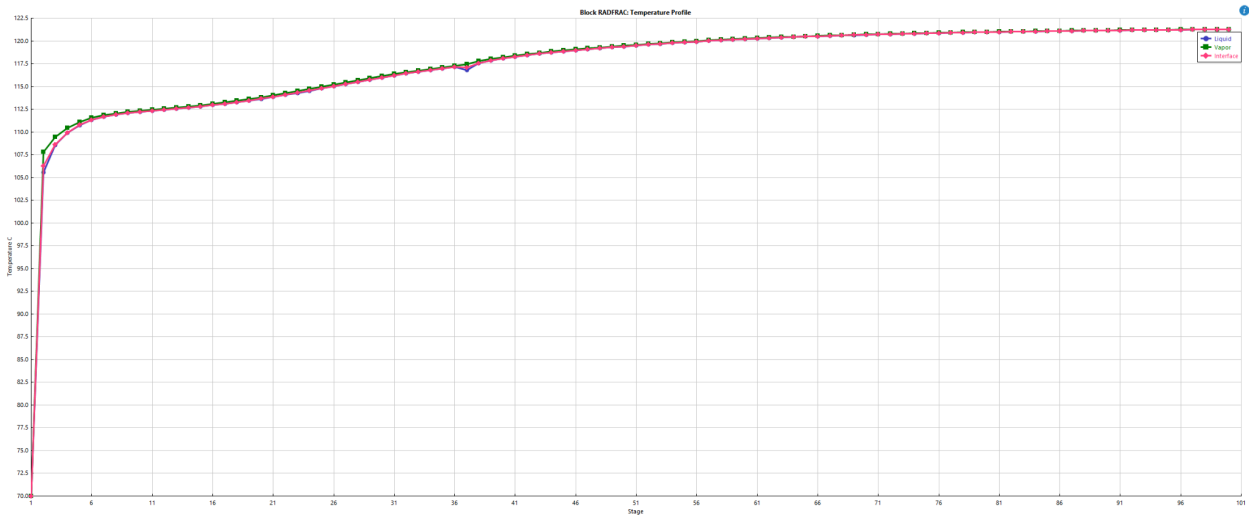

Figure J8. Temperature profile plot for RadFrac unit stream results *Figure 7.*Vapor composition plot for RadFrac unit stream results

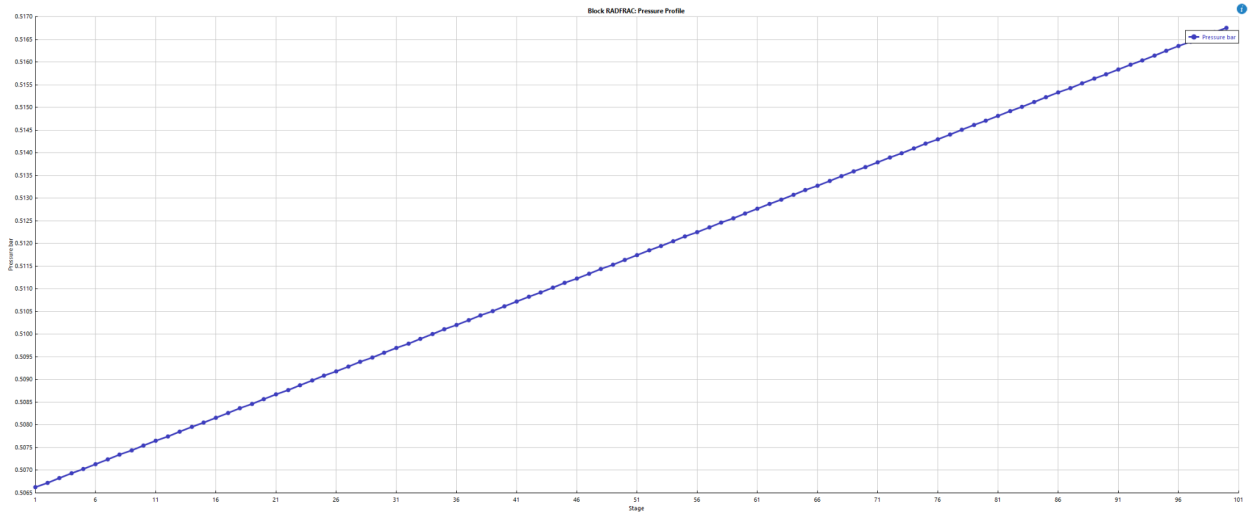

Figure J9. Pressure profile plot for RadFrac unit stream results

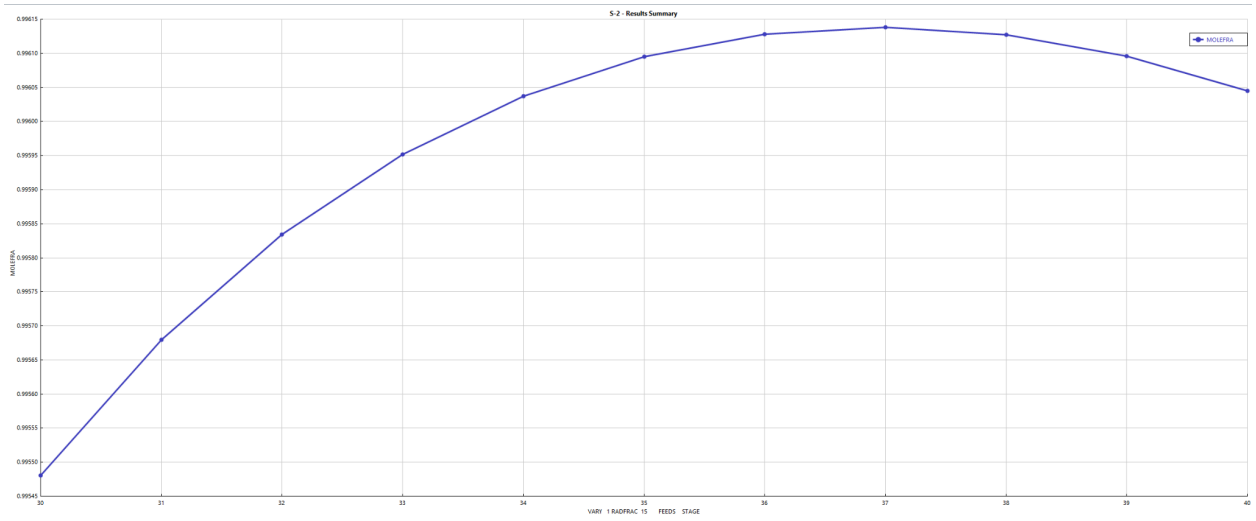

Figure J10. Sensitivity analysis for feed stage location for pure styrene purity

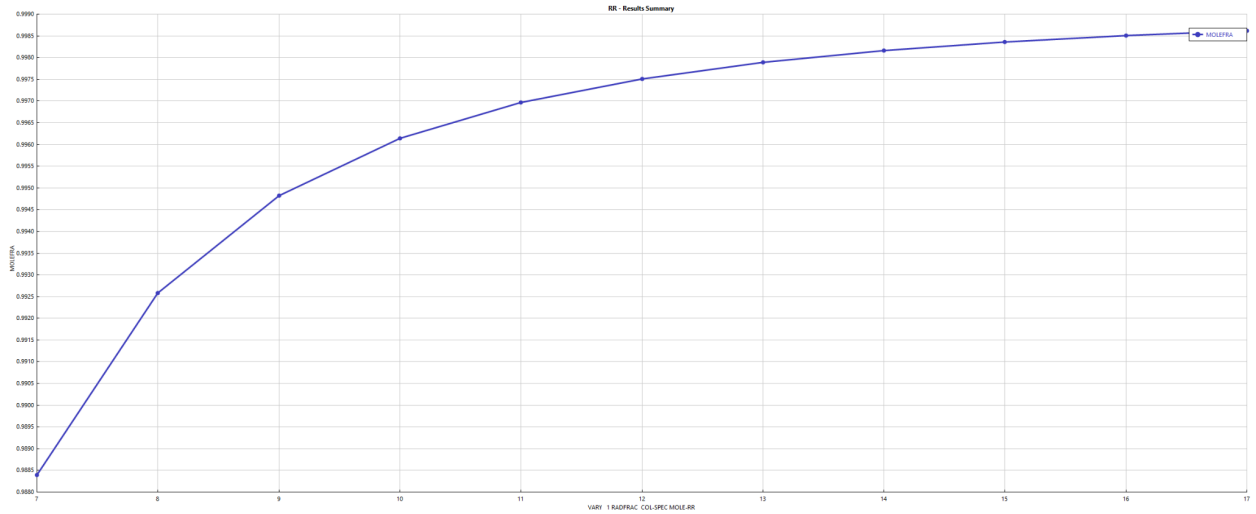

Figure J11. Sensitivity analysis for reflux ratio and styrene mole fraction in bottoms product

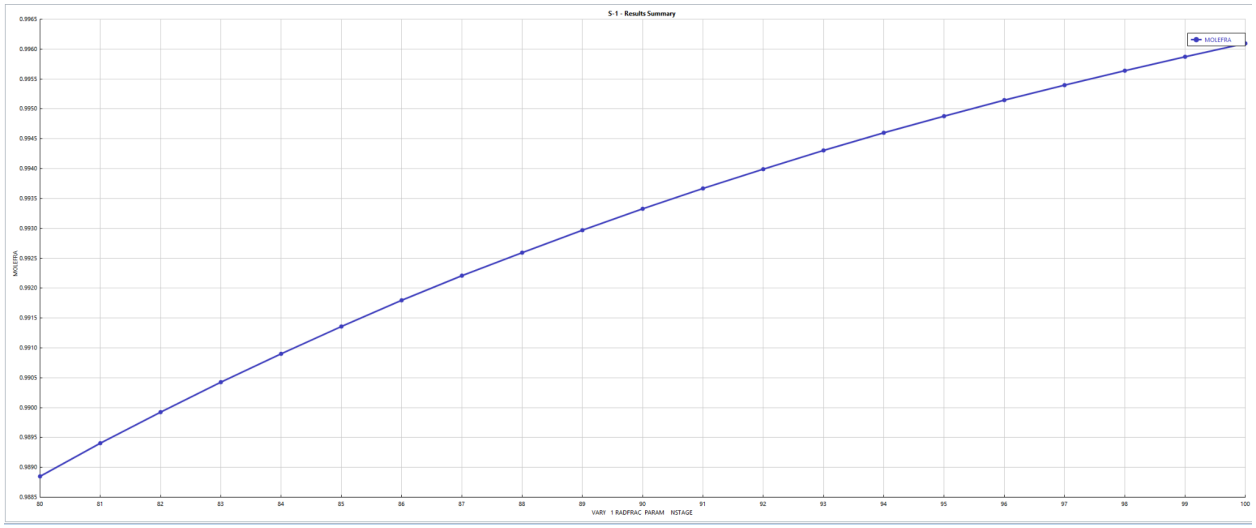

Figure J12. Sensitivity analysis for number of stages and styrene mole fraction in bottoms product

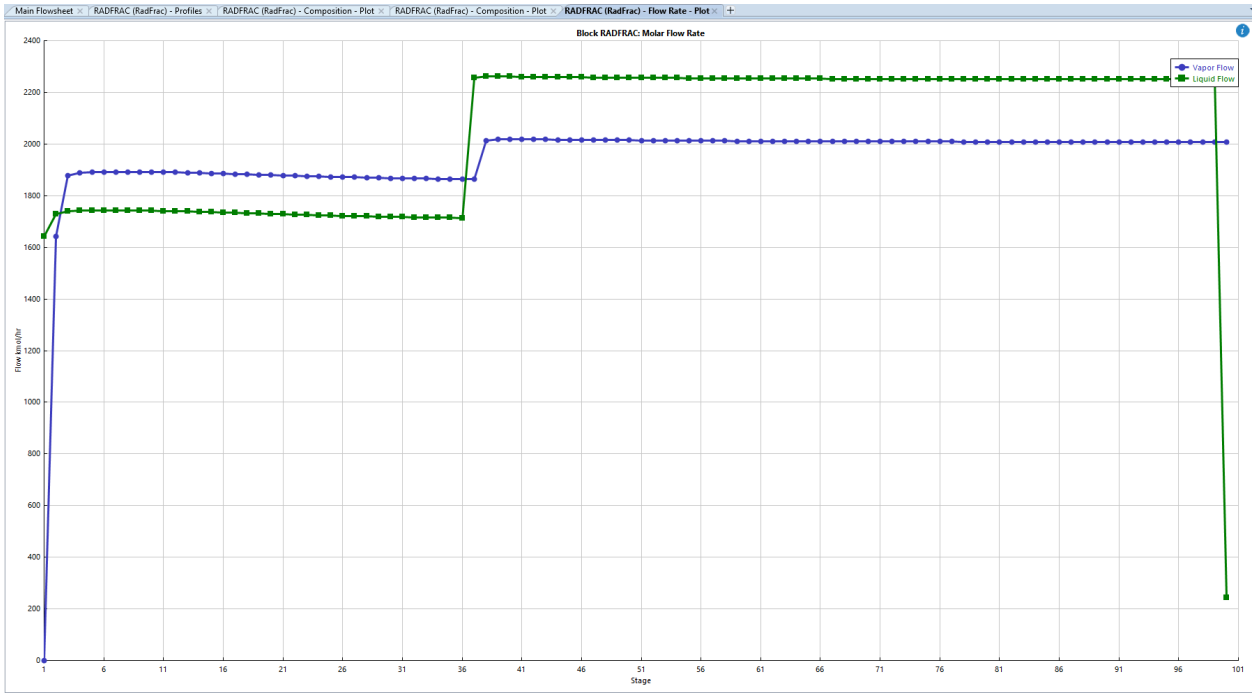

Figure J13. Flow rate profile at different stages of the column

Appendix K

K.1 Design details and calculations for T-102

Table K1. Summary of the design of the sieve plate [40]

Illustration	
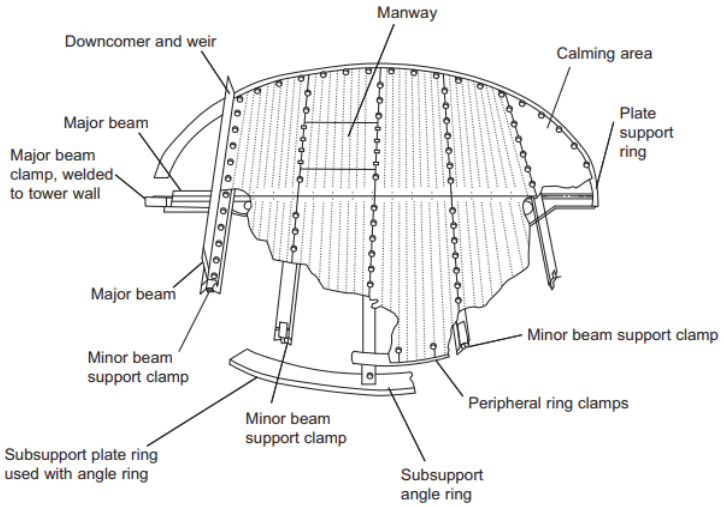	Sectional Construction A typical tray consists of a perforated plate supported by a welded ring along the vessel wall and beams spaced about 0.6 m apart. The beams, usually made of folded sheet metal in angle or channel sections, provide structural support. Special fasteners allow for easy assembly from one side. One section is designed to be removable, serving as a manway to facilitate maintenance and reduce the need for additional vessel openings.
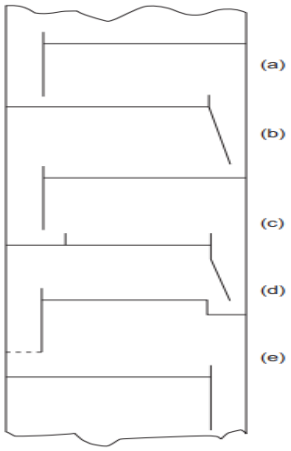 Segment (chord) downcomer designs: (a) vertical apron; (b) inclined apron; (c) inlet weir; (d) recessed well; (e) truncated downcomer[40]	Downcomers The segmental (chord) downcomer is the simplest and most cost-effective design, suitable for most applications. It consists of a flat apron extending downward from the outlet weir, which can be vertical or sloped to maximize perforated plate area, commonly seen in high-capacity trays. For better sealing, an inlet weir or recessed seal pan may be added. Circular downcomers are used for low liquid flow rates, while curved and truncated downcomers optimize space and capacity in large columns.

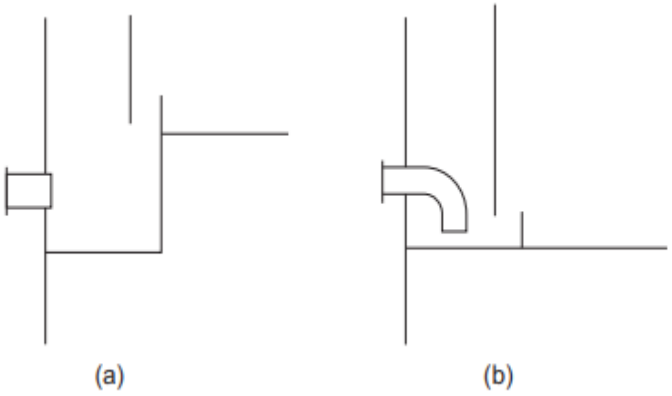	Side Stream and Feed Points Side streams require a liquid seal at the withdrawal point to ensure proper flow. Pipes and rundown lines must be designed for self-venting to prevent vapor buildup. A correlation by Sewell (1975) helps determine the minimum pipe diameter for this purpose[40].

Table K2. Feed and Product Composition with Relative Volatility for Fenske Equation

Compound	x_f	x_d	x_b	Relative Vol.
EB	0.724	0.031	0.935	1
Steam/water	0.012	0.054	0.000	2.99
ST	0.050	0.000	0.065	0.76
Toluene	0.187	0.803	0.0002	2.14
Benzene	0.026	0.112	0.000	5.15

Table K3. The saturation pressure and relative volatility of feed components

Component	Condenser		Reboiler		Geom. Average
	P_{sat}, atm	Relative Vol.	P_{sat}, atm	Relative Vol.	Relative Vol.
EB	0.11	1	1.43	1	1
Steam/water	0.31	2.75	4.66	3.25	2.99
ST	0.08	0.72	1.13	0.79	0.76

Toluene	0.27	2.41	2.72	1.90	2.14
Benzene	0.72	6.50	5.84	4.07	5.15

$$\frac{N_r}{N_s} = [(\frac{B}{D})(\frac{x_{HK}}{x_{LK}})_F(\frac{x_{LK,B}}{x_{HK,D}})^2]^{0.206} \quad \text{(Eq. K.1)}$$

where, N_r is the number of stages above the feed, N_s is the number of stages below the feed, B is the molar flow rate of bottom products, D is the molar flow rate of distillate products. Feed stage is estimated to be at 4th stage. The thickness of the vessel was calculated in the same way as for T-101 and is provided in the Excel file for T-102.

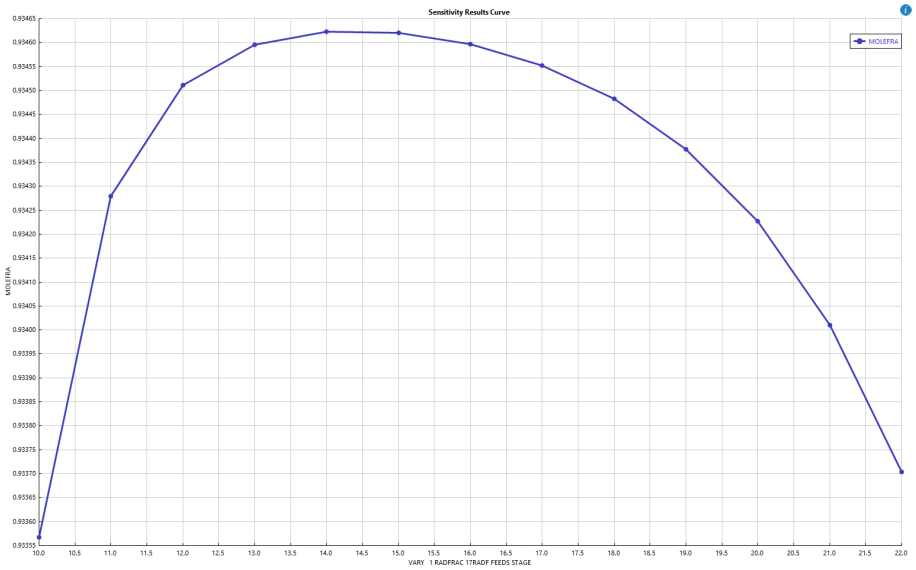

Figure K1. Sensitivity analysis for feed stage location

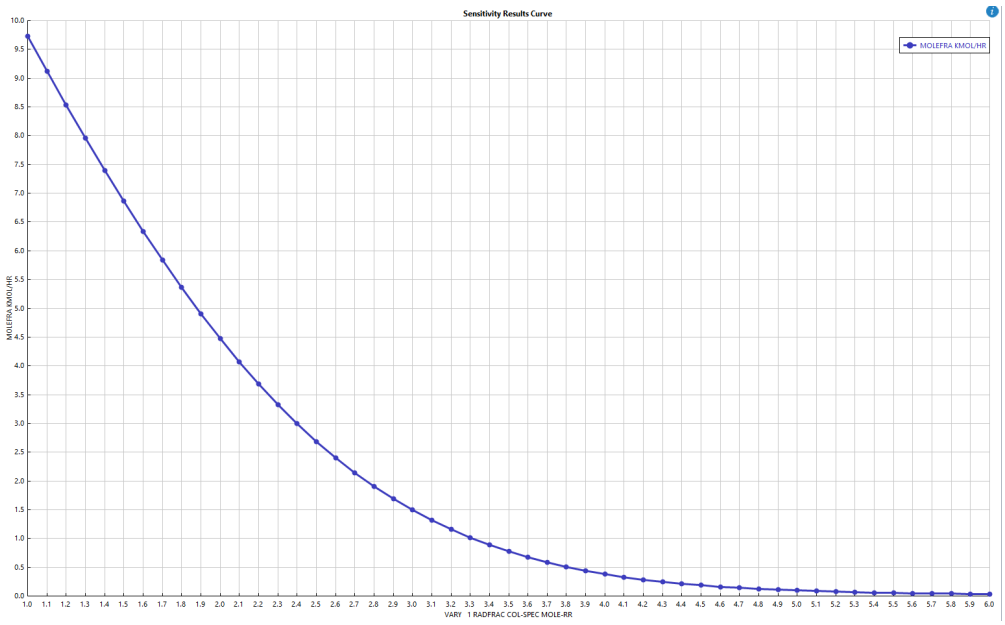

Figure K2. Sensitivity analysis for reflux ratio and toluene molar flow rate in bottoms product

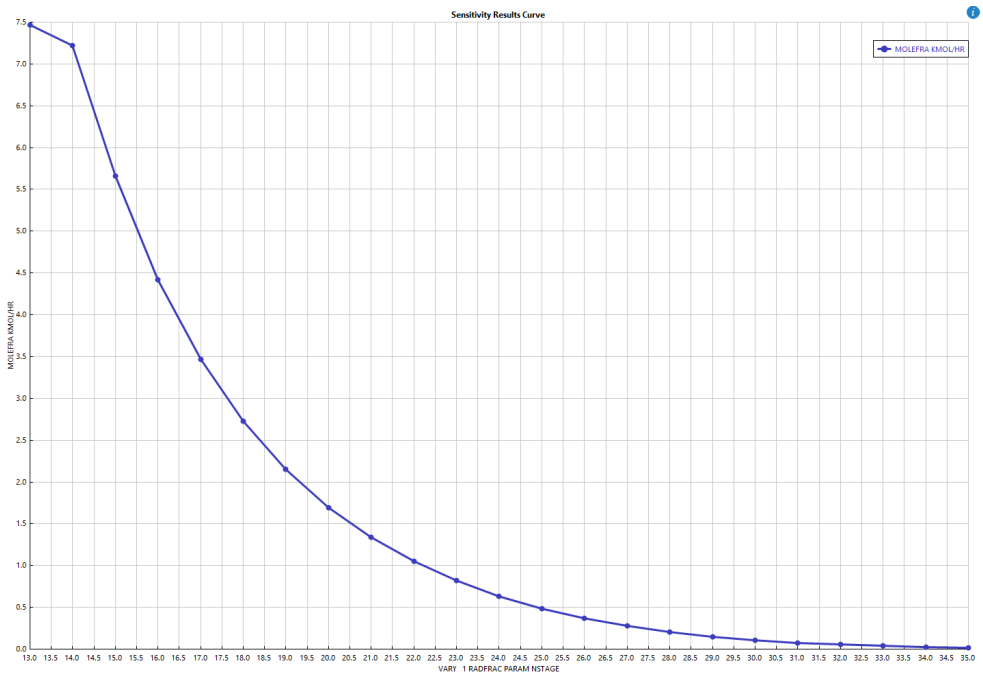

Figure K3. Sensitivity analysis for number of stages and toluene molar flow rate in top product

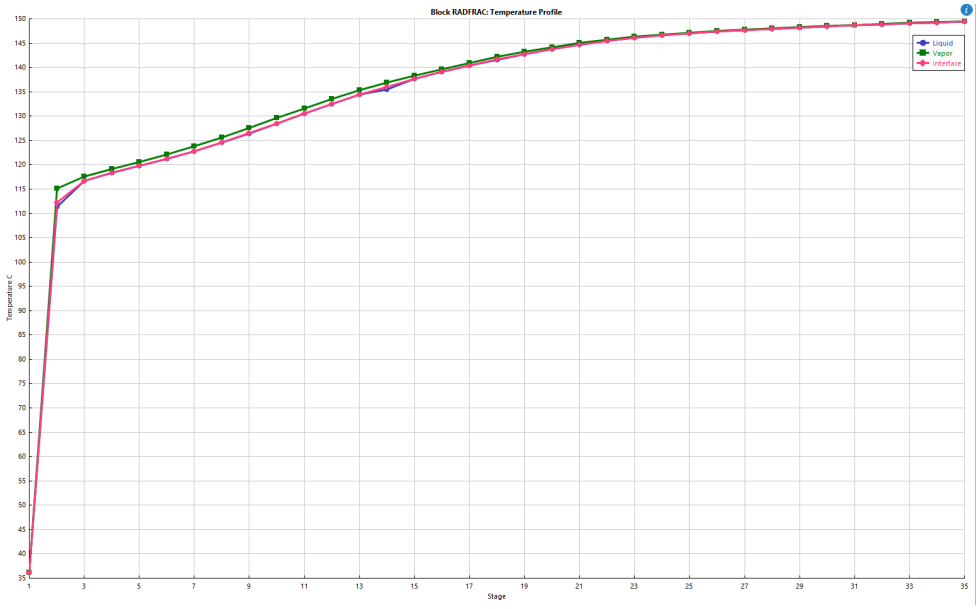

Figure K4. Temperature profile plot for RadFrac unit stream results

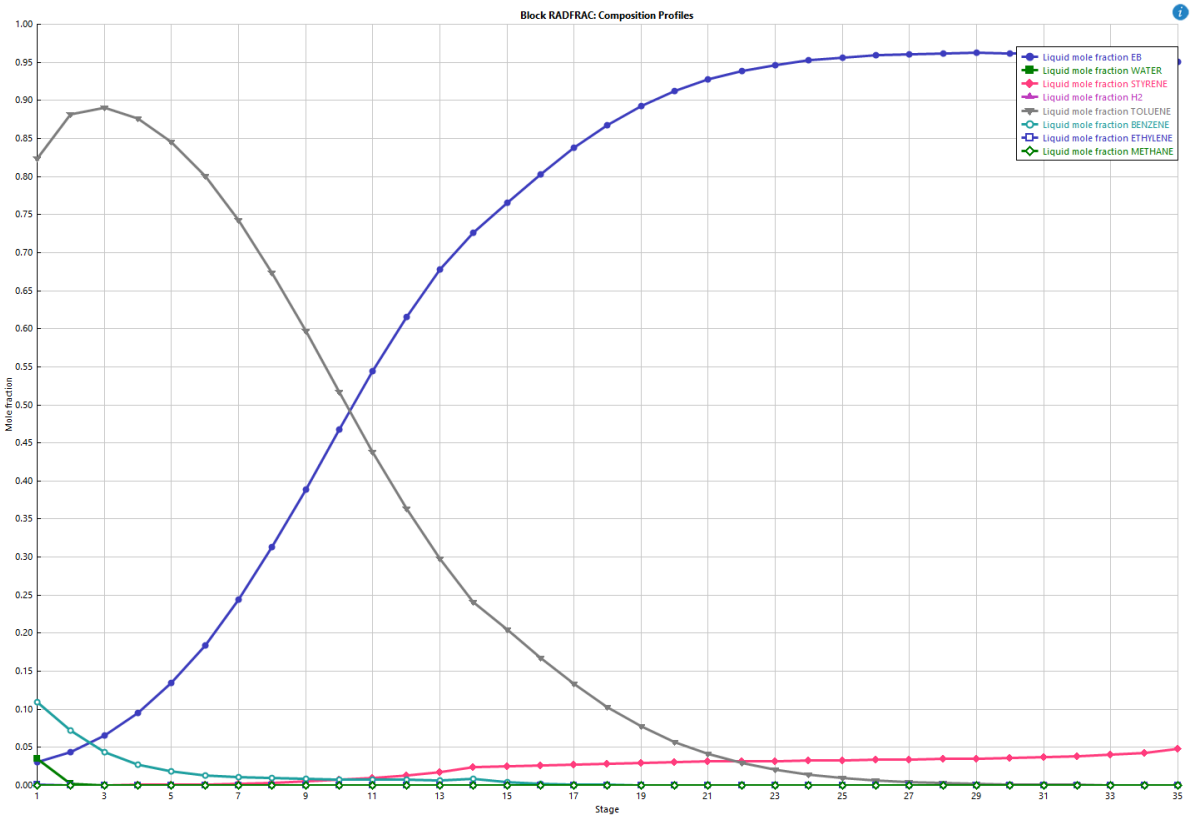

Figure K5. Liquid composition plot for RadFrac unit stream results

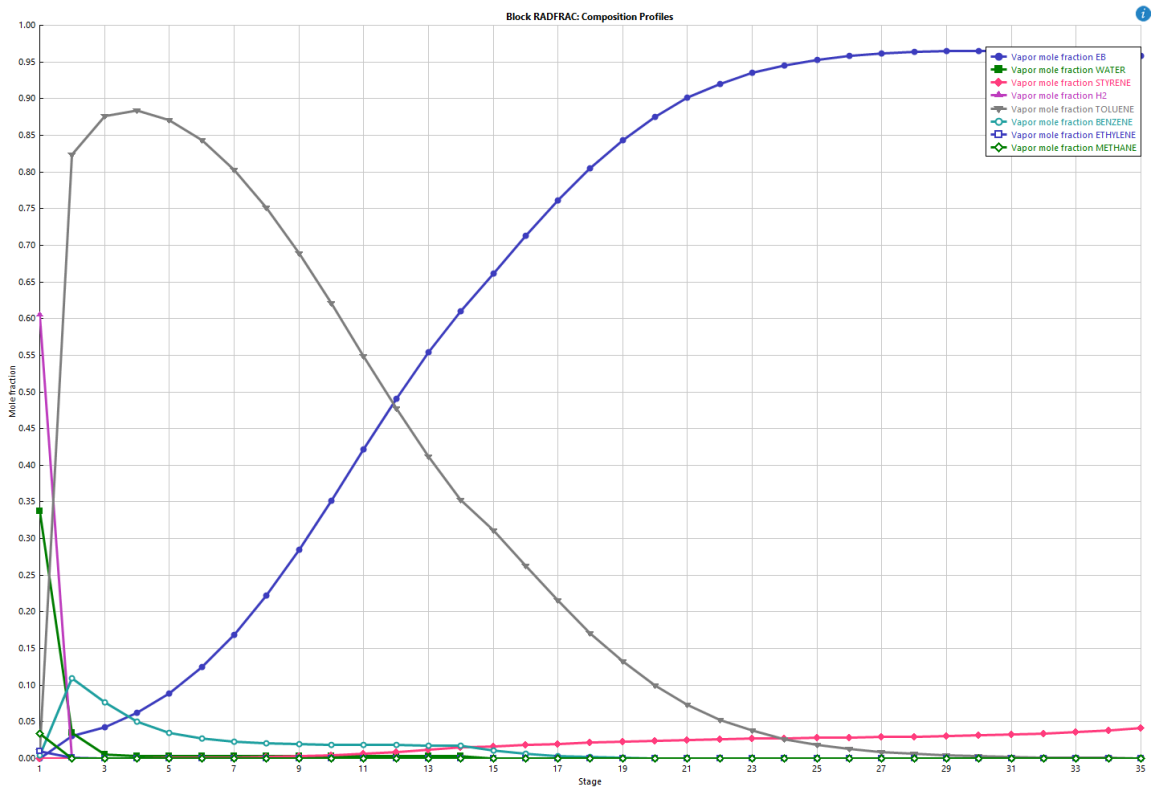

Figure K6. Vapor composition plot for RadFrac unit stream results

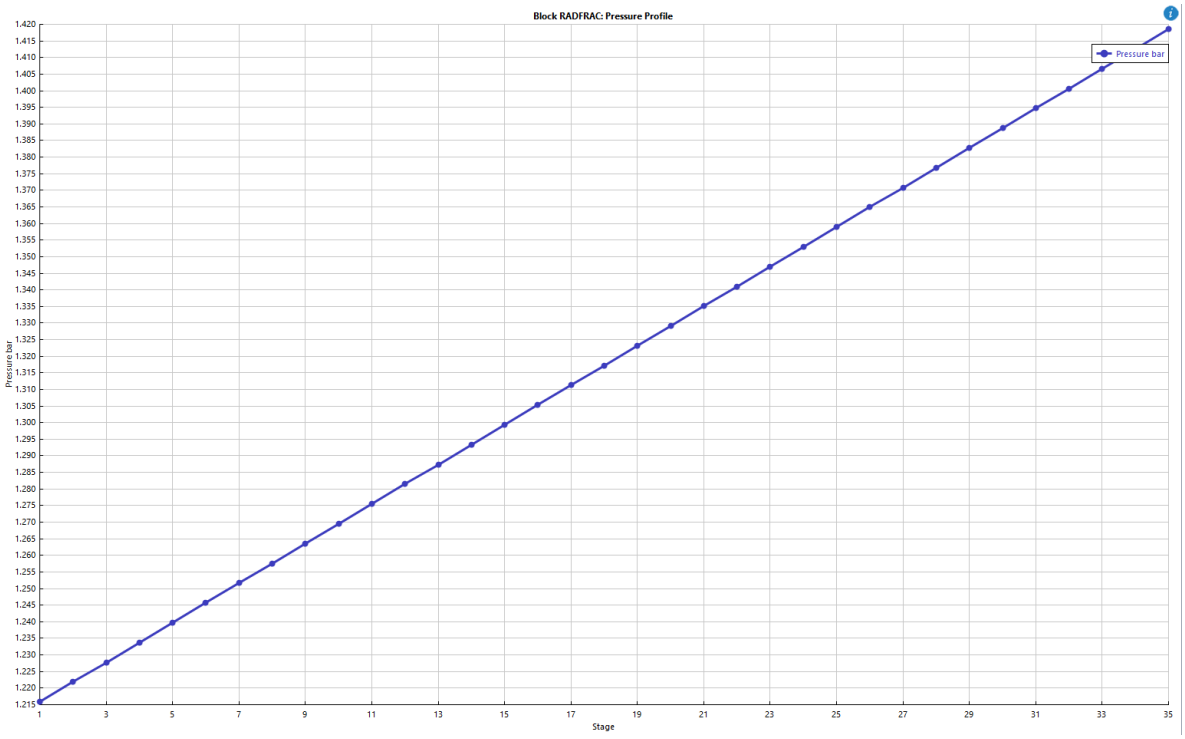

Figure K7. Pressure profile plot for RadFrac unit stream results

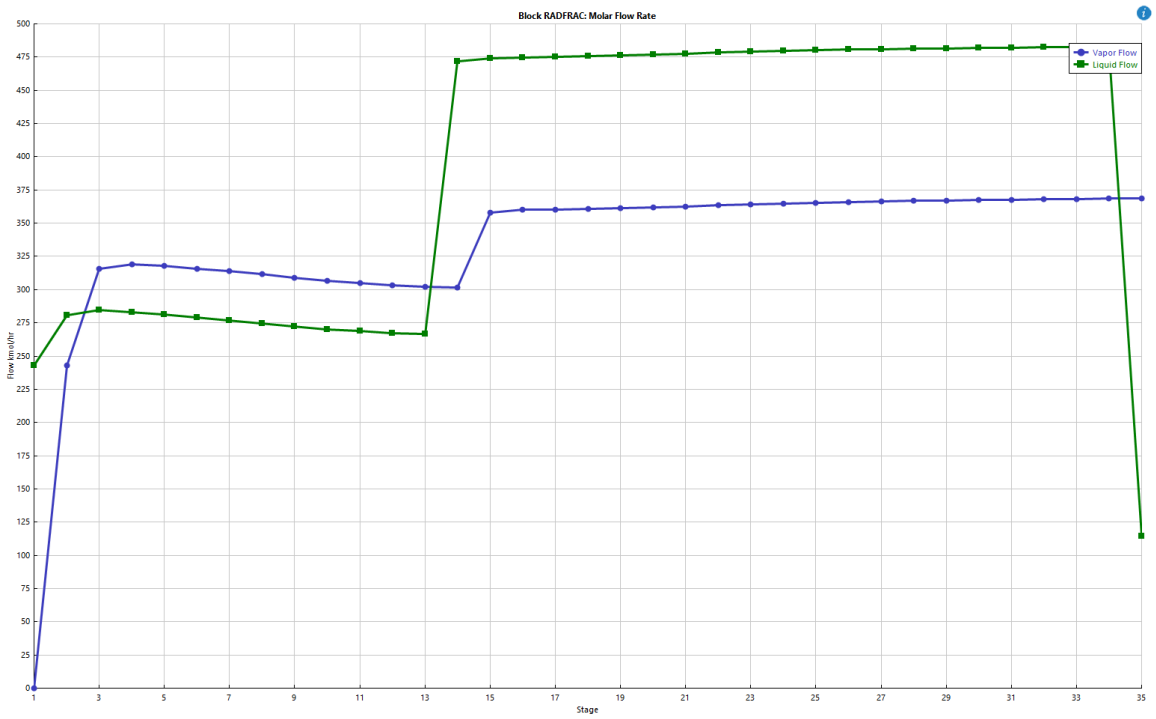

Figure K8. Flow rate profile at different stages of the column

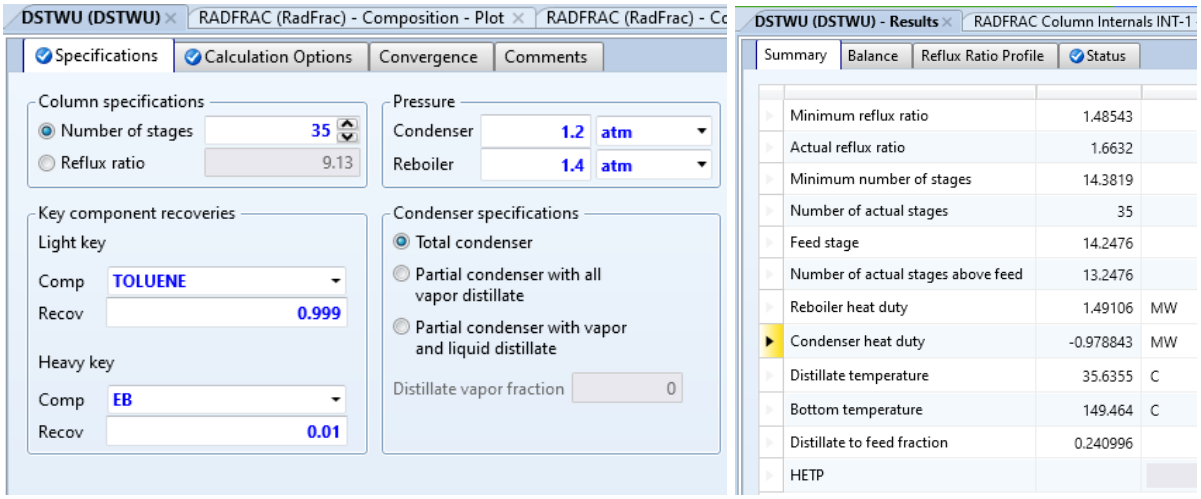

Figure K9. DSTWU Inputs and Results Summary

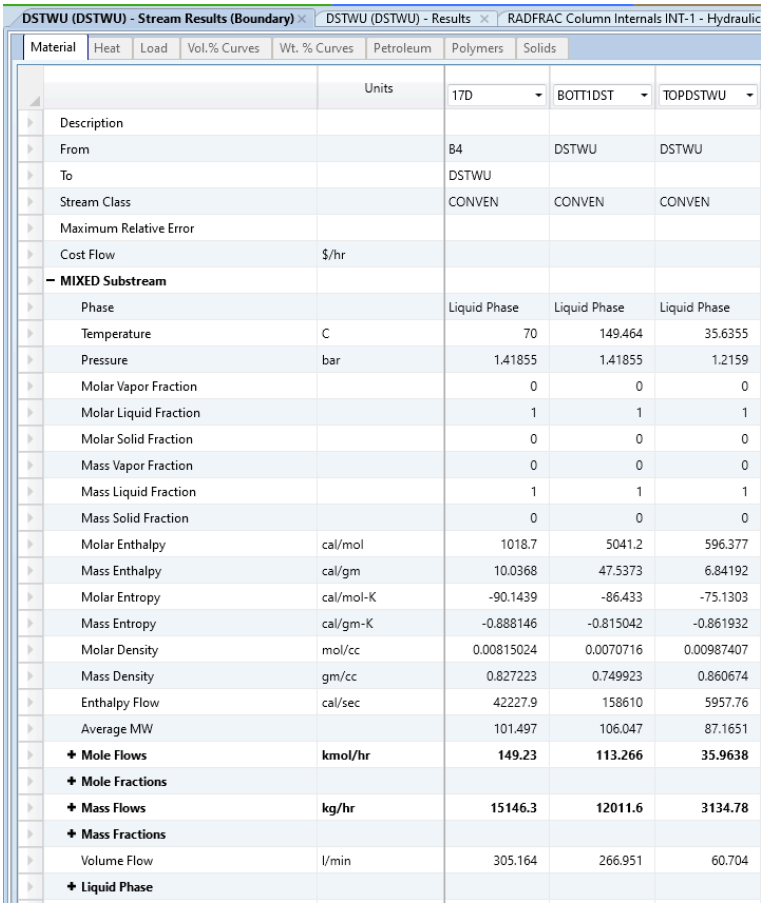

DSTWU (DSTWU) - Stream Results (Boundary) | DSTWU (DSTWU) - Results | RADFRAC Column Internals INT-1 - Hydraulic

Material | Heat | Load | Vol.% Curves | Wt. % Curves | Petroleum | Polymers | Solids

	Units	17D	BOTT1DST	TOPDSTWU
Description				
From		B4	DSTWU	DSTWU
To		DSTWU		
Stream Class		CONVEN	CONVEN	CONVEN
Maximum Relative Error				
Cost Flow	$/hr			
MIXED Substream				
Phase		Liquid Phase	Liquid Phase	Liquid Phase
Temperature	C	70	149.464	35.6355
Pressure	bar	1.41855	1.41855	1.2159
Molar Vapor Fraction		0	0	0
Molar Liquid Fraction		1	1	1
Molar Solid Fraction		0	0	0
Mass Vapor Fraction		0	0	0
Mass Liquid Fraction		1	1	1
Mass Solid Fraction		0	0	0
Molar Enthalpy	cal/mol	1018.7	5041.2	596.377
Mass Enthalpy	cal/gm	10.0368	47.5373	6.84192
Molar Entropy	cal/mol-K	-90.1439	-86.433	-75.1303
Mass Entropy	cal/gm-K	-0.888146	-0.815042	-0.861932
Molar Density	mol/cc	0.00815024	0.0070716	0.00987407
Mass Density	gm/cc	0.827223	0.749923	0.860674
Enthalpy Flow	cal/sec	42227.9	158610	5957.76
Average MW		101.497	106.047	87.1651
Mole Flows	**kmol/hr**	**149.23**	**113.266**	**35.9638**
Mole Fractions				
Mass Flows	**kg/hr**	**15146.3**	**12011.6**	**3134.78**
Mass Fractions				
Volume Flow	l/min	305.164	266.951	60.704
Liquid Phase				

Figure K10. DSTWU Stream Results

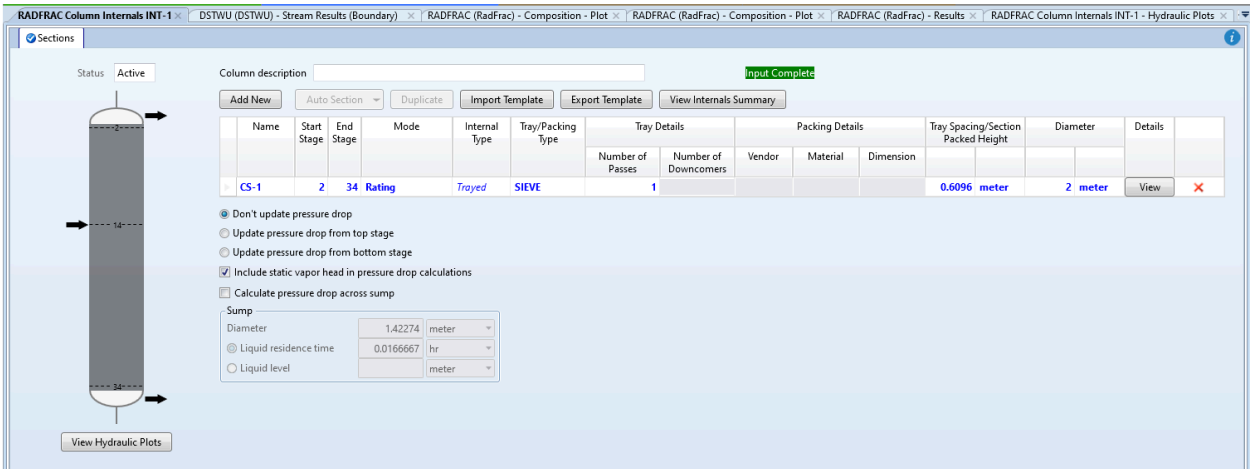

RADFRAC Column Internals INT-1 | DSTWU (DSTWU) - Stream Results (Boundary) | RADFRAC (RadFrac) - Composition - Plot | RADFRAC (RadFrac) - Composition - Plot | RADFRAC (RadFrac) - Results | RADFRAC Column Internals INT-1 - Hydraulic Plots

Sections

Status Active

Column description

Input Complete

Add New | Auto Section | Duplicate | Import Template | Export Template | View Internals Summary

Name	Start Stage	End Stage	Mode	Internal Type	Tray/Packing Type	Tray Details: Number of Passes	Tray Details: Number of Downcomers	Packing Details: Vendor	Packing Details: Material	Packing Details: Dimension	Tray Spacing/Section Packed Height		Diameter		Details
CS-1	2	34	Rating	Trayed	SIEVE	1					0.6096	meter	2	meter	View

Don't update pressure drop

Update pressure drop from top stage

Update pressure drop from bottom stage

Include static vapor head in pressure drop calculations

Calculate pressure drop across sump

Sump

Diameter	1.42274	meter
Liquid residence time	0.0166667	hr
Liquid level		meter

View Hydraulic Plots

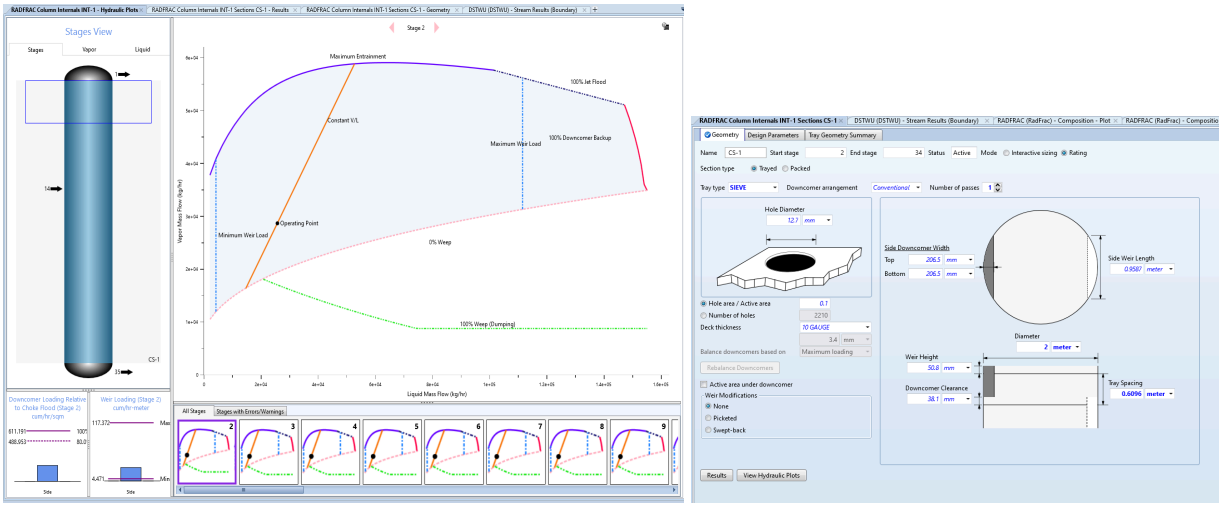

Figure K11. RadFrac Column Internals, Hydraulic Plots and Geometry

RADFRAC Column Internals INT-1 Sections CS-1 - Results | RADFRAC Column Internals INT-1 - Hydraulic P

Summary | By Tray | Messages

Name: CS-1 Status: Active

Property	Value	Units
Section starting stage	2	
Section ending stage	34	
Calculation Mode	Rating	
Tray type	SIEVE	
Number of passes	1	
Tray spacing	0.6096	meter
Section diameter	2	meter
Section height	20.1168	meter
Section pressure drop	0.207451	bar
Section head loss (Hot liquid height)	2790.22	mm
Trays with weeping	None	
Section residence time	0.0145284	hr

Limiting conditions

Property	Value	Units	Tray	Locati
Maximum % jet flood	62.2782		26	
Maximum % downcomer backup (aerated)	38.8299		34	
Maximum downcomer loading	407.385	cum/hr/sqm	34	Side
Maximum % downcomer choke flood	66.6544		34	Side
Maximum weir loading	57.3407	cum/hr-mete	34	Side
Maximum aerated height over weir	0.181997	meter	31	
Maximum % approach to system limit	41.9693		27	
Maximum Cs based on bubbling area	0.0713175	m/sec	25	

Rate-Based design

Calculated diameter		meter

RADFRAC (RadFrac) - Results | DSTWU (DSTWU) - Stream Results (Boundary)

Summary | Balance | Split Fraction | Reboiler | Utilities | Stage Utilities

Basis: Mole

Condenser / Top stage performance

Name	Value	Units
Temperature	35.6351	C
Subcooled temperature		
Heat duty	-3.19785	MW
Subcooled duty		
Distillate rate	35.9638	kmol/hr
Reflux rate	215.783	kmol/hr
Reflux ratio	6	
Free water distillate rate		
Free water reflux ratio		
Distillate to feed ratio		

Reboiler / Bottom stage performance

Name	Value	Units
Temperature	149.464	C
Heat duty	3.71007	MW
Bottoms rate	113.266	kmol/hr
Boilup rate	380.157	kmol/hr
Boilup ratio	3.35631	
Bottoms to feed ratio		

RADFRAC (RadFrac) - Results | DSTWU (DSTWU) - Stream Results (Boundary) | DSTWU (DSTWU) - Results | RADFRAC Column Internals INT-1 - Column H

Column Internals Summary

Summary

	Value	Units
Number of Trayed/Packed stages	33	
Total height	20.1168	meter
Total head loss (Hot liquid height)	2.79022	meter
Total pressure drop	0.207451	bar
Number of sections	1	
Number of diameters	1	
Pressure drop across sump		bar
Total residence time	0.0145284	hr

Sections

	Start Stage	End Stage	Diameter		Section Height		Internals Type	Tray Type or Packing Type	Section Pressure Drop		% Approach to Flood	Limiting Stage	
CS-1	2	34	2	meter	20.1168	meter	Trayed	SIEVE	0.207451	bar	62.2782	26	View

Figure K12. RadFrac block results

RADFRAC (RadFrac) - Stream Results (Boundary) | RADFRAC Column Internals INT-1 Sections CS-1 - Geometry | RADFRAC

Material | Heat | Load | Vol.% Curves | Wt. % Curves | Petroleum | Polymers | Solids

	Units	17RAD	20	21
To		RADFRAC		
Stream Class		CONVEN	CONVEN	CONVEN
Maximum Relative Error				
Cost Flow	$/hr			
− MIXED Substream				
Phase		Liquid Phase	Liquid Phase	Liquid Phase
Temperature	C	70	35.6351	149.464
Pressure	bar	1.41855	1.2159	1.41855
Molar Vapor Fraction		0	0	0
Molar Liquid Fraction		1	1	1
Molar Solid Fraction		0	0	0
Mass Vapor Fraction		0	0	0
Mass Liquid Fraction		1	1	1
Mass Solid Fraction		0	0	0
Molar Enthalpy	cal/mol	1018.7	597.566	5040.84
Mass Enthalpy	cal/gm	10.0368	6.85559	47.5338
Molar Entropy	cal/mol-K	-90.1439	-75.1286	-86.4336
Mass Entropy	cal/gm-K	-0.888146	-0.861915	-0.815047
Molar Density	mol/cc	0.00815024	0.00987413	0.00707158
Mass Density	gm/cc	0.827223	0.860676	0.749923
Enthalpy Flow	cal/sec	42227.9	5969.65	158599
Average MW		101.497	87.1648	106.047
− Mole Flows	**kmol/hr**	**149.23**	**35.9638**	**113.266**
EB	kmol/hr	107.768	1.07564	106.692
WATER	kmol/hr	1.87994	1.87994	1.869e-07
STYRENE	kmol/hr	6.55215	0.00655395	6.5456
H2	kmol/hr	0	0	0
TOLUENE	kmol/hr	29.126	29.0975	0.0285417
BENZENE	kmol/hr	3.90411	3.90411	1.69245e-05
ETHYLENE	kmol/hr	0	0	0
METHANE	kmol/hr	0	0	0
+ Mole Fractions				
+ Mass Flows	**kg/hr**	**15146.3**	**3134.77**	**12011.6**
+ Mass Fractions				
Volume Flow	l/min	305.164	60.7037	266.951
+ Liquid Phase				

Figure K13. RadFrac Stream Results

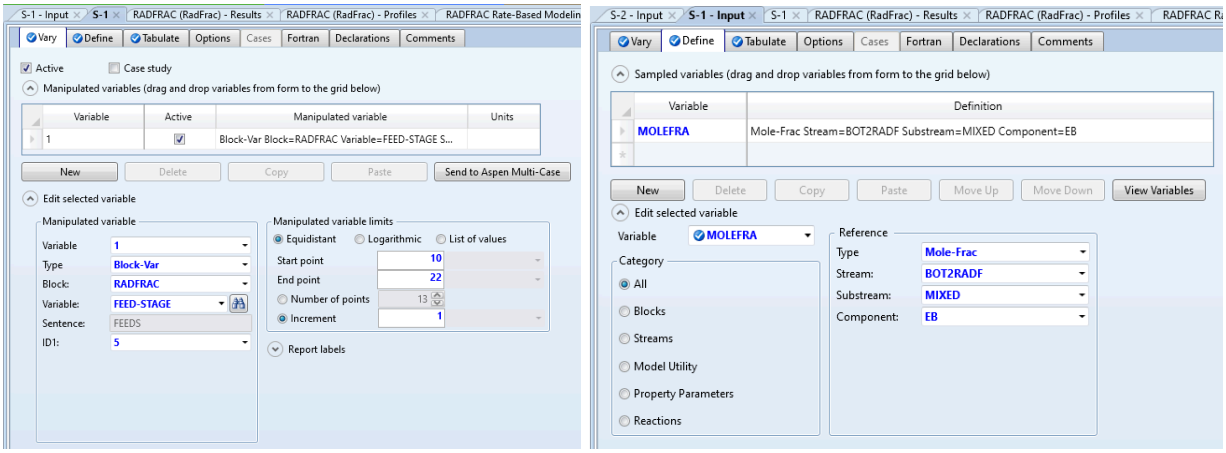

Figure K14. Sensitivity inputs for feed stage location

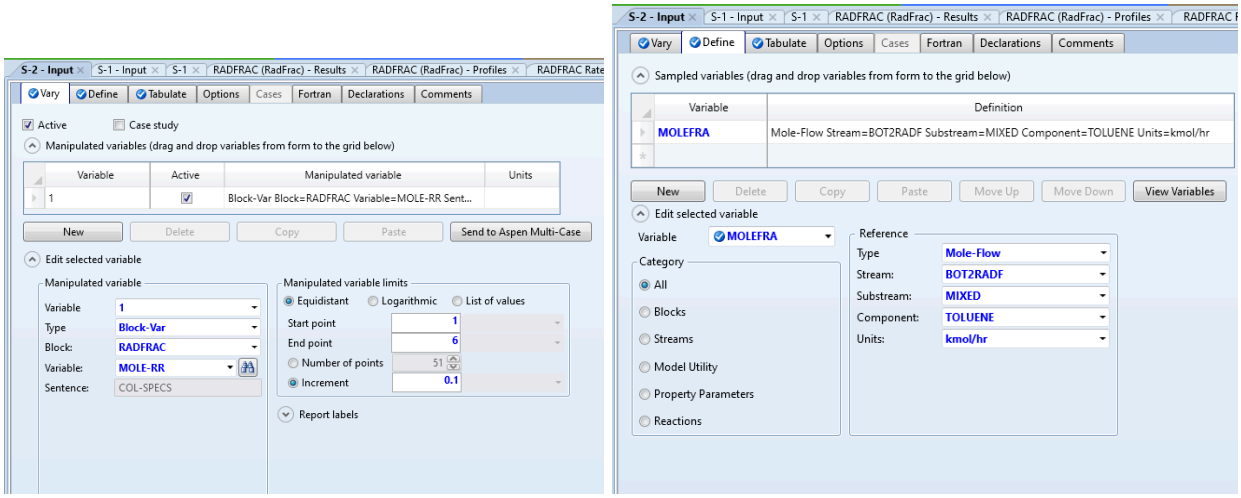

Figure K15. Sensitivity inputs for reflux ratio optimization

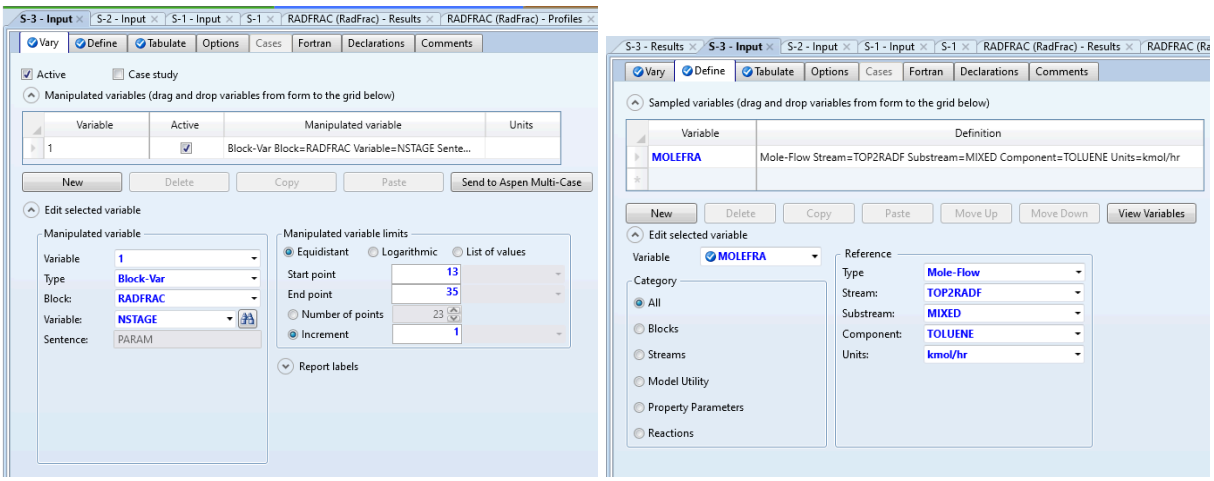

Figure K16. Sensitivity inputs for number of stages optimization

Appendix L

Table L1. Cash flow

Project Yr	CapEx & OPEX (M$)	Revenue(M$)	CCOP(M$)	Gross Profit(M$)	Depreciation(M$)	Taxable income(M$)	Cash flow(M$)	PV of CF(M$)	NPV(M$)
1	-$21.4	$0	$0	$0	$0	$0	-$21.4	-$18.62	-$18.62
2	-$32.1	$0	$0	$0	$0	$0	-$32.1	-$24.29	-$42.91
3	-$15.13	$314.7	$236.3	$78.4	$5.35	$73.1	$63.3	$41.61	-$1.30
4	$0	$314.7	$236.3	$78.4	$9.64	$68.8	$78.4	$44.83	$43.53
5	$0	$314.7	$236.3	$78.4	$7.71	$70.7	$78.4	$38.99	$82.52
6	$0	$314.7	$236.3	$78.4	$6.16	$72.3	$78.4	$33.9	$116.42
7	$0	$314.7	$236.3	$78.4	$4.93	$73.5	$78.4	$29.48	$145.89
8	$0	$314.7	$236.3	$78.4	$.96	$74.5	$78.4	$25.63	$171.53
9	$0	$314.7	$236.3	$78.4	$3.53	$74.9	$78.4	$22.29	$193.82
10	$0	$314.7	$236.3	$78.4	$3.53	$74.0	$78.4	$19.38	$213.2
11	$0	$314.7	$236.3	$78.4	$3.53	$74.9	$78.4	$16.86	$230.06
12	$0	$314.7	$236.3	$78.4	$3.53	$74.9	$78.4	$14.66	$244.71
13	$0	$314.7	$236.3	$78.4	$1.77	$76.7	$78.4	$12.74	$257.46

Note: there is no tax column, as it is considered to be zero dollars per year.